

Design and Optimization of Printed Antennas for Wireless Powering

Vom Fachbereich Maschinenbau
an der Technischen Universität Darmstadt

zur
Erlangung des akademischen Grades Doktor der Philosophie (Dr. phil.)
genehmigte

D i s s e r t a t i o n

vorgelegt von

Ardeshir Hakimi Tehrani, M.A.

aus Isfahan, Iran

Gutachter: 1. Prof. Dr.-Ing. Edgar Dörsam

2. Prof. Dr.-Ing. Klaus Hofmann

Datum der Einreichung: 18.05.2015

Datum der mündlichen Prüfung: 16.07.2015

Darmstadt 2015

D17

Erklärung

Hiermit erkläre ich, dass ich die vorliegende Arbeit, abgesehen von den in ihr ausdrücklich genannten Hilfen, selbständig verfasst habe.

05.08.2015, Ardeshir Hakimi Tehrani

Ardeshir Hakimi Tehrani

Design and Optimization of Printed Antennas for Wireless Powering

URN: urn:nbn:de:tuda-tuprints-46863

URI: <http://tuprints.ulb.tu-darmstadt.de/id/eprint/4686>

Dieses Dokument wird bereitgestellt von tuprints.

E-Publishing-Service der Technische Universität Darmstadt

<http://tuprints.ulb.tu-darmstadt.de/>

Kurzfassung

Das Ziel der vorliegenden Untersuchung war die Auslegung und Optimierung von gedruckten Spiralinduktionsspulen als Antennen für die drahtlose Stromversorgung. Die Leistungsübertragung wurde über einen Abstand von mehreren Zentimetern im Mega Hertz Frequenzbereich für niedrigen Stromverbrauch bei Gütern wie Desktop-Zubehör und Verpackung auf einige Milliwatt beschränkt. Im Allgemeinen ist der Wirkungsgrad der Leistungs Übertragung durch gedruckte Antennen weniger als bei herkömmlichen Spulen aufgrund einiger Eigenschaften der leitfähigen Tinten und Druckverfahren. In dieser Arbeit wurde die Auslegung und Optimierung von gedruckten Antennen unter Berücksichtigung der Grenzen der Druckverfahren dargelegt, geometrische Parameter der Spiralantennen und deren Wirkung auf induktive Stromversorgung überprüft. Drei Layouts für den Siebdruck der Antennen wurden verwendet: ein vorläufiges Layout für Praxistests auf feinen Liniendruck und Abmessungseigenschaften der Antennen; ein Vergleichs-Layout für den Vergleich zwischen der elektromagnetischen Eigenschaften von Antennen; und ein endgültiges Layout für die Verwendung in der drahtlosen Stromversorgung. Zum Drucken der Proben auf PET-Träger wurden zwei Arten von Maschensieben und drei Arten von leitenden Silbertinten aufgebracht. Die Charakterisierung von bedruckten Proben wurde durch Anwendung eines Netzwerkanalysators basierend auf Reflexionsverfahren in Frequenzbereich von 100 Hz bis 40 MHz durchgeführt. Der Betrag und die Phasenlage des Impedanzspektrums wurden aufgetragen, und die Induktivität, Widerstand und die parasitäre Kapazität wurden basierend auf äquivalente RLC-Modelle berechnet. Die erste Resonanzfrequenz der meisten Antennen ist in dem Frequenzbereich der Messung enthalten. Der Phasenwinkel hat 90° in allen Proben nicht überschritten. Die Resonanzfrequenz wurde extrem verbessert durch Erhöhen der Spurweite und der Verringerung der Zahl der Windungen. Die Anwendung der verschiedenen Druckfarben konnte den Impedanzwert erheblich verändern. Die Messungen zeigten, dass die Verluste durch den Nachbarschaftseffekt wirksamer als der Skin-Effekt in bedruckten Proben sein können. Auch durch Erhöhung der Kettenlänge oder Windungszahlen kann die parasitäre Kapazität und Induktivität erhöht werden. Die Ergebnisse haben dargestellt, dass der Gütefaktor ein problematischer Faktor für den Vergleich zwischen verschiedenen Geometrien sein könnte. Der Wert des Gütefaktors wurde für den Vergleich zwischen verschiedenen Antennen bezogen auf den Gesamtbereich der Antennen angewendet. Die Gesamtfläche wurde durch den mit Tinte bedruckten Bereich ersetzt, um das Verhältnis von Wirkungsgrad zu Tintenverbrauch zu repräsentieren. Der Gütefaktor von gedruckten Antennen in der vorliegenden Untersuchung war relativ weniger als der von PCB-Antennen, was durch hohe Widerstandsverluste von leitfähigen Tinten verursacht werden könnte. Schließlich wurde die Funktionalität der gedruckten Antennen von einem Demonstrator nachgewiesen. Auch ein Konzept für den Software-Workflow für die Gestaltung von gedruckten Antennen wurde vorgestellt.

Abstract

The aim of this research was to design and optimize printed spiral inductor coils to use as antennas for wireless powering. Power transfer was limited to some milliwatts over several centimeters with mega Hertz range frequency for low-power consumer products, such as desktop accessories or packaging. Due to some characteristics of conductive inks and printing processes, the efficiency of power transfer through printed antennas is generally less than conventional coils. In this thesis, we considered the impact of printing limits on the design and optimization of printed antennas. We also studied the geometrical parameters of spiral antennas and their effect on inductive powering. Three layouts for screen printing of the antennas were represented: A Preliminary layout for practical tests on fine line printing and the dimensional characteristics of antennas; A Comparative layout for comparing the electromagnetic characteristics of antennas; and a Final layout for use in wireless powering. Two types of mesh screens and three types of conductive silver inks were used to print the samples on PET substrates. The characterization of printed samples was done with a network analyzer based on the reflection method in the frequency range of 100 Hz to 40 MHz. The magnitude and phase angle of the impedance spectrum were plotted and the inductance, resistance, and parasitic capacitance were calculated based on the equivalent RLC model. The first resonance frequency for most of the antennas was included in the frequency range of the measurements. The phase angle was 90° or less in all of the samples. The resonance frequency improved dramatically by increasing the track width and decreasing the number of turns. By using different inks, the impedance value could be changed significantly. The measurements showed that proximity-effect-losses could be more effective than skin-effects in printed samples. Also, it was possible to increase the parasitic capacitance and inductance by increasing the track length or turn number. Our results show that the quality factor could be problematic when comparing different geometries. Figure-of-merit was applied when comparing different antennas based on the overall antenna area. The overall area was replaced by the ink area to represent the ratio of efficiency to ink consumption. The FOM of the printed antennas used in our research was less than that of PCB antennas, which might have been caused by high resistive losses in the conductive inks. Finally, the functionality of printed antennas was validated by a demonstrator and a software workflow concept for the design of printed antennas was introduced.

Acknowledgements

I wish to thank my supervisor Prof. Dr.-Ing. Edgar Dörsam who gave me this opportunity to do present research. I am grateful to colleagues in IDD (Institut für Druckmaschinen und Druckverfahren, TUD) for their support, especially Dr. Hans Martin Sauer the group leader of functional printing at IDD, and also Prof. Dr.-Ing. Klaus Hofmann from IES (Fachgebiet Integrierte Elektronische Systeme, TUD) as the advisor of my thesis, and Mr. Jan Lotichius from EMK (Institut für Elektromechanische Konstruktionen, TUD) for his advices on high frequency measurements. I would like to say my thanks to Dr. Martin Schmitt-Lewen and Mr. Martin Filsinger from Heidelberger Druckmaschinen AG for their help and support on this research.

Table of Contents

Notations.....	v
1 Introduction	1
1.1 Motivation	1
1.2 Objectives	6
1.3 Overview of the Thesis.....	7
2 Fundamentals.....	8
2.1 Printing Technology for Electronic Applications.....	8
2.2 Screen Printing Process	12
2.2.1 Printing Parameters	14
2.2.2 Thick Film Screen Printing	21
2.3 Antennas	23
2.4 Electrical Principles in Wireless Powering Antennas	26
2.4.1 Conductivity, Resistance and Impedance.....	26
2.4.2 Dielectric Properties and Parasitic Capacitance	31
2.4.3 Inductivity.....	33
2.4.4 Resistance, Capacitance and Inductance Model (RLC Model).....	40
2.4.5 Wireless Power Transmission	41
2.5 Measurement and Characterization of Printed Antennas	45
3 Geometrical Design and Optimization of Printed Antennas.....	48
3.1 Geometrical Design of Printed Antennas	48
3.1.1 Shape	49
3.1.2 Outer Diameter	51
3.1.3 Inner Diameter.....	53
3.1.4 Track Width.....	54
3.1.5 Track Spacing.....	55
3.1.6 Track Thickness.....	56

3.1.7	Number of Turns	56
3.1.8	Geometrical Design Optimization.....	57
3.2	Concept of Software Workflow for Printed Antennas	58
3.2.1	Software Workflow	61
4	Experimental Setup	66
4.1	Layout design and Software Settings	67
4.1.1	Preliminary Layout.....	67
4.1.2	Comparative Layout	69
4.1.3	Final Layout.....	71
4.1.4	Software Settings.....	74
4.2	Mesh Screen	80
4.3	Ink.....	81
4.4	Printing Procedure and Curing	82
4.5	Experiments.....	86
5	Electrical Characterization.....	88
5.1	Setup Definition.....	88
5.2	Categorization of Printed Samples for Measurement.....	90
6	Results and Discussion	93
6.1	Microscopic Controlling of Ink Thickness and Line Width Deviations	93
6.2	The Influence of Design, Ink and Mesh Screen on Electrical Characteristics .	101
6.2.1	Impedance.....	101
6.2.2	AC Resistance	106
6.2.3	DC Resistance	112
6.2.4	Parasitic Capacitance.....	114
6.2.5	Inductance.....	116
6.2.6	Frequency of Resonance.....	118
6.2.7	Quality Factor	118
6.2.8	Figure-of-merit	121
7	Application of Printed Antennas in Demonstrator.....	124
8	Conclusion and Outlook.....	128

References..... 131

Appendix 138

A1. Measured values for all of the samples 138

A2. Silver ink NCS-500AG Nicomatic 138

A3. Silver ink SunTronic™ PTF CXT-0644 Sun Chemical 140

A4. Silver ink Acheson Electrodag PF-050 Henkel 141

A5. PET film Hostaphan® GN..... 143

Notations

Symbols

Symbol	Description	Unit or Value
$ Z $	magnitude of impedance	[Ω]
\square	Square	[-]
$^\circ$	Degree	[-]
$^\circ\text{C}$	Celsius degree	[-]
A	Ampere	[-]
A	area	[m^2]
A	cross sectional area of conductive part	[m^2]
A	decimal equivalent of openness percentage of mesh screen	[-]
A_0	effective plate capacitor area	[m^2]
B	magnetic flux density or magnetic inductance	[N/A.m]
C	capacitance	[F]
C	capacitor	[-]
c	speed of light	299,792,458 m/s
c_i	layout dependent coefficients	[-]
cm	centimeter	[-]
d	diameter	[m]
D	diameter of screen wire	[mil] = 25.4 μm
d	distance	[m]
D	flexural rigidity	[N·m]
d_w	wire diameter of screen	[m]
e	Euler's number	≈ 2.72
E	Young's modulus	[N/m ²]
F	Farad	[-]
f	frequency	[Hz]

f_0	self-resonant frequency	[Hz]
H	Henry	[-]
H	magnetic field strength	[A/m]
H	mesh thickness	[mil]
h_s	thickness of screen	[m]
Hz	Hertz	[s ⁻¹]
I	electric current	[A]
j	imaginary quantity	$j^2 = -1$
k	coupling coefficient or coil coupling factor	[-]
k	kilo	[-]
k_r	relative openness of mesh screen	[m]
L	inductance	[H]
L	Inductor	[-]
L	length	[m]
l	length	[m]
L_1	self-inductance	[H]
m	meter	[-]
M	number of meshes per unit length	[-]
m	screen wire pitch	[-]
M_{12}	mutual inductance	[H]
mil	mil	25.4 μm
mm	millimeter	[-]
n	nano	[-]
N	Newton	[-]
N	number of loops	[-]
Pa	Pascal	[-]
Q	quality factor	[-]
Q_{\max}	peak quality factor	[-]
r	cylindrical radius	[m]
R	radius	[m]
r	radius of coil antenna	[m]
R	resistance	[Ω]
rad	radian	$\approx 57.30^\circ$
S	maximum side dimension of rectangular spiral inductor	[cm]

s	second	[-]
s	track space	[m]
s ⁻¹	reciprocal second(s)	[1/s]
sq	square	[-]
t	thickness	[m]
t	time	[s]
T _w	relative thickness	[mil]
V	voltage	[V]
V	Volt	[-]
w	track width	[m]
W	Watt	[-]
w	width	[m]
X	reactance	[Ω]
Z	impedance	[Ω]
δ	skin depth	[m]
ε	strain	[-]
ε ₀	dielectric constant in vacuum	[F/m]
ε _r	dielectric material constant	[F/m]
θ	phase angle	°
λ	wavelength	[m]
μ	magnetic permeability in free space	[H/m]
μ	micro	[-]
μ ₀	magnetic field constant	[H/m]
μ _r	relative magnetic permeability	[-]
ν	Poisson ratio	[-]
ξ _m	transmission efficiency	[-]
π	ratio of a circle's circumference to its diameter	≈ 3.14
ρ	fill ratio	[-]
ρ	resistivity	[Ω·cm]
σ	conductivity	[1/Ω·m]
Φ	magnetic flux	[V·s]
Ψ	total flux	[V·s]
Ω	Ohm	[-]
ω ₀	frequency of resonance	[rad/s]

Acronyms

Abbreviation	Description
AC	alternating current
AI	Adobe Illustrator
ASCII	American standard code for information interchange
CAD	computer aided design
CMYK	cyan, magenta, yellow, and black
CSV	comma separated values
DC	direct current
DPI	dots per inch
DXF	drawing interchange format
EAS	electronic article surveillance
FOM	figure-of-merit of inductor
IC	integrated circuit
IFBW	intermediate frequency bandwidth
ISM	industrial, scientific, and medical
LED	light-emitting diode
MEMS	microelectromechanical systems
MUT	material under test
OLED	organic light-emitting diode
PCB	printed circuit board
PDF	portable document format
RF	radiofrequency
RFID	radiofrequency identification
RLC	resistor, inductor and capacitor
S-parameter	scattering parameter
UHF	ultra high frequency
WPT	wireless power transfer

1 Introduction

1.1 Motivation

With conventional printing technology, text and graphics are created for such applications as newspapers, packaging, and textiles. Here, the aim of printing is to deposit ink(s) on a substrate to generate a pattern from a given layout. If the printed text is legible and the images look good, then the major goals of printing have been achieved. In addition to conventional printing, however, there is also so-called functional printing. Here, special inks are deposited on substrates so that the printed samples can perform a function, such as an electromagnetic or mechanical activity.

Functional printing samples may look good visually, but this is not enough for a reliable evaluation of printing quality. For example, Figure 1.1 shows two screen-printed antennas. Figure 1.1 (a) was printed with normal black ink, whereas Figure 1.1 (b) was printed with conductive silver ink, with the same screen and on the same type of substrate. Both of them look good, but some electrical characterizations are necessary to evaluate the functionality in sample (b). In any case, sample (a) has no functionality, due to the type of ink used.

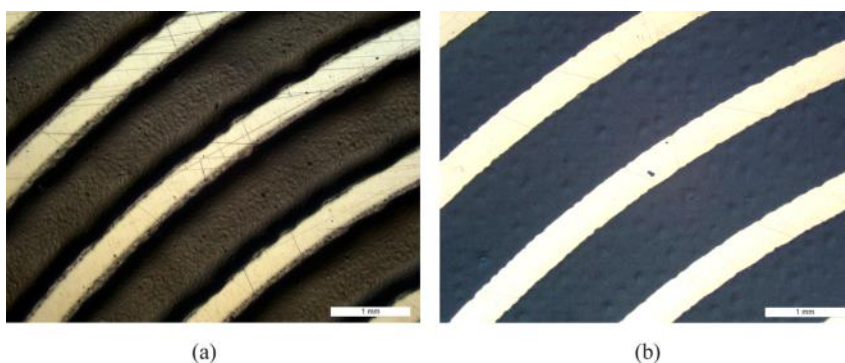


Figure 1.1: (a) A screen-printed antenna with normal black ink. (b) A screen-printed antenna with conductive silver ink. Both samples were printed with the same screen and on the same type of substrate. The samples look good visually, but some electrical characterizations are necessary to evaluate the functionality of sample (b).

Printing parameters play an important role in functional printing processes. Some of the critical parameters are the deposition technique, type of ink, substrate, printing form, geometrical design, post-processing steps, printing runs, printing speed, and printing pressure. Therefore, the essential question when designing pattern for functional printing is on how to optimize it for printing production. For example, how wide do the fine lines in a printed electronic circuit need to be to decrease the risk of disconnection during ink transfer from plate to substrate? Similarly, how wide do the track gaps need to be to prevent interconnection between the lines after ink bleed out? Sung et al. [92] believe that the requirements of printed electronics are pushing the limits of conventional printing. In addition to the limits, there are some freedoms in the “design of innovative structures” by functional printing and printed electronics, in compare with conventional techniques, e.g. in the field of printed antennas and wireless powering.

Wireless power transfer (WPT) systems [91] or inductive powering systems [99] work on the basis of the inductively coupled model [91], which means that two inductors make a link to transfer electric power. WPT is a reliable and simple method for transferring power and data over short distances without cables [99]. Nicola Tesla first presented the concept of WPT at the end of 19th century. He applied for the related patent in 1902. After Tesla, other scientists developed WPT systems. For example, in 2006, Professor Marin Soljačić and his research team at the Massachusetts Institute of Technology demonstrated a mid-range WPT based on magnetic resonance. In 2007, they were able to wirelessly light a 60 watt (W) lamp across a 200 cm gap [49]. Figure 1.2 shows these two significant steps in the development of WPT systems.

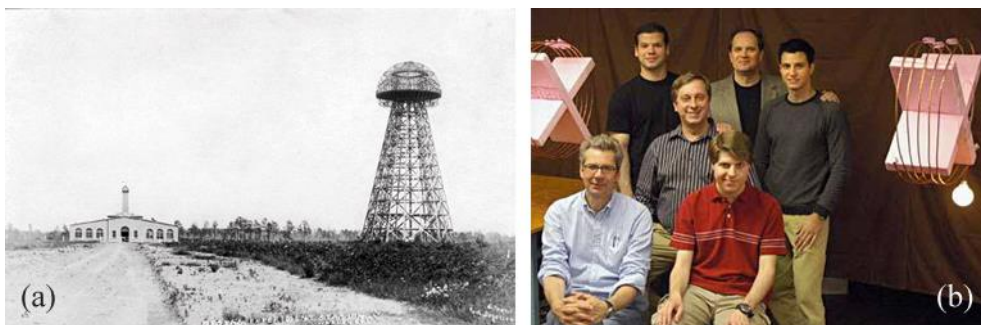


Figure 1.2: Two significant steps in wireless powering development: (a) Nicola Tesla's power transfer tower [80] from the end of 19th century [49]. (b) Lighting up a 60 W lamp via antennas by Marin Soljačić and his research team [36] in 2007 [49].

A successful experiment on a wirelessly powered laptop was reported by Sample et al. [78]. The WPT system provides laptop's peak power of 12 W across a 70 cm gap, with an efficiency of 50%. Figure 1.3 shows the wirelessly powered laptop.

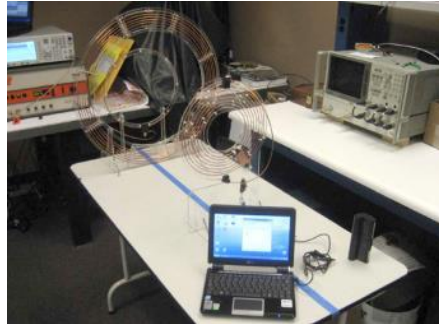


Figure 1.3: A laptop powered wirelessly at 12 W across a 70 cm gap with an efficiency of 50% [78].

The principal concept of wireless powering is simple: A fluctuating current, voltage or electric field generates a time-varying magnetic field at the transmitter side [21]. The transmitter antenna establishes electromagnetic fields around itself. The receiver antenna, located at a distance from the transmitter, collects the magnetic fields. A rectifier at the receiver side converts alternating current (AC) power to direct current (DC) power. In addition to power transfer, data communication through the power link is possible by modulating the AC power [53]. Figure 1.4 illustrates the WPT concept. The transmitter and receiver antennas are produced by different technologies and from various types of conductive materials having different electromagnetic characteristics. Although one prevalent type of antenna is wire-wound coils, other solutions are available too, such as etching printed circuit boards (PCBs) or depositing conductive inks on polymer substrates.

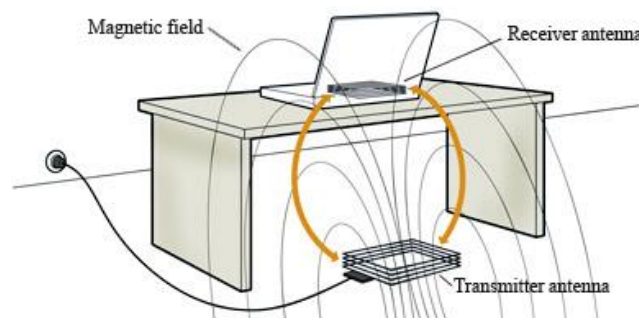


Figure 1.4: The concept of WPT [81]. The magnetic field is transferred from transmitter antenna to receiver antenna to generate power for an electrical appliance.

What advantages do WPT systems have over systems using wire connections? Wireless systems are cheaper and can be used over long distances. For example, long-distance telephone lines with wire cables are expensive and it is not possible to connect wires to a satellite. Wireless systems can also overcome physical barriers in many cases, as with biomedical implants inside the human body. Moving systems, especially in unknown locations, can be improved by wireless powering. For example, WPT can solve the problem of metal fatigue in moving cables [99]. There is a wide range of applications for inductive wireless powering. For example, powering biomedical implants [86], [44], electric power supplies, battery chargers, power transfer among integrated circuits (ICs) [86] and radiofrequency identification (RFID) [99]. The potential for new cordless utilization is also considerable. Displacement sensors [60] and paper computing [108] are two examples. Figure 1.5 shows inductive wireless powering in two applications, a wireless mobile phone charger and a printed RFID antenna.

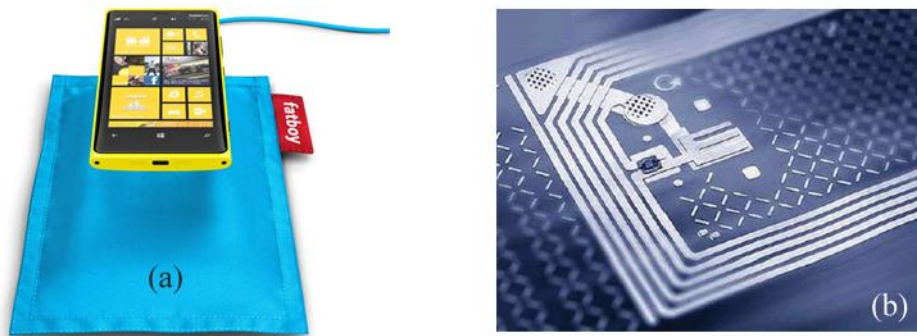


Figure 1.5: Use of inductive wireless powering in 2 applications: (a) A wireless charger for mobile phones [24]; (b) a printed RFID antenna [54].

Wireless powering is not the only possibility for cordless power transfer. There are several others, such as radiative, conductive and capacitive powering [53] and even batteries. Each of these has its own benefits. For example, compared with traditional batteries, WPT systems have a long lifetime, are biocompatible and compact [99], [91]. Planar antennas based on polymer substrates have some advantages over conventional wire wound coils. For example, flexibility, miniaturization, batch-fabrication and easy integration with circuitries [44]. However, the major challenge with implanted WPT systems is the short transmission distance and low energy efficiency caused by microelectromechanical systems (MEMS) receiver antennas [91].

There are two approaches to overcoming the challenges of printed WPT antennas: optimizing printing process parameters and using inductive antennas and prevalent hints on the efficiency of WPT systems. Some parameters impact the efficiency of WPT systems. For example, the antenna shape, distance, alignment, outer diameter, inner diameter, number of turns, track width, track spacing, and frequency of operation [45]. Also, the quality factor and mutual coupling are two key features of wireless powering. These depend on the geometries, dimensions and relative positions of the antennas [42]. The quality factor affects the power transfer efficiency between antennas [25]. Planar spiral antennas have a lower quality factor than wire antennas [62]. This means that the printed antennas must be optimized to obtain the highest possible power transfer efficiency [25]. The efficiency of the powering system is in direct proportion to the inductivity of the antenna. The inductivity depends strongly on the conductivity of the printed antenna. Because of some unfavorable characteristics of conductive inks and printing processes, the conductivity of printed lines is less than that of bulky metals or even of thin foil-clad substrates (such as PCBs). Consequently, the efficiency of power transfer through printed antennas is normally less than that of conventional coils. Therefore, every printing parameter that effects conductivity can also change power efficiency.

There are benefits and drawbacks to different printing techniques for printed antennas. Using offset lithography has been reported for printing conductive inks on a wide range of flexible materials. The use of gravure printing and flexography in the fabrication of conductors has also been reported [54]. Sidén et al. [87], however, have discussed some problems associated with printing antennas with flexography. Depending on the application, inkjet and screen printing are more common in printed electronics [54]. As reported by Salmerón et al. [77], the result of screen-printed RFID tags was better than inkjet with regard to sheet resistance and quality factor. Moreover, Arenas et al [10] believe that the geometry of square spiral inductors is adaptable to screen printing. The forty years of experience using screen printing in the electronics industry [54], [67] explains its reliability. The screen-printing process is on-demand and inexpensive. Also, the ink used for screen printing is easier to formulate than the ink for other printing processes [18]. Nevertheless, there are still some challenges in fabricating antennas with screen printing. The major influences on RF performance are line thickness, edge definition, layout accuracy, and printing resolution [77]. The printing resolution achieved with screen printing is relatively low [18]. Moreover, to improve conductivity,

thicker printed lines are desirable. Achieving thick lines with screen printing is difficult, and fine-line screen printing requires stricter process control [67]. There is a huge number of process variables available for screen printing optimizations. The effects of over 280 different parameter combinations has been mentioned in some references [74], [104]. There may be many new challenges also.. For example, as Horwood [41] mentioned, it is difficult to repeatedly deposit precise amounts of ink. Moreover, Brown [15] believes that attaining a smooth surface and rectangular cross section are critical targets for minimizing ohmic loss in printed conductors, such as antennas.

In summary, the most important challenges in the field of printed antennas could be seen as follows:

- Conductivity of printed traces
- Dimensional consistency of printed traces
- Quantity of printed traces in a specified area

1.2 Objectives

The general aim of this dissertation is the design and optimization of printed antennas for the application of wireless powering. A wireless powering system may include several elements, as shown in Figure 1.6. The aim of this research is to replace transmitter antenna L_1 and receiver antenna L_2 with screen-printed antennas.

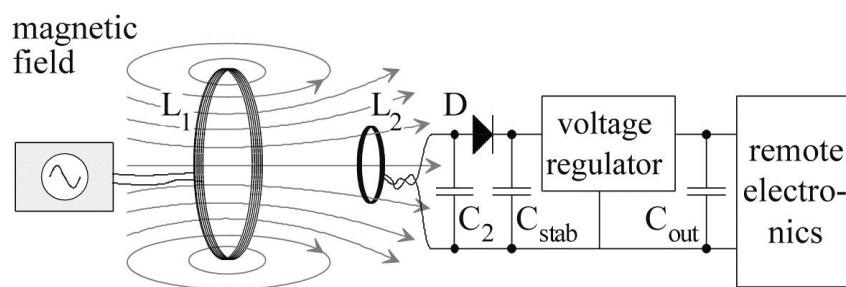


Figure 1.6: Structure and elements of a wireless powering system. L_1 is the transmitter antenna, L_2 is the receiver antenna, D is the rectifier, C_2 is a capacitor for developing link efficiency, C_{stab} is a stabilizer capacitor, and C_{out} is an output ripple regulator or load variations filter [99]. The aim of this research is to replace transmitter antenna L_1 and receiver antenna L_2 with screen-printed antennas.

The major question in the present research is this: is it possible to print the antenna for WPT systems? If it is possible, how can one meet the challenges of improving magnetic

efficiency in screen-printed antennas, as discussed previously? What is the best software and/or software workflow for the geometrical design of antennas? To answer these questions, one must pay attention to the geometrical parameters and design optimization of printed antennas.

In this research project, the rate of power transfer is limited to a few milliwatts across several centimeters of distance. The range of the operating frequency is several mega Hertz (Hz). The printed antennas would be used in low-power consumer products, such as desktop accessories, showcases, supermarket shelves, and packaging.

1.3 Overview of the Thesis

The following chapters of this thesis introduce the theoretical and experimental context of screen-printed antennas for the application of wireless powering. Chapter 2 includes the fundamentals of printing, antennas and WPT. It contains some general information about screen printing technology, its capabilities for electronic applications, and the electrical principles of wireless powering antennas. Chapter 3 covers the design and optimization of WPT antennas for printing. It focuses on spiral antennas for wireless powering applications and includes information on the delimitations of research, the geometrical design of printed antennas, the optimization of artwork for printing. It also presents a concept for the software workflow for the geometrical design of printed antennas.

Chapter 4 deals with the experimental setup for printing antennas. It contains detailed information on the layouts of experiments, screens, the squeegee blade, conductive inks, the substrate, the printing procedure, the curing of printed samples and the number of experiments.

Chapter 5 describes the characterization and electrical measurement of printed antennas. It includes measurements of some key features for the electromagnetic characterization of printed samples. After explaining and discussing experimental results in Chapter 6, the usability of printed antennas will be considered in a demonstrator in Chapter 7, which also describes the prototype and potential applications of printed antennas. Chapter 8 is a brief conclusion containing the scientific achievements, outlook and next steps of the work.

2 Fundamentals

This part contains the theoretical framework of thesis. The aim of this chapter is to express a review on printing and wireless powering antennas. The context sequence is starting with printing technology for electronic applications, and after it, moving on to fundamentals of printing and antennas. Finally, electrical principles in wireless powering antennas and measurement and characterization of them are considering.

2.1 Printing Technology for Electronic Applications

Considering the goal of this research to wireless powering by printed antennas, the starting point is selection of feasible printing process for manufacturing WPT antennas. A general review on flexible electronics and printing technology for electronic applications can be useful to show the position of printing in electronics. The benefits and drawbacks of printed electronics in compare to conventional methods will be represented, too.

Flexible Electronics and Printed Electronics

The background of flexible electronics is more than forty years. Some famous applications of flexible electronics are solar cells, organic light-emitting diode (OLED) displays, medical image sensors, and electronic papers. Generally, flexible electronic products are more rugged, lighter, portable, and less expensive [105]. They are combinable with novel consumer products and can be produced with ultra-low cost and large-area processes [57]. Figure 2.1 shows a flexible color display, and a wraparound display as a potential of wearable devices.



Figure 2.1: Two examples on application of flexible electronics in new products: (a) A flexible color display [72] that is already available, and (b) a wraparound display [71] as a concept design for wearable devices.

In flexible electronic structures, all components must be relatively bendable. These structures can include four major parts [105]:

- a) Substrate
 - b) Backplane
 - c) Frontplane
 - d) Encapsulation
- a) Substrates should have some specific characteristics. These characteristics include optical features, surface roughness, and chemical, mechanical, thermal, thermo mechanical, electrical, and magnetic properties. Three types of substrate materials are available in the field of flexible applications: organic polymers, metals, and flexible glass.
 - b) Backplane provides power and signal for frontplane. It can also collect them from frontplane. Two types of backplane are available: active and passive.
 - c) Frontplane is an optoelectronic part. It can include a transmissive display, an emissive display, or a sensor.
 - d) Encapsulation is a barrier layer on top of substrate devices. It protects them and increase their life time [105]. High transparency and dimensional stability are additional features for encapsulation. It may include inorganic and hybrid materials that deposited by vacuum or wet methods [57].

Generally, flexible structures are classified in three fields: bendable, stretchable, and permanently shaped [105]. Flexibility of the substrate can effect dramatically on electrical properties of structures like antennas. An important factor in flexibility of substrate is flexural rigidity D as

$$D = \frac{Et^3}{12(1-\nu^2)} \quad (2.1)$$

Where E is Young's modulus, t is thickness of substrate, and ν is Poisson ratio. If a sheet of substrate that is mechanically homogeneous will be bent to a cylindrical shape, during this deformation, the outside surface of substrate will expand, while the inside surface will compressed. The bending strain ε of deformation is calculated as

$$\varepsilon = \frac{t}{2r} \quad (2.2)$$

Where t is thickness of substrate, and r is cylinder radius. The value of bending strain should be kept less than critical values, especially in sensitive functional cases [105].

The ε value can be a challenge for some production processes such as printing. In some printing processes, the bending strain of the substrate can exceed ε value. Additional problems can be caused by stretch and compression of substrate during printing process.

Printed electronics can be defined as a part of flexible electronics, depends on the type of substrate and the ink. Printed electronics may use every printing technology [54] that is employed in graphic art industry [84] to fabricate electronic circuits, electronic devices, electrical components, and interconnects [54]. Printed electronics is an additional part for silicon electronics [18]. A wide range of functional materials and substrates can be used by printing [54]. Maybe the first application of printing in electronic industry is deposition of metal conductors for solar cells with inkjet printing in 1980s. After it, other electronic devices have been attempted to produce by printing, e.g. flexible displays, polymer light emitting diode displays [84], ultra high frequency (UHF)-RFID antennas, interdigitated capacitors, spiral inductors [92], sensors, batteries, security devices, and quality indicators [54]. As instance of printed electronics, Figure 2.2 shows the schematic of a differential amplifier and the microphotograph of screen printed amplifier.

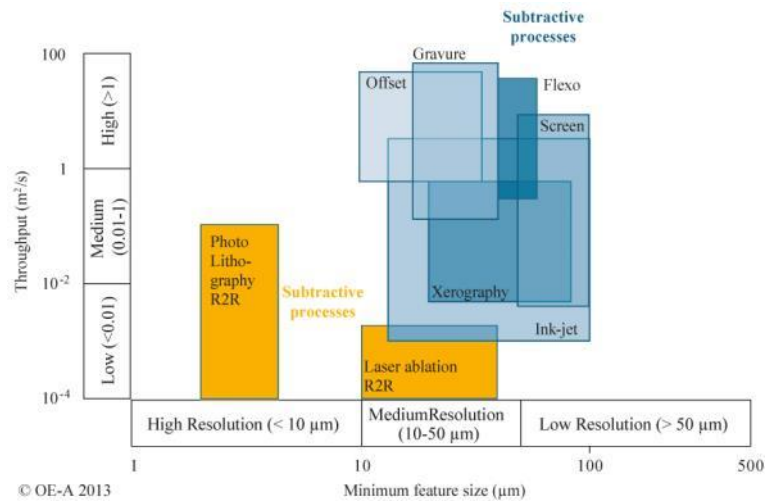


Figure 2.3: The comparison between additive and subtractive processes. The highest achievable resolution and the throughput represented on horizontal and vertical axis respectively [65]. Subtractive process are more accurate but the highest speed of production is for additive process including gravure, offset, flexography, screen, inkjet and xerography.

Quality of printed elements in some cases like conductivity and inductivity is less than conventional ones. That makes them less efficient in e.g. antenna for inductive powering. Resolution, registration and process stability are other challenges. The speed of printed electronics is slow and the carrier mobility is low [18]. On the other hand, there are some advantages. Sung et al. [92] mentioned some printing characteristics. Printing is a large area, roll-to-roll, and all-additive process for different substrates. It does not need expensive processes like vacuum or photolithography. In addition, printing is almost low cost [84] with low environmental impact [54], [34].

2.2 Screen Printing Process

Screen printing or silk-screen printing [32] has been applied in visual arts for near two millenniums [15]. The origin of screen printing comes from reproduction of paintings by stencils in ancient Chinese art. During World War II, it was applied for mass production of electronic circuits. The printing was substituted with manual routing of wires. Throughout the space programme in the sixties, it was used for miniaturization of electronic circuits. Later, screen printing was developed into a branch of electronic manufacturing which is called thick film [74] deposition. By considering the opinion of

Horwood at 1974, screen printing has been determined as a low cost and repeatable process for high quality patterns from many years before [41].

The screen is a woven fabric that coated with a masking material in non-imaging areas. Although in ancient era, the fabric was made from silk but nowadays nylon and stainless steel are more conventional. During printing, the screen takes place over the substrate and the ink is transferring through the imaging areas of screen by pressure of a flexible blade which is called squeegee [32]. Figure 2.4 shows a screen printing machine, a printing screen, and microscopic view of a screen woven fabric.

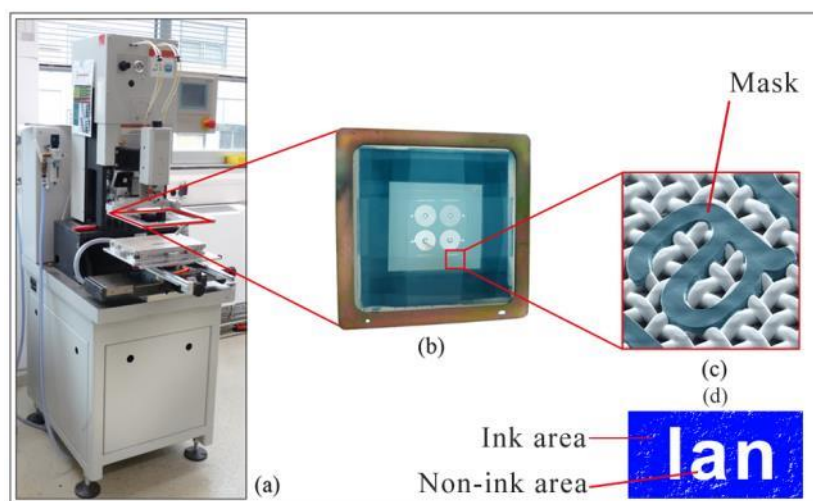


Figure 2.4: (a) A screen printing machine Kammann-K15Q SL from IDD (Institut für Druckmaschinen und Druckverfahren, TUD), (b) Stainless steel mesh screen, (c) Microscopic view of a screen woven fabric [29], and (d) The transferred ink on a substrate.

A basic concept of screen printing is transferring the ink via open areas of a mesh and deposition on substrate [41]. An inking blade spreads the ink on screen. The flexible squeegee is moving over the surface of screen (Figure 2.5) and filling open parts of the mask by ink [15], [41]. Some parts of the both sides of screen were covered with a photo emulsion mask to do not transfer the ink. The resolution of pattern depends on the number of meshes. The mesh number is determined by threads per inch [41] or centimeter [82]. At the same time that squeegee is moving, screen is pushed down to transfer the ink on substrate [15]. Figure 2.5 shows the process.

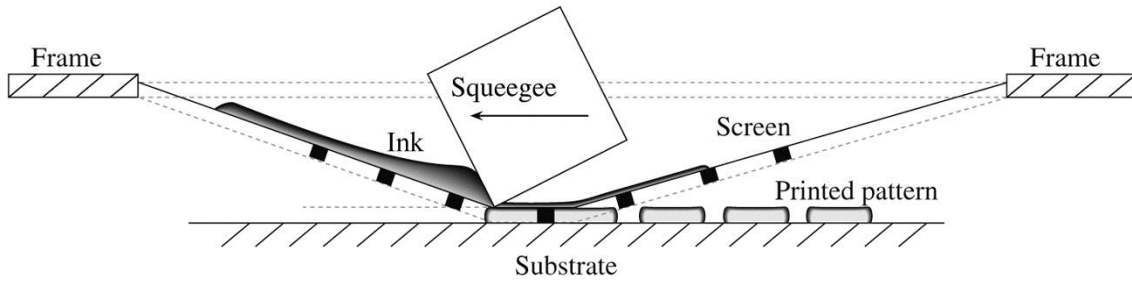


Figure 2.5: Screen printing process. The arrow indicates printing direction [96]. The squeegee is moving on screen and pushing the ink through screen meshes on substrate.

2.2.1 Printing Parameters

Although the process of screen printing appears simple but the quality of the process can be defined with several parameters, such as fine line resolution, print thickness average, thickness uniformity, and the number of voids [67]. As mentioned by Brown [15] more than 50 printing parameters can effect on process. Pan et al. [67] have been proposed 45 effective parameters in 6 different categories, as represented in Figure 2.6:

- Printing machine
- Screen
- Ink
- Squeegee
- Substrate
- Printing process

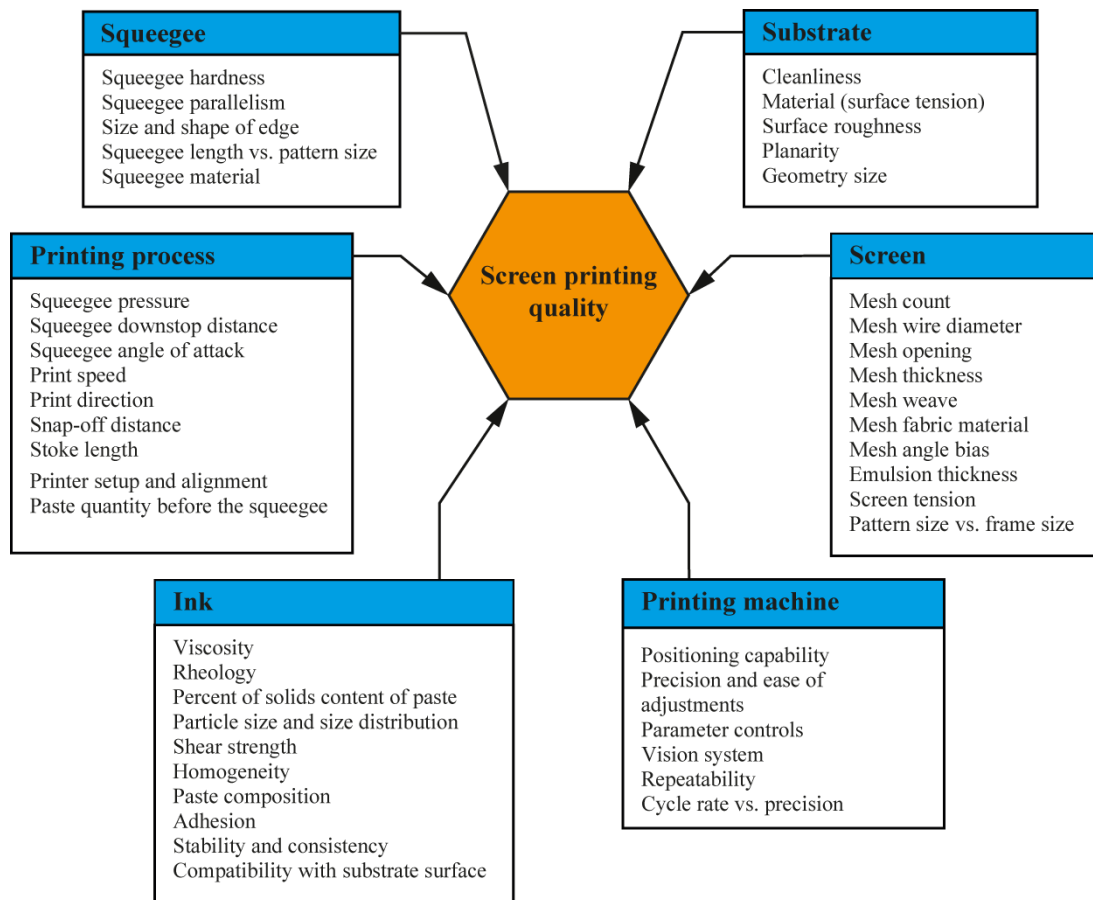


Figure 2.6: The factors that influence screen printing quality, re-drawn from [67]. The number of factors is 45 that are distributed in six categories including printing machine, screen, ink, squeegee, substrate, and printing process.

In addition, there are several typical quantitative values for screen printing parameters, e.g. screen length, screen snap off, screen tension, mesh wire diameter and separation, ink density and surface tension, squeegee velocity, and tip height and curvature of it. Table 2.1 contains some typical quantitative values of screen printing.

Table 2.1: Some typical quantitative values of screen printing, including screen length, screen snap off, screen tension, mesh wire diameter and separation, ink surface tension and density, and velocity, tip height and tip curvature of squeegee. Data from [96], [104].

Parameter	Value
Screen length	10^{-1} m
Screen snap off	10^{-3} m
Screen tension	10^3 Nm $^{-1}$
Mesh wire diameter	0.5×10^{-4} m
Mesh wire separation	1.5×10^{-4} m
Ink surface tension	10^{-3} Nm $^{-1}$
Ink density	103 kgm $^{-3}$
Squeegee velocity	10^{-1} ms $^{-1}$
Squeegee tip height	10^{-4} m
Squeegee tip curvature	10^2 – 10^4 m $^{-1}$

Mesh Screen

A screen is composed of three parts: a stencil that defines the pattern, a mesh that supports the stencil, and a frame that supports the mesh [39]. Figure 2.7 shows a microscopic view of the mesh.

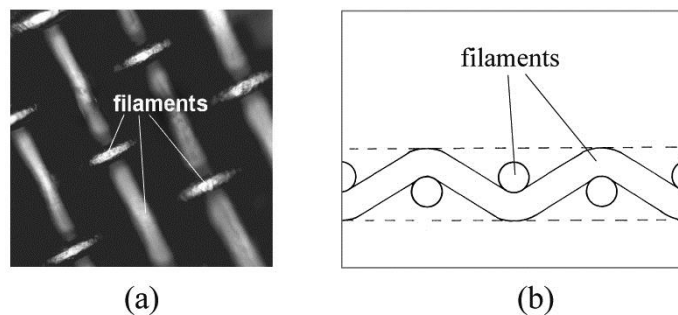


Figure 2.7: (a) A microscopic view of stainless steel mesh [40], and (b) Section view of stainless steel mesh [41]. The stainless steel filaments are represented in both of images.

Stencil defines the shape of printing pattern. In electronics applications, there is an additional role for the stencil. It has a major influence on print thickness. Generally, there are three types of stencil: photo-emulsions, metal masks and plastic sheets [39]. Conventional materials for screen meshes are stainless steel (type 304), monofilament nylon (polyamide), monofilament Dacron (polyester), and metalized polyester [67]. Nylon monofilament screens are strong and resilient but they are not so stable and can absorb water. Polyester is more stable than nylon. That is resilient and flexible. Stainless steel is stronger and more stable than nylon and polyester, with a higher elastic modulus and lower elastic limit. Stainless steel screens are long life but can be damaged by mechanical impacts. Frames almost made of metal for electronics applications. The strength and stability of metal is necessary. The flatness tolerances of frame is in the range of ± 0.15 mm [39]. Stainless steel [104], [96] and polyester are conventional screens that applied for industrial screen printing [39]. Usually, optimum dimensional stability and abrasion resistance of stainless steel mesh are its advantages, as well as lower cost and higher flexibility of polyester monofilament mesh [69].

Squeegee

Actually, the squeegee carries the ink on screen and in front of itself [35]. The squeegee over screen must be so adjusted that to wipe ink off the screen surface [74], as represented in Figure 2.8 (a). By moving squeegee, the screen takes the shape of it [40] temporarily, as schematic is represented in Figure 2.8 (b).

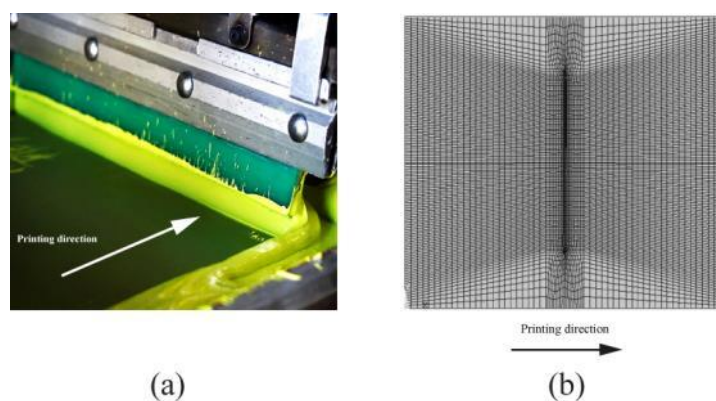


Figure 2.8: (a) A squeegee blade during printing process. The squeegee is wiping off the ink from screen surface. The arrows show the printing direction [97], and (b) Deformation of screen by moving the squeegee over it [40].

Polyurethane is the most conventional material for squeegee. That is wear resistance and durable in contact with chemical agents [35]. The hardness of squeegee is the most important parameter that effects on printing results. For printing the fine lines, a hard squeegee should be used. Also, the speed of squeegee can effect on fine lines that are parallel to traveling direction of it [67]. Generally, an attack angle of 45 degrees is a good adjustment for travelling the squeegee on screen [35].

Ink

Deposition of viscous ink through a mesh is base of screen printing [15]. Ink roll in front of squeegee forms a hydrodynamic pump. This pump injects ink to substrate, through open parts of the mesh [74]. Every viscous thick film ink with a non-Newtonian rheology is suitable for screen printing [40]. The viscosity of thick film inks should be on the order of 10 Pascal-second (Pa·s) at a shear rate of about 600 reciprocal seconds (s^{-1}) [35]. Thick film inks are composed of two phases: vehicle phase for development of rheology, and functional phase for final electrical characteristics [15]. Generally, metallic particle inks consist of silver, copper, or gold particles dispersed in a solvent matrix. The particles can be micro particles with diameter of 2 μm to 40 μm , or nanoparticles with diameter of 2 nm to >50 nm [77]. Figure 2.9 shows different types of silver inks after sintering. Figure 2.9 (a) includes a low curing temperature metallo-organic-decomposition silver ink. Figure 2.9 (b) shows a conventional type of silver ink with micro particles, flakes and polymeric binder matrix, and Figure 2.9 (c) represents a developed type of silver nano ink.

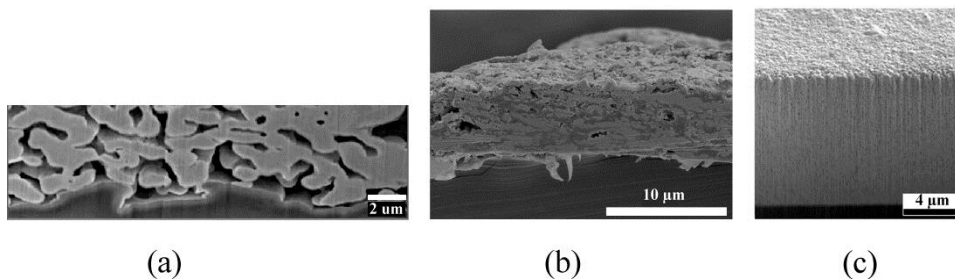


Figure 2.9: The section view of different types of sintered silver inks: (a) A low curing temperature metallo-organic-decomposition silver ink [55], (b) A conventional silver ink with micro particles, flakes and polymeric binder matrix, and (c) A developed silver nano ink [84].

Silver ink can be bonded with high strength to the substrate. Considering skin effect, silver can be an excellent conductor at high frequencies [35].

***Contact* Screen Printing and *Off-contact* Screen Printing**

Screen printing process is divided to two major types: *contact* and *off-contact*. In *contact* process, the screen is placing over substrate. The surface of screen touches the substrate. Generally, this process is not preferred. Lifting the screen from substrate can destroy fine patterns.

In *off-contact* process, screen is holding above substrate. The screen is under high tension [104] and there is a snap-off between screen and substrate [96]. Snap-off is a several millimeters gap between screen and substrate to limit their contact during squeegee movement. Because of the snap-off between the screen and substrate, the contact of screen with substrate is just a line [41]. This line-contact effects on ink thickness [15]. Off-contact process is almost standard printing method in microelectronics industry [104]. Figure 2.10 shows the off-contact screen printing process.

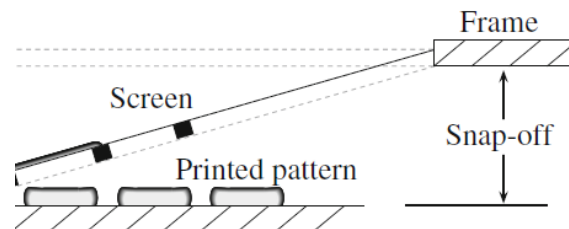


Figure 2.10: *Off-contact* screen printing process [96]. Snap-off is a several millimeters gap between screen and substrate and caused to limit their contact to a line, during squeegee movement.

By moving the squeegee over screen, the screen peels behind squeegee. Figure 2.11 depicts the squeegee moving at $t = 0$ and $t > 0$, assume that as the squeegee moves, a printed layer is quickly established, and also the screen peels behind the squeegee slower than the squeegee moving [96].

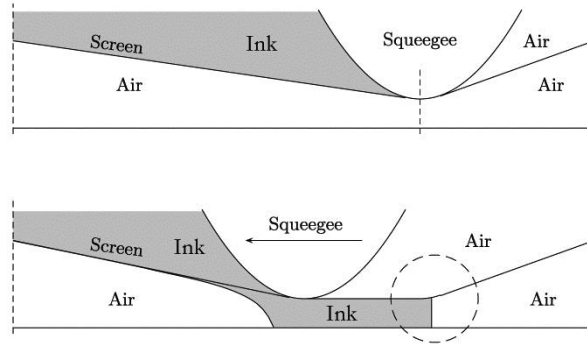


Figure 2.11: By moving the squeegee, the screen peels behind squeegee. Above image shows the position of squeegee at $t = 0$, and the below one shows it at $t > 0$. The dashed line circle in below image indicates where peeling dynamics is appeared. The arrow indicates printing direction. The width of squeegee tip is exaggerated [96].

While the squeegee is moving, the stretched screen returns to previous situation. The ink remains on substrate and is wetting it in the form of small globules. The globules come together to form a continuous layer [15], as represented in Figure 2.12.

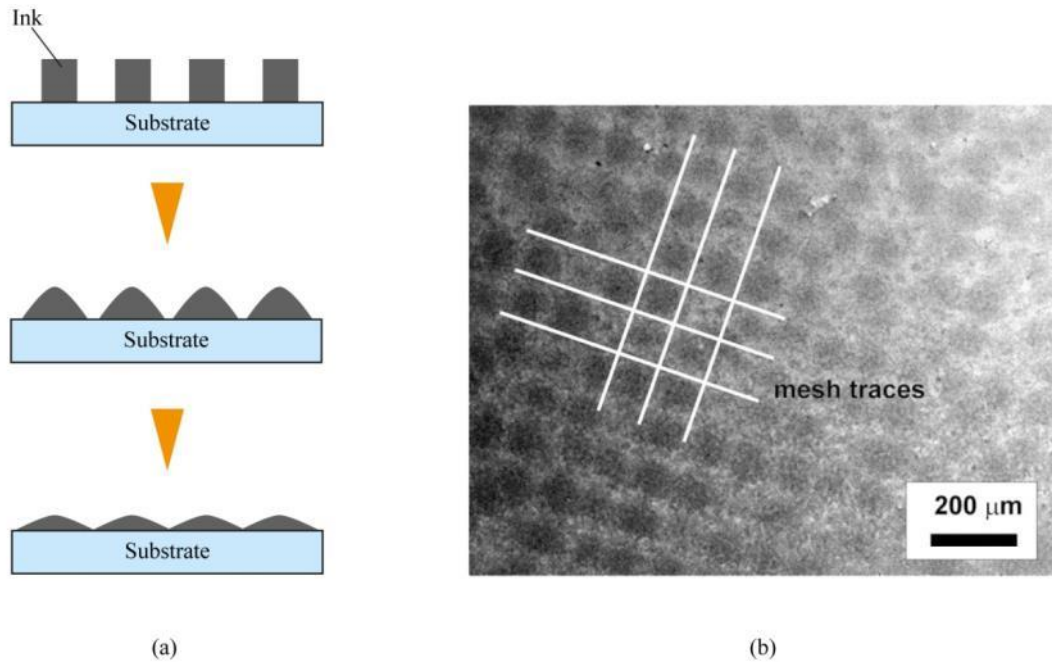


Figure 2.12: (a) Ink deposition and wetting the substrate, re-drawn from [74], and (b) Printed pattern including the remained effect of mesh traces. The effect of mesh traces is depicted by white lines [84].

For more details on screen printing process and parameters, please refer to Siebdruck-Handbuch [79].

2.2.2 Thick Film Screen Printing

The term thick film means the cured film is relatively thick in compare to conventional deposition techniques. The variety of film thickness is 76 to 127 μm [35] or maybe more. In thick film technology, the film layers are adding to substrate [47]. Paste or slurry, which is often called ink, is deposited through a screen [35] on substrate. For almost seventy years, screen printing has been a regular process for fabrication of thick film patterns for electronic applications [15]. Figure 2.13 shows the steps of conventional thick film process for fabrication of some electronic devices. Ink is deposited on substrate. Depends on the complexity of electronic component, the process of deposition may be repeated for several times. After drying and curing the ink, some additional processes will be done, such as trimming resistors for accurate adjustment, mounting, attachment, and protective encapsulation.

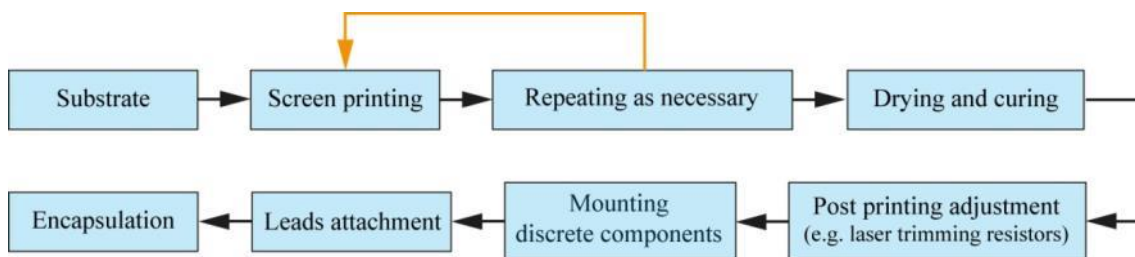


Figure 2.13: Conventional thick film process for fabrication of some electronic devices, re-drawn from [35].

Theoretical Model for Film Thickness in Screen Printing

The thickness of printed conductive inks is a critical feature. As an instance, in printed inductive antennas, the power efficiency depends on conductivity, while conductivity subordinates the thickness of printed ink. The relative thickness of wet film that deposited by screen printing can be calculated from [35]

$$T_w = D \left(2 - \frac{D\pi}{2ma} \right) \quad (2.3)$$

where T_w is relative thickness in mils (1 mil = 25.4 μm), D is diameter of screen wire in mils, m is 1000/ M in mils (M is number of meshes per inch), and a is equal to $\cos(\arctan DM/1000)$. Also

$$T_w = HA \quad (2.4)$$

where H is mesh thickness and A is decimal equivalent of openness percentage.

The thickness of wet film h_w can be calculated based on the mesh dimensions of the screen. Assume that only 70% of included ink in mesh volume is emptied during squeegee stroke, the thickness of wet film is calculated as

$$h_w = 1.3 h_s k_r \quad (2.5)$$

where h_s is thickness of screen (usually $2 \times d_w$), d_w is wire diameter of screen, k_r is relative openness of screen ($[(m - d_w)/m]^2$), m is screen wire pitch ($1/M$) and M is number of meshes per unit length. This equation can also be applied as $h_w = h_s k_r$ [74]. Figure 2.14 depicts the screen thickness, wire diameter of screen and the thickness of wet film on substrate after printing.

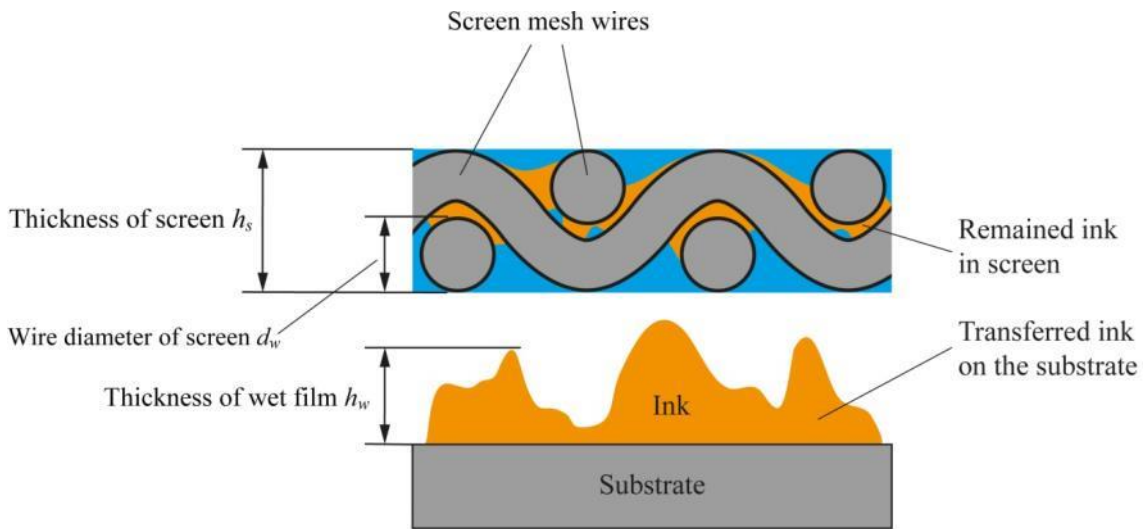


Figure 2.14: The thickness of wet film on substrate after printing. Thickness of screen h_s is usually twice the wire diameter of screen d_w .

2.3 Antennas

Every structure carrying radio frequency (RF) current generates an electromagnetic field around carrier structure and can radiate RF power through space. Such a structure is named antenna. An antenna can transmit or receive the RF power. A transmitter antenna transforms the RF energy into an electromagnetic field and a receiver antenna transforms the electromagnetic field into RF energy [76]. In the field of RF energy transfer, Hertz was the first person that has demonstrated the generation of radio waves at UHF in Germany in 1885–1886. In next ten years, Tesla in America, Marconi in Italy, Popov in Russia, and Bose in India represented wireless telegraphy. Tesla explained the “transmitting intelligence without wires” in London in 1892, and he transmitted the signals that were detected 80 km away in 1895 [101].

Antennas are key features of wireless communication systems [101]. There are different types and classes of antennas such as aperture antennas, reflector antennas, wire element antennas (including monopole, dipole, and loop structures), micro strip antennas [14], slot-type antennas [101], meander antennas, coil antennas [20], frequency-independent antennas, leaky-wave antennas, reconfigurable antennas, fractal antennas, wideband and traveling-wave antennas [14] as well as arrays of some of these [101].

The structure of RF carrier in every antenna can be different. As an example, the coil antennas include a simple straight conductor that is wound into a helix so that the conductor is contained in a short housing and can be flexible [20].

Printed Antennas

Printed antennas or patch antennas are kind of slot-type [101] or micro strip or planar antennas [28]. Micro strip patch antennas include metal patches that radiate the magnetic field from its margin edges [59]. In simplest form, a patch antenna consists of a metallized printed circuit board. By the application of PCB etching technology, this type of antennas can be produced in low cost and high level of reproducibility [28]. Figure 2.15 shows a patch antenna on PCB (type F4B) with operating frequency range of 10.29–11.66 GHz.

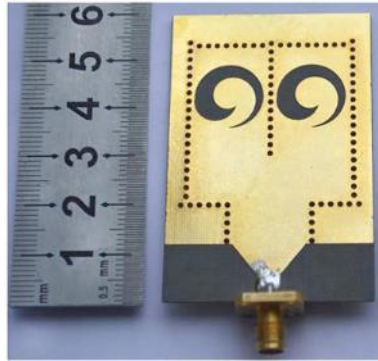


Figure 2.15: A patch antenna with operating frequency range of 10.29–11.66 GHz on PCB (type F4B) [56].

Patch antennas are using in some communication devices, e.g. latest generations of mobile telephones and RFID systems [28]. Printed antennas can be integrated within various types of substrate, e.g. dielectric substrates, paper, and textile [73] as represented in Figure 2.16.

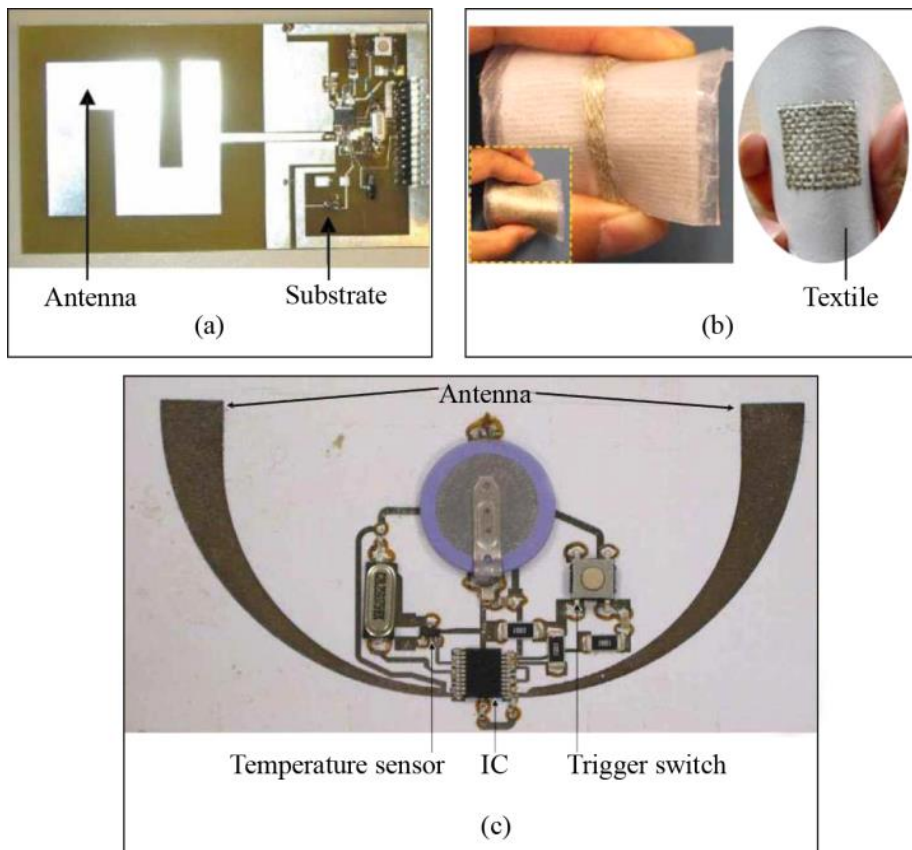


Figure 2.16: Printed antennas integrated within (a) Dielectric substrates, (b) Textile, and (c) Paper [73].

In addition of flat substrates, the printed antennas can be fabricated in three-dimensions. One solution is ink deposition on flat substrate and thermoforming the substrate to three-dimensional surface [107], as represented in Figure 2.17 (a). Direct ink deposition on three-dimensional substrate is possible, too [1] (see Figure 2.17 (b)).

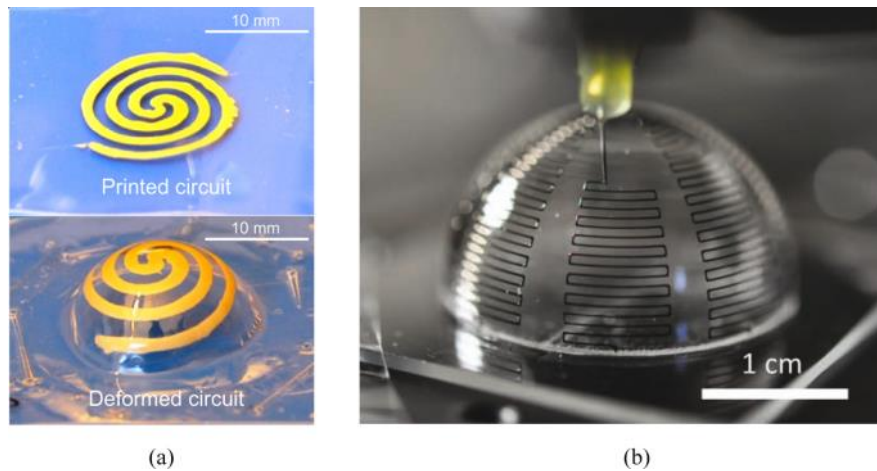


Figure 2.17: (a) Ink deposition on flat substrate and thermoforming the substrate to three-dimensional surface [107], and (b) Direct ink deposition on three-dimensional substrate [1].

One of the most conventional patterns in planar antennas is spiral patterns including Archimedean and equiangular ones. These shapes are represented in Figure 2.18.

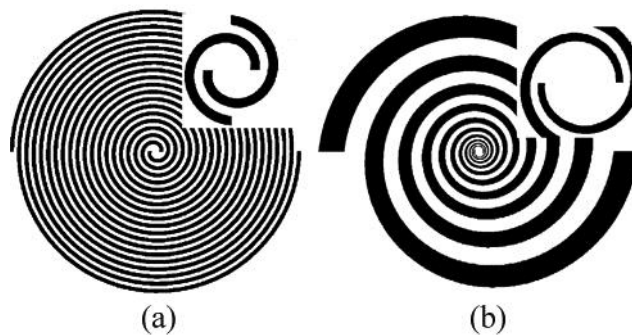


Figure 2.18: (a) Archimedean spiral, and (b) Equiangular spiral are conventional patterns in planar antennas [17].

In Archimedean spirals, the track width and the track spacing of the spiral are constant values, while in equiangular spirals, the track width and the track spacing are increasing as they are going far away from the center of spiral.

2.4 Electrical Principles in Wireless Powering Antennas

Conductivity, inductivity, and parasitic capacitance of printed antennas are features that strongly effect on efficiency of wireless powering. These electrical phenomena can be different in various conditions of material such as bulky state, thick film or ink. Present part includes an overview on these electrical principles, as well as the generalities of wireless powering.

2.4.1 Conductivity, Resistance and Impedance

Electrical conductivity σ explains the potential of material to transport charge or current. Based on definition of conductivity, resistivity ρ is defined as

$$-\tag{2.6}$$

Subsequently, the resistance R of a conductive part can be determined as

$$-\tag{2.7}$$

where L is length and A is cross sectional area of conductive part, respectively.

The DC conductivity σ can be calculated as [88]

$$-\tag{2.8}$$

where l is length, R is resistance, w is width, and d is thickness of conductor.

A solution on resistance measurement of a piece of material is application of Ohm's law. Two probes apply a direct current through the piece of material and the voltage drop is recorded. The resistance is calculated by Ohm's law as

$$(2.9)$$

where V is voltage and I is electric current [88].

The impedance Z is an important parameter for characterization of electronic circuits, electronic components, and the materials that used to make components. Impedance can

be defined as total opposition that offered by device or circuit to alternating current at a given frequency. Impedance as a complex quantity can be expressed with rectangular-coordinate form or polar form, respectively as

$$Z = R + jX = |Z|\angle\theta \quad (2.10)$$

where R is resistance, j is the imaginary quantity, X is reactance, $|Z|$ is magnitude, and θ is phase angle of impedance [9].

The resistive losses of the antenna can affect significantly on wireless powering performance [99]. The AC resistance of the antenna can be increased by skin effect [42] at higher frequencies e.g. more than 10 MHz [25]. The AC resistance at high frequency R can be determined based on the real part of impedance value, as [9]

$$R = |Z| \cos \theta \quad (2.11)$$

where $|Z|$ is magnitude of impedance, and θ is phase angle of impedance.

Thick Film Printed Conductors

Thick film conductors have the highest rank of material usage in thick film hybrid circuits. The major application of them is interconnection of circuit components. The functional phase of the ink is a key feature in characteristics of thick film conductors. Conductive inks include metal particles, e.g. silver, gold, platinum, palladium, aluminum, copper, nickel, chromium, tungsten or molybdenum. Distribution, dimension, and shape of particles effect on electrical and physical characteristics of thick film conductors. Silver ink is one of the first materials that developed for thick film conductors. However, there are some drawbacks on application of pure silver. For example, that is influenced by air, moisture, temperature and bias voltage [47].

Conductivity can be different for various conditions of the same material, such as thick film and bulky shape. Table 2.2 shows the measured conductivity of several materials in various conditions, including etched bulk copper, electro less deposited copper, bulk silver, and two types of conventional silver inks. The measurement is based on DC resistance, length, and cross sectional area [93]. As represented, the conductivity of bulk copper is relatively higher than electro less deposited copper, and the conductivity of bulk silver is several times higher than silver ink.

Table 2.2: Measured conductivity σ of several materials in various conditions. The measurement is based on DC resistance, length, and cross sectional area. Silver ink A and B are two types of conventional silver inks [93]. The conductivity of bulk copper is relatively higher than electro less deposited copper, and the conductivity of bulk silver is several times higher than silver ink.

Material	Conductivity σ [1/Ω·m] x 10 ⁶
Bulk copper	58
Electro less deposited copper	50
Bulk silver	61.8
Silver ink A	5.1
Silver ink B	4.2

The resistance of conductive film can be calculated as [47]

$$R = \frac{\rho l}{wt} \quad (2.12)$$

where ρ is bulk resistivity, and l , w , and t are length, width and thickness of conductive film after curing, as depicted in Figure 2.19.

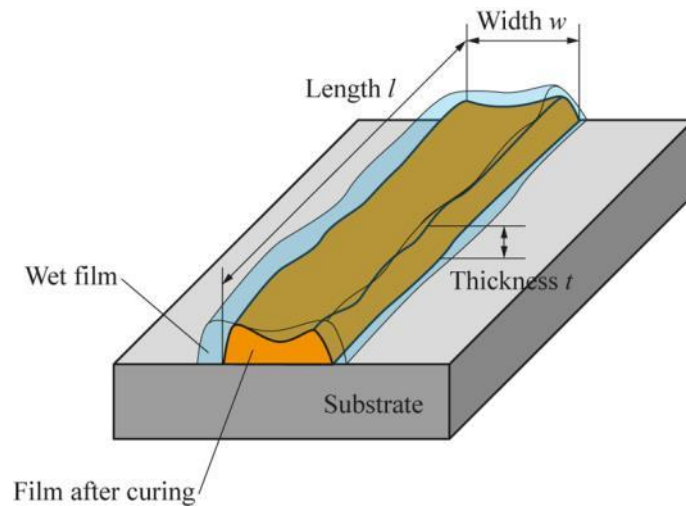


Figure 2.19: Length l , width w and thickness t of printed film, before and after curing. For calculation of resistivity R , the dimensional values of the cured ink will be taken into account.

A typical term for determination of thick film resistivity is sheet resistivity. That is explained in ohms per square [Ω/\square]. The sheet resistivity is equal to bulk resistivity at the specified thickness (ρ/t). The thick film resistivity can be calculated by multiplying the value of sheet resistivity by film aspect ratio (l/w).

Skin Effect and Proximity Effect Losses at High Frequency

Skin effect and proximity effect can cause power losses in conductive structures. The AC magnetic field inside of conductor causes skin effect. This magnetic field concentrates current charges of conductor to surface [99]. Figure 2.20 demonstrates flux lines and current density through a bulky and a thin conductor.

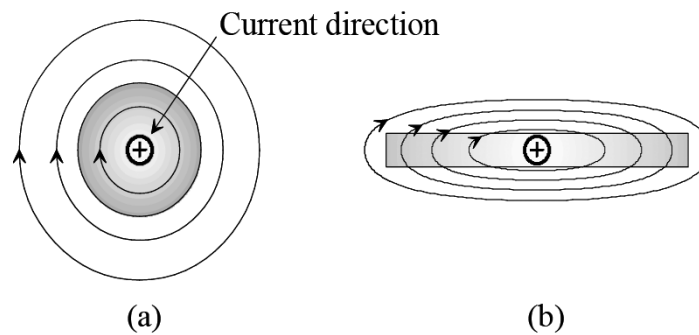


Figure 2.20: Flux lines and current distribution in a bulky conductor (a) and a thin conductor (b). The current density is represented by shading [99].

A significant parameter in skin effect is skin depth. Skin depth δ is a distance beneath conductor surface. At that distance, the current decreased to $1/e$ of its value at the surface, where e is Euler's number. Skin depth is calculated by

$$\delta = \frac{1}{\sqrt{\pi\sigma\mu f}} \quad (2.13)$$

where σ is conductivity, μ is permeability, and f is frequency [99]. Table 2.3 contains the calculated skin depths of some bulky and deposited materials including etched bulk copper, electro less deposited copper, bulk silver, and two types of conventional silver inks. The measured conductivity of them mentioned earlier in Table 2.2 [93]. Obviously, the rate of skin depth is different for bulky and deposited materials.

Table 2.3: Measured conductivity σ and calculated skin depth δ of several materials in various conditions. Silver ink A and B are two types of conventional silver inks [93]. The rate of skin depth is different for bulky and deposited materials. The rate of skin depth is in inverse relation with the conductivity of various samples, according to Equation (2.13).

Material	Conductivity σ [$1/\Omega \cdot m$] $\times 10^6$	Skin depth δ [μm] at 915 MHz
Bulk copper	58	2.18
Electro less deposited copper	50	2.35
Bulk silver	61.8	2.1
Silver ink A	5.1	7.31
Silver ink B	4.2	8.11

Figure 2.21 presents the influence of skin effect on a single turn coil antenna. The plot includes AC resistance and frequency for different conductor widths [25]. As represented, by increasing of frequency, the AC resistance increasing significantly. Although the increasing of conductor width caused to reduce the AC resistance, but the slope of the curves are almost similar.

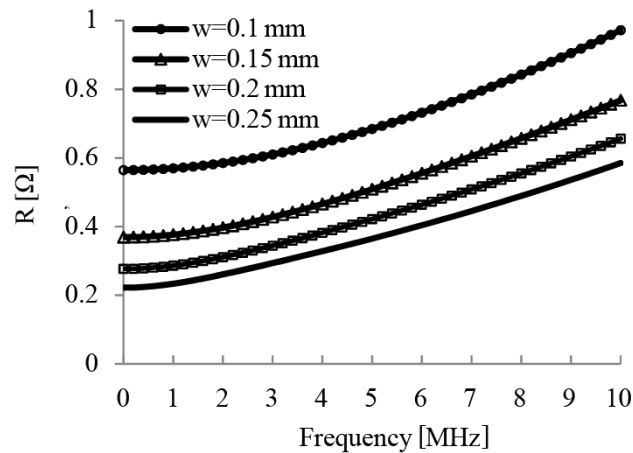


Figure 2.21: AC resistance R and frequency of a single turn coil with conductor width w 0.1 mm, 0.15 mm, 0.2 mm and 0.25 mm [25]. By increasing of frequency, the AC resistance is increasing significantly. The increasing of conductor width w caused to reduce the AC resistance.

In addition of skin effect, the proximity effect can cause power losses in conductive tracks. The current through the conductor generates a magnetic field that may redistribute the current of adjacent conductors. The name of this phenomenon is proximity effect. Proximity effect adds to skin effect and enhance the resistance of conductor [99]. By increasing frequency, the proximity effect is increasing at the edges of conductor [68], as well as Joule heating near the surface of conductor [35].

2.4.2 Dielectric Properties and Parasitic Capacitance

Although the dielectric substrate loss is not the most effective parameter on power dissipation in conductive structures with conventional substrate thicknesses [77] but in some cases is not negligible. In this part, the focus is mostly on dielectric properties and parasitic capacitance that appears between printed conductive lines.

Dielectric characteristics of materials explain some of the electrical features of them such as energy transfer, energy storage, and losses. Energy loss depends on scattering, radiation, or conversion of electrical energy to thermal energy or Joule heating. Practically, in dielectric materials, the processes that result in power loss are more relevant [88]. The capacitance C can be determined as

$$C = \frac{\epsilon_0 A_o}{d} \epsilon_r \quad (2.14)$$

where ϵ_0 is dielectric constant in vacuum, A_o is effective plate capacitor area, d is distance between metal plates, and ϵ_r is dielectric material constant. Reduction of dielectric material constant of isolator can affect directly on parasitic capacitance [22].

Parasitic capacitance appears between conductive traces, as represented in Figure 2.22. C_s is parasitic capacitance through the air or coating layer, and C_{sub} is parasitic capacitance through the substrate [42].

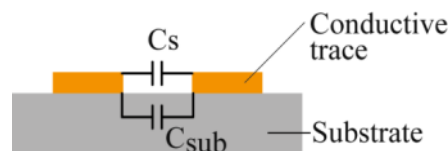


Figure 2.22: Parasitic capacitance between conductive traces via air or coating layer C_s , and via the substrate C_{sub} , re-drawn from [42].

The parasitic elements of a spiral inductor are depicted in Figure 2.23 (a, b); where L_s is desired inductance, R_s is resistance of spiral traces, C_s is parasitic capacitance between spiral traces and underpass, C_{ox} is oxide capacitance, R_{sub} is resistance of substrate, and C_{sub} is capacitance of substrate. C_{ox} , R_{sub} and C_{sub} are coupled into lossy substrate [22]. Also the equivalent parasitic elements of a screen printed spiral antenna with silver ink are depicted in the Figure 2.23 (c).

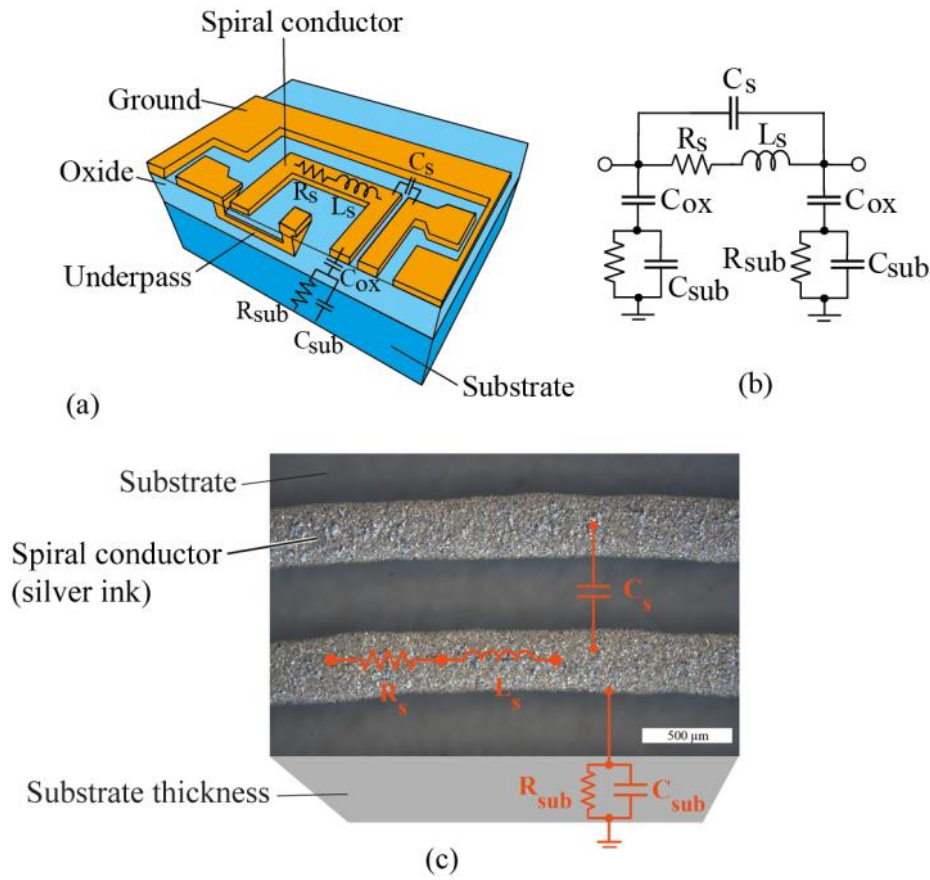


Figure 2.23: A spiral inductor including parasitic elements. L_s is desired inductance, R_s is traces resistance, C_s is parasitic capacitance, C_{ox} is oxide capacitance, R_{sub} is resistance of substrate, and C_{sub} is capacitance of substrate. (a) Cross section of spiral inductor, (b) Equivalent circuit of spiral inductor [22], and (c) Equivalent parasitic elements on a screen printed spiral antenna with silver ink.

Parasitic capacitance C can be calculated as

$$C = \frac{1}{\omega_0^2 L} \quad (2.15)$$

where ω_0 is frequency of resonance, and L is low frequency inductance of the coil [25].

2.4.3 Inductivity

Inductivity phenomenon is a key feature of inductive wireless powering. This part of text contains a general view on electromagnetic fields, self-inductance, mutual inductance, and coupling coefficient of inductive antennas that will be the fundamental of the next chapters.

Electromagnetic Fields and Frequency of Resonance

Electric currents generate magnetic field around conductor. The low frequency magnetic fields can cause direct and indirect effects. For example, deflection of electron beam according to force is a direct effect, while induction of current in a conductor is an indirect effect [31].

Magnetic field strength H is the magnitude of magnetic field, regardless of material properties of the space. Figure 2.24 depicts the magnetic flux lines encircling a straight conductor and a coil.

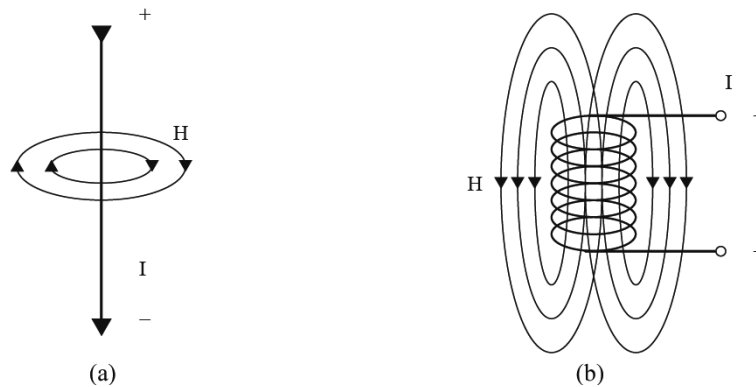


Figure 2.24: (a) Magnetic flux lines encircling a straight conductor, and (b) A cylindrical coil. I is current, and H is magnetic field strength [28].

Magnetic flux Φ indicates the total number of magnetic lines that are passing through a defined object. Magnetic flux density B , also named magnetic inductance, is determined as subsequent equation, based on area A

$$B = \frac{\Phi}{A} \quad (2.16)$$

Figure 2.25 delineates the relation between magnetic flux density and magnetic flux.

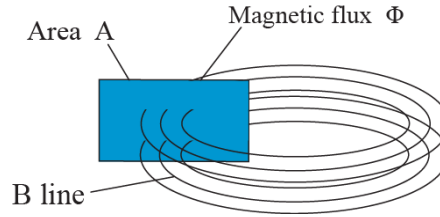


Figure 2.25: The relation between magnetic flux density B and magnetic flux Φ [28]

The relation between magnetic flux density and magnetic field strength is determined as

$$B = \mu_0 \mu_r = \mu H \quad (2.17)$$

where μ_0 is the magnetic field constant ($\mu_0 = 4\pi \times 10^{-6} \text{ V}\cdot\text{s}/\text{A}\cdot\text{m}$) and explains the permeability or magnetic conductivity of a vacuum. μ_r is relative permeability of material in compare to μ_0 , and μ is permeability.

A magnetic field, and in consequence, a magnetic flux can be generated surrounding every conductor. For the shapes such as loop or coil, the effect is increasing. The total magnetic flux ψ of multiple loops is determined as

$$\psi = \sum_N \Phi_N = N\Phi = N\mu HA \quad (2.18)$$

where N is number of loops, and A is the loop area [28]. Figure 2.26 (a) represents the magnetic flux surrounding a one-turn loop conductor that is generated by current I [28], and Figure 2.26 (b) depicts the magnetic flux density B and the magnetic field strength H between two antennas by application of computational software [98].

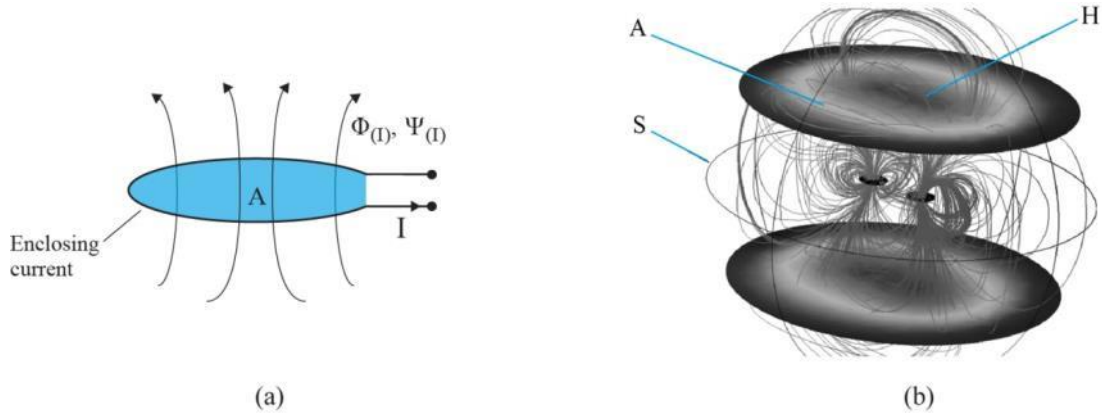


Figure 2.26: (a) The magnetic flux surrounding a one-turn loop conductor. A is the loop area, I is current, Φ is magnetic flux, and ψ is total magnetic flux [28]. (b) Magnetic flux density and magnetic field strength between two antennas by application of a computational software. S is the computational boundary sphere with radius 80 cm. The lines B passing through and around the antennas are magnetic flux density. The ovals H on top and bottom are magnetic field strength. The shadows from light to dark show the magnetic field strength emitted by the antennas [98].

Inductance L in a conductor loop can be defined as subsequent equation, based on the interlinked flux ψ

$$L = \frac{\psi}{I} = \frac{N\Phi}{I} = \frac{N\mu HA}{I} \quad (2.19)$$

The inductance of a conductor loop or coil depends on geometry of the layout and permeability. Permeability includes material properties of surrounding space of the coil [28]. If diameter of the wire is very smaller than diameter of conductor coil, the inductance can be calculated as

$$L = N^2 \mu_0 R \ln\left(\frac{2R}{d}\right) \quad (2.20)$$

where R is the radius of the conductor loop, d is diameter of the wire and $d/D < 0.0001$ where D is diameter of conductor coil [28].

In practical cases, parasitic capacitance cause the coils to resonate [99]. The self-resonant frequency f_0 can be calculated as [35]

$$f_0 = \frac{1}{\sqrt{2\pi(LC_d)}} \quad (2.21)$$

where C_d is the inter-winding capacitance. Dimensions of the coil and constructive wire should be much smaller than operating wavelength λ [53], where λ is equal to speed of light c divided by frequency f [28].

Self-inductance, Mutual Inductance and Coupling Coefficient

The inductance of a coil is proportional to magnetic flux density. By increasing the magnetic flux, the overall inductance value will be increased [42]. The self-inductance L_1 of a closed circuit is determined as

$$L_1 = \frac{\Phi_1}{I_1} \quad (2.22)$$

where Φ_1 is magnetic flux, and I_1 is electric current that producing this flux [53].

Mutual inductance describes the coupling of two circuits via a magnetic field. The dimension and unit of mutual inductance are like the same as inductance [28]. The mutual inductance M_{12} is determined as

$$M_{12} = \frac{\Phi_2}{I_1} \quad (2.23)$$

where Φ_2 is magnetic flux enclosed by a secondary circuit to the current I_1 in a primary circuit that producing the flux. It can be proved that $M_{21} = M_{12} = M$ [53].

Considering the fact that inductive coupling describes signal transmission from one system to another through magnetic field [31], so, coupling coefficient can be a critical factor in inductive wireless powering systems. The coupling coefficient k [28] or coil coupling factor dominates the power transfer efficiency [99]. It is an important feature that can enable WPT systems to achieve high efficiency near 90% or more [50]. As an example, Figure 2.27 shows the relation between coupling coefficient and calculated efficiency for an antenna. By decreasing of coupling coefficient, the efficiency is decreasing rapidly.

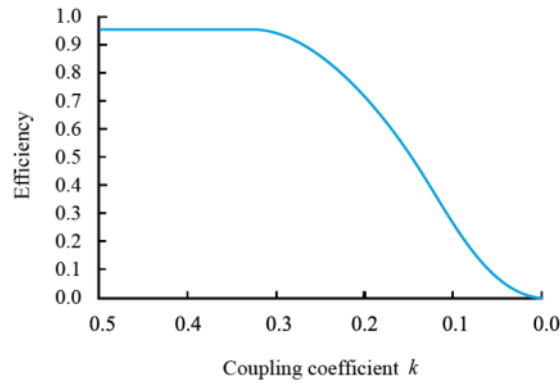


Figure 2.27: The relation between coupling coefficient and calculated efficiency for an antenna, re-drawn from [50]. By decreasing of coupling coefficient from 0.3 to 0.0, the efficiency is decreasing rapidly.

The coupling coefficient can make a qualitative prediction on coupling of conductor loops. This qualitative prediction is independent of geometric dimensions of the conductor loops [28]. The coupling coefficient k is described as [28], [23]

$$k = \frac{M}{\sqrt{L_1 L_2}} \quad (2.24)$$

where M is mutual inductance, and L_1 and L_2 are self-inductance of transmitter and receiver antennas.

Coupling coefficient is varying between the two extreme values $0 \leq k \leq 1$. The condition of $k = 0$ means full decoupling between antennas. Full decoupling is caused by large distance between transmitter and receiver antennas. Also, magnetic shielding can cause full decoupling. The condition of $k = 1$ or total coupling means that both antennas are subject to the same magnetic flux [28].

The distance between transmitter and receiver antennas can significantly effect on coupling factor. Figure 2.28 shows coupling factor versus antenna distance for different samples. By increasing the antennas distance, coupling factor decreasing significantly.

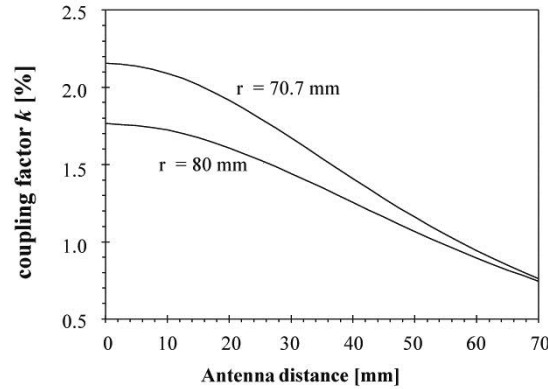


Figure 2.28: Coupling factor versus antennas distance for two different transmitter coil antennas with 70.7 mm and 80 mm radius. The radius of receiver antennas is 10 mm [99]. By increasing the antennas distance, coupling factor decreasing significantly.

Quality Factor

The quality factor Q can be calculated as [102]

$$Q = \frac{2\pi f_{res}L}{R_L} \quad (2.25)$$

where f_{res} is resonant frequency, and L is inductance. R_L can be determined as parasitic resistance of the inductor [102], or series resistance of inductor [35], or frequency dependent resistance that extracted from measured impedance [25].

Figure-of-merit

Although the quality factor can demonstrate characteristics of efficiency of WPT systems, but figure-of-merit is a sufficient factor for comparison of different printing layouts and optimization of design. Generally, the highest possible inductance and quality factor at the targeted frequency [42], [94] is an aim of antenna design. To give a fair evaluation of overall performance of inductors with different sizes, a figure-of-merit of inductor (FOM) is often used, as defined by Tai et al. [94] and Islam et al. [42]

$$FOM = \frac{LQ_{max}}{A} \quad (2.26)$$

where Q_{max} is peak quality factor and unit less, L is inductance at low frequency in nH, and A is the overall area of inductor in mm^2 .

Thick Film Printed Inductors

An ideal inductor is a magnetic field energy storage device that owns linear voltage-current derivative [102]. Generally, the role of inductor is opposing the current change through it. For opposing the current change in inductor, a voltage drop should be generated against current change. If the current is at a maximum, the voltage will be zero, as represented in Figure 2.29 for a sinusoidal waveform [100].

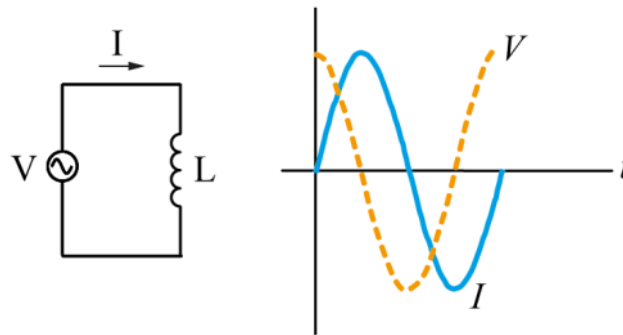


Figure 2.29: Voltage V and current I waves of an inductor versus time t . The continuous and dashed sine waves demonstrate voltage and current, respectively. If the current is at a maximum, the voltage will be zero for a sinusoidal waveform [100].

Typically, the term thick film inductor refers to inductors that mainly fabricated by a printed conductor coil [35]. Spiral planar inductors include metallic layers that deposited on printed circuit boards, ceramic substrates or silicon integrated circuits [68]. The conductive layer of thick film inductors can contain gold with or without magnetic material. Gold is preferred to silver or copper for fine-line definition. Metal electro migration in silver and special curing conditions for copper can cause problem with thick film inductors [35].

Thick film inductors and related magnetically coupled devices are expected to behave in a non-ideal manner. As mentioned by Wager et al. [102], two main reasons underlie the non-ideal behavior of a transparent thin film inductors. Those could be generalizable across thick film inductors, too. First, the conductivity of these materials compared to metals is relatively poor. Therefore, transparent thin film inductors will possess a

significant amount of parasitic resistance. Second, efficient magnetic field coupling is strongly facilitated by the use of a magnetically permeable insulator. Thus, realizing high performance for such a devices is expected to be a challenging task.

Inductance L in a rectangular spiral inductor is determined as

$$L \propto SN^2 \quad (2.27)$$

where S is maximum side dimension in cm, and N is number of turns. The Equation (2.27) shows that to earn a large inductance, the inductor should cover a large area and has a large number of turns. The large area is not always problematic but the large number of turns can cause problem. Large number of turns will increase parasitic resistance and perhaps parasitic capacitance of the inductor [102]. Table 2.4 includes the typical values of deposited thick film inductors [35] including DC resistivity, skin depth at 100 MHz, inductance, number of turns, and quality factor at 100 MHz for thick film deposited silver, copper, gold, and aluminum.

Table 2.4: Typical values of deposited thick film inductors [35]. The DC resistivity, skin depth at 100 MHz, inductance, number of turns, and quality factor at 100 MHz for thick film deposited silver, copper, gold, and aluminum.

Material	DC resistivity ρ [$\mu \Omega \cdot \text{cm}$]	Skin depth δ at 100 MHz [μm]	Inductance L [nH]	Number of turns N	Quality factor Q at 100 MHz
Silver	1.59	6.40	20	1(3/4)	60
Copper	1.67	6.60	28	2(3/4)	45
Gold	2.35	7.86	44	3(3/4)	42
Aluminum	2.65	8.14	64	4(3/4)	36

2.4.4 Resistance, Capacitance and Inductance Model (RLC Model)

Every component in circuit exhibits three characteristic properties: resistance, capacitance and inductance [15]. In a practical point of view, coils are not ideal because of parasitic coil losses and parasitic resonances [99]. The equivalent model of a coil can

be represented by a lumped resistor, inductor and capacitor (RLC) model [66]. Measurements indicated that the lumped coil model, for frequencies below and around the first resonance frequency, can be accurately represented by three separate equivalent elements: an ideal coil L_s , a series loss resistor R_s , and a parallel parasitic capacitor C_s [99]. Figure 2.30 shows equivalent RLC model of a coil.

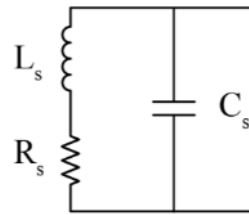


Figure 2.30: Equivalent RLC model of a coil. C_s is parallel parasitic capacitor, L_s is ideal coil, and R_s is series loss resistor [99].

2.4.5 Wireless Power Transmission

All wireless links have a device at transmitter side that converts electric signals to acoustic waves, light, magnetic or electric fields; for example, ultrasound speaker, LED or antenna. The reverse process is happening at receiver side [99]. Figure 2.31 shows the concept of electromagnetic WPT system, where two antennas are using at transmitter side and receiver side for transferring electromagnetic fields.

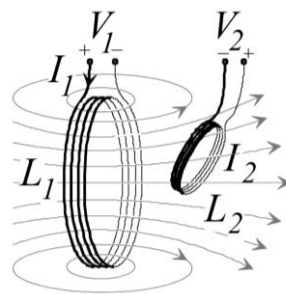


Figure 2.31: The concept of electromagnetic wireless links, where V is voltage, I is current, and L is inductance. The 1 and 2 subscripts refer to transmitter and receiver antennas, respectively [99].

The transmitter antenna is driving by voltage V_1 . The current I_1 generates a magnetic flux Φ through the receiver antenna. If this flux is changed by changing the I_1 current,

an induced electromotive force appears in the receiver antenna, in order to the voltage V_2 across the coil terminals with the number of windings N_2 becomes as [99]

$$V_2(t) = N_2 \frac{d\Phi(t)}{dt} \quad (2.28)$$

This system can be represented as a simplified equivalent lumped circuit model as depicted in Figure 2.32. The left side is transmitter and the right side is receiver. The system includes two resonant circuits that are linked magnetically. At the left loop, transmitter is excited by a source, where V_1 is source voltage, R_1 is source impedance, C_1 is a capacitor to make resonance at desired frequency, and L_1 is an inductor. On the receiver side, L_2 is load inductor, C_2 is load capacitor, R_2 is load impedance, and V_2 is load voltage. The Inductors L_1 and L_2 are connected with mutual inductance M [43].

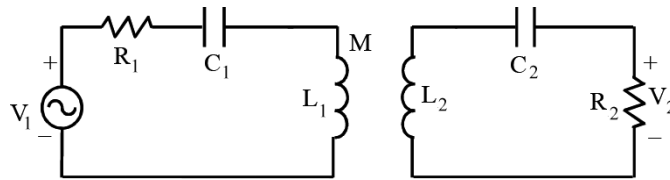


Figure 2.32: Equivalent circuit model of an inductive wireless powering system. V_1 is source voltage, R_1 is source impedance, C_1 is resonance capacitor, L_1 is inductor, L_2 is load inductor, C_2 is load capacitor, R_2 is load impedance, V_2 is load voltage, and M is mutual inductance [43].

A complete WPT system includes an inverter at transmitter side. The inverter is converting DC power to AC for driving the antenna [53]. Selection of driver topology is the first step in circuit design of transmitter. A saturating class C or class D amplifier is more appropriate for a moderate and variable coupling, while a class E amplifier is better for weak or constant coupling [99]. On the receiver side, a resonance capacitor cancels the inductive impedance of receiver antenna. A rectifier converts the received AC power to DC. In addition, a voltage regulator prepares an appropriate and fixed voltage for system [53]. The block schematic of a complete WPT system would be like Figure 2.33.

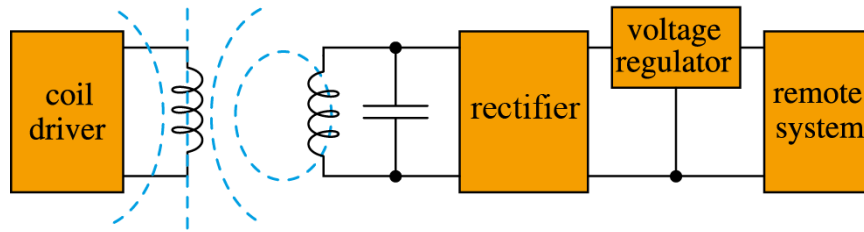


Figure 2.33: Block schematic of a complete WPT system. The coil driver is generating power at the left side. On the right side, the inductive impedance of receiver antenna is cancelling by a resonance capacitor. The received AC power is converting to DC by a rectifier. The appropriate and fixed voltage for remote system is preparing by voltage regulator [53].

Power Efficiency in Wireless Power Transmission Systems

In WPT systems, separation between transmitter and receiver windings is an important factor that effects on magnetic flux coupling. Smaller separation of printed windings cause to reach higher magnetic flux coupling [95]. Figure 2.34 shows the effect of antenna distance on power transmission efficiency, as well as coupling factor. By increasing the distance, the transmission efficiency and coupling factor are decreasing steadily.

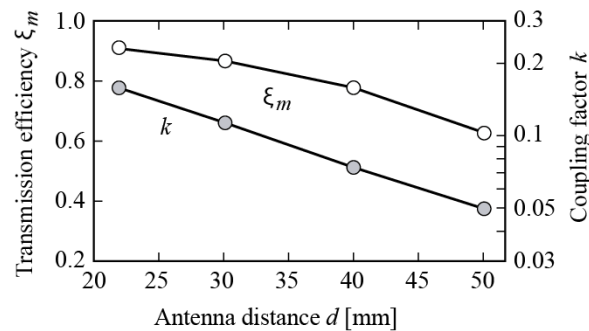


Figure 2.34: The relation between coupling factor k and power transmission efficiency ξ_m with antenna distance d [89]. By increasing the distance, the transmission efficiency and coupling factor are decreasing steadily.

Geometrical dimensions and relative position of each winding are two important features of coupling [27]. The alignment of transmitter and receiver antennas is an important factor in WPT systems. The lateral and angular misalignments can change coupling rate, output voltage, output power, and transmission efficiency. Figure 2.35

demonstrates the schematics of lateral misalignment and angular misalignment of two spiral circular antenna.

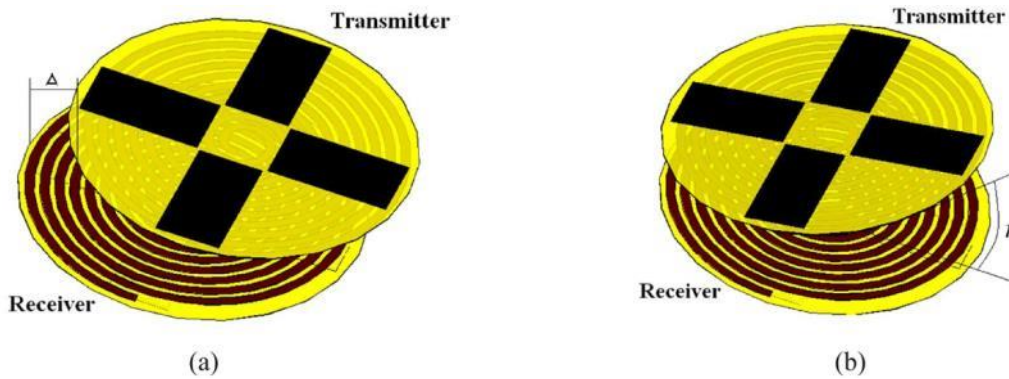


Figure 2.35: Schematics of transmitter and the receiver spiral circular antennas; (a) Lateral misalignment Δ [mm], and (b) Angular misalignment γ [°] [103].

Figure 2.36 shows the relation between receiver output voltages and frequency for lateral misalignment and angular misalignment in a simulation. By increasing the value of lateral and angular misalignments, the rate of output voltage in receiver antenna decreases.

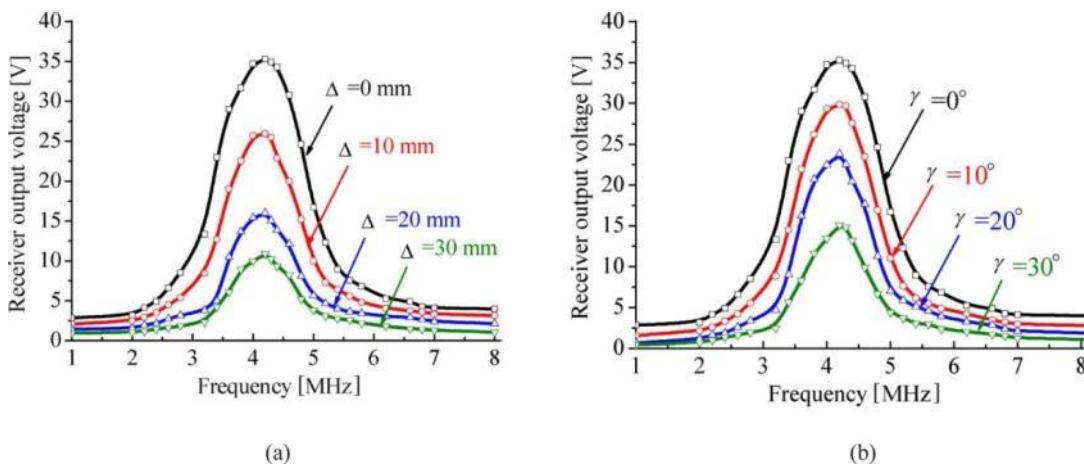


Figure 2.36: Relation between receiver output voltages and frequency in a simulation at the distance of 5 cm; (a) Lateral misalignment Δ [mm], and (b) Angular misalignment γ [°] [103].

Frequency of operation is other important factor in power transfer efficiency. Figure 2.37 represents the effect of frequency on efficiency and gained voltage in different cases. Figure 2.37 (a) shows that by increasing the frequency, the efficiency is

increasing. In addition, Figure 2.37 (b) represents that by increasing the frequency from 45 kHz to near 54 kHz, the voltage of receiver antenna is increasing. Higher frequency values cause to reduce the voltage.

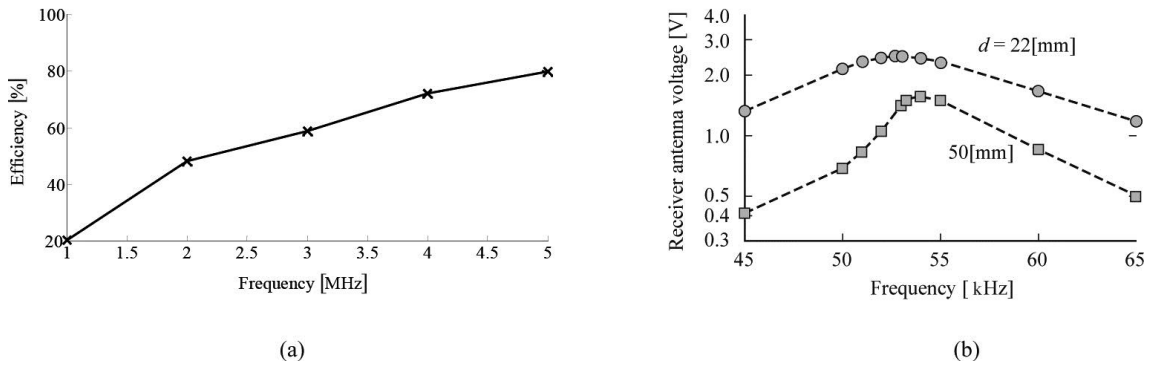


Figure 2.37: (a) The effect of frequency on power transfer efficiency. The transmitter is a 2-layer coil antenna with turn number 17 and measured quality factor 18.5 at 1 MHz. The receiver is a 2-layer coil antenna with turn number 8 and measured quality factor 10.2 at 1 MHz. The distance between antennas is 5 mm and $R_L = 270 \Omega$ [11]. (b) The effect of frequency on the voltage of receiver antenna. The frequencies are around resonant frequency. The antenna distance d is set to 22 mm and 50 mm [89].

2.5 Measurement and Characterization of Printed Antennas

Impedance measurement can give reliable data in a wide range of frequency. Figure 2.38 shows the magnitude and phase angle of impedance vs. frequency for a sample coil. The first peak point of impedance is coinciding with the phase change at resonance frequency.

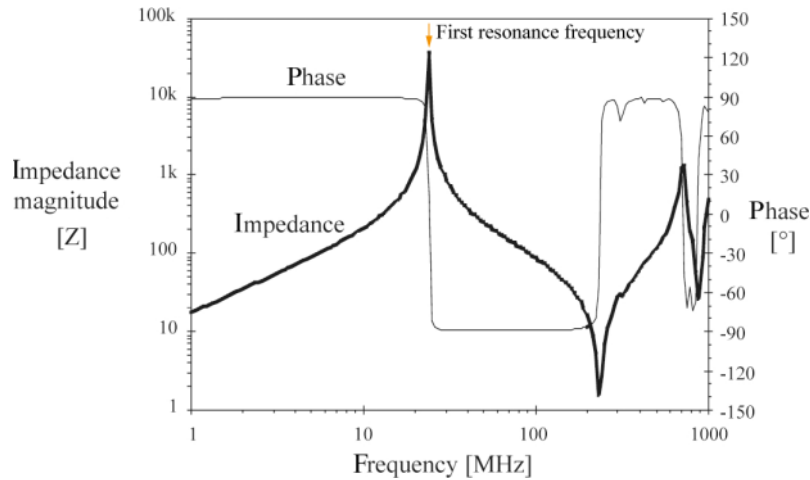


Figure 2.38: Magnitude and phase angle of impedance for an air-cored coil with 25 windings of enamelled copper wire 0.7 mm, with a diameter of 11 mm and a length of 22 mm [99]. The first peak point of impedance is coinciding with the phase change at resonance frequency.

Conventional methods of passive intermodulation characterization of microwave laminates are based on two-port measurements of the transmitted and reflected waves. Transmitted wave is forward propagating signal at the device output, and reflected wave is reverse propagating signal at the device input [85]. A microwave network analyzer is an instrument for measurements of the incident, reflected, and transmitted electromagnetic waves. Reflection and transmission characteristics of a material under test (MUT) can be calculated based on amplitude and phase of reflected and transmitted waves of network analyzer. The reflection and transmission parameters can be expressed as vector (magnitude and phase), scalar (magnitude only), or phase-only quantities. In a network analyzer, the reflected wave is measured at port 1, and the transmitted wave is measured at port 2 [88], as represented in Figure 2.39.

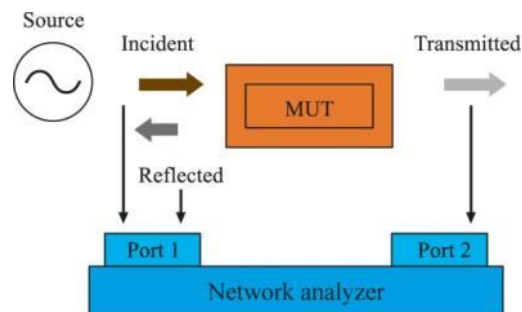


Figure 2.39: Block diagram of a network analyzer, including the incident, reflected, and transmitted waves for characterization of a material under test (MUT). The reflected wave is measured at port 1, and the transmitted wave is measured at port 2 [88].

A Network analyzer can have two types of test ports, as represented in Figure 2.40 (b):

- Scattering parameter (S-parameter) test port
- Gain-phase test port

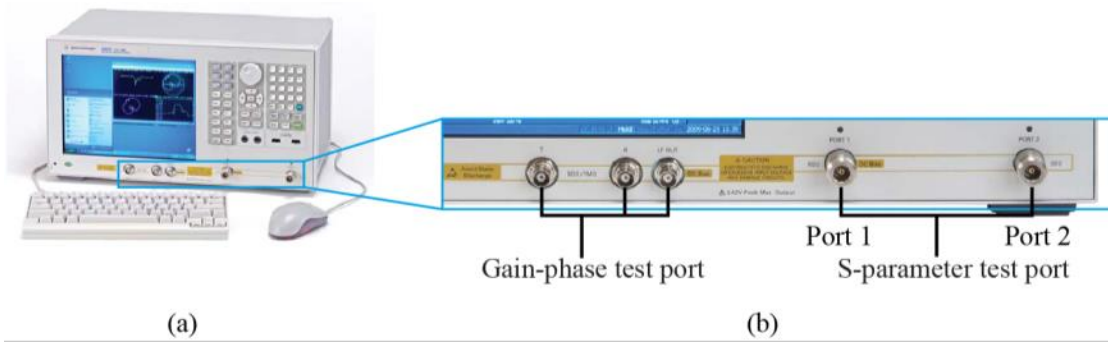


Figure 2.40: (a) Network analyzer Agilent E5061B, and (b) S-parameter test port and Gain-phase test port on network analyzer [7].

In the instrument that represented in Figure 2.40 (Agilent E5061B), the S-parameter test port covers the range of 5 Hz to 3 GHz with input impedance of 50Ω . This port can be useful for measurement of RF devices (filters, amplifiers, antennas, etc.), low frequency devices, and broadband devices. On the other side, the gain-phase test port covers the range of 5 Hz to 30 MHz with input impedance of $1 M\Omega$ or 50Ω . This port can be useful for measurement of low-frequency applications that need direct source and receiver access and high-impedance probing [7].

3 Geometrical Design and Optimization of Printed Antennas

This chapter aims to explain the process of design optimization for printed spiral coil antennas. The first part summarizes recent research on geometrical parameters of spiral antennas. The second part represents a software workflow concept for printed antennas.

Delimitations on Frequency of Operation

The printed spiral coil antenna for WPT is a type of inductors. Considering the fact that the optimal operating frequency of inductors is strongly affected by geometry [66], taking decision on a fixed operating frequency for this research is not easy. Therefore, the characterization of printed antennas is taking place in the frequency range of 100 Hz to 40 MHz. Considering the application of present printed antennas for consumer goods and products, eligible targeted frequency of operation is 13.56 MHz. This range of frequency belongs to the license-free industrial, scientific, and medical (ISM) band [42] and includes electronic article surveillance (EAS) applications in shops [28].

3.1 Geometrical Design of Printed Antennas

Antenna is an important variable in characterization of WPT design [99]. Although similar coupling can be achieved with different designs [27] but there are some variables that limit the design, e.g. dimensions of instrument that includes antenna. The importance of geometric design is mostly on inductive characteristics of antennas which includes the self-inductance, mutual inductance and leakage inductance [95]. Although the number of available references on printed antennas is not so high, but there are several studies on other types of flatten spiral coils and antennas that the result of them can be generalized for printed antennas. Several recent studies emphasized on some specific parameters that should take in account for geometrical design of antennas:

- Shape [45], [103]
- Outer diameter [23], [25], [38], [45], [62], [66], [95], [103]
- Inner diameter [23], [45], [62], [66], [103], [106]
- Track width [23], [38], [42], [45], [62], [66], [103], [106]
- Track spacing [23], [38], [42], [45], [62], [66], [103], [106]
- Track thickness [45], [66], [103]
- Number of turns [23], [25], [27], [35], [38], [42], [45], [62], [95], [103], [106]

Figure 3.1 represents the mentioned parameters on a circular spiral antenna.

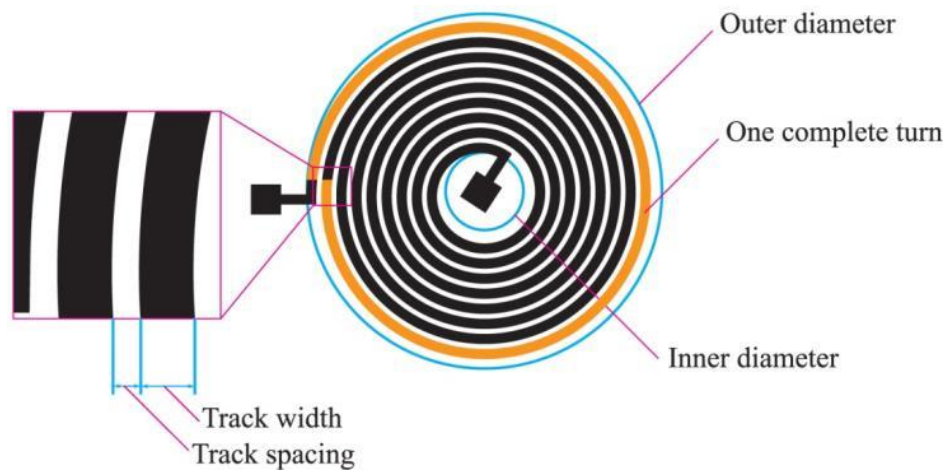


Figure 3.1: The outer diameter, inner diameter, track width, track spacing, and a complete turn in a circular shape spiral antenna.

In addition, there are other parameters that are rarely mentioned in references, e.g. number of segments [23]. Tang et al. [95] believe that there is no effect for track width and track thickness, while the inner diameter and track spacing just can effect on functionality of the antenna. As reported by Sidén et al. [87], some investigations show that mainly, the total amount of deposited ink determines the printed antennas' radiation efficiency and not how it is distributed throughout the structures.

3.1.1 Shape

Generally, spiral configuration is optimum for reducing resistance and improving coupling in the windings [26] and circular spirals provide the greatest inductance [95]. Although circular spirals provide higher inductance but square spirals are more

conventional because of the ease of their layout. Additionally, some designers prefer polygons with more than four sides e.g. hexagonal and octagonal ones to improve performance [62]. Figure 3.2 represents different conventional shape types.

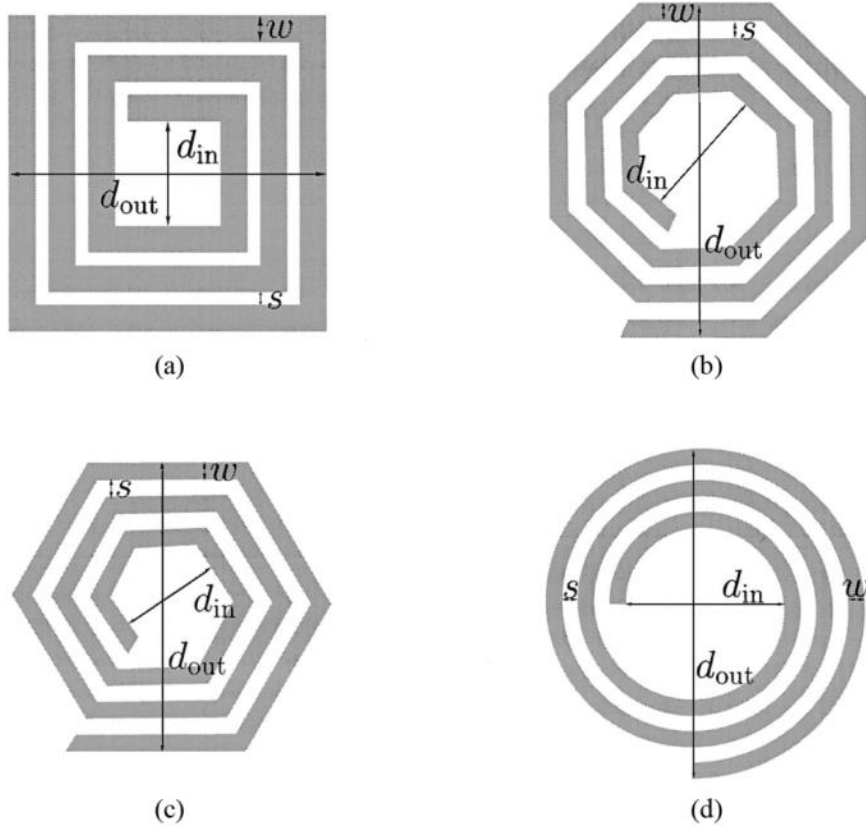


Figure 3.2: Spiral antenna shape types: (a) square, (b) hexagonal, (c) octagonal, and (d) circular. d_{in} is inner diameter, d_{out} is outer diameter, w is track width, and s is track spacing [62].

For evaluation of inductivity in different shapes, Mohan et al. [62] assumed the subsequent equation after Greenhouse [33], which is known as the *Greenhouse* formula [42]

$$L_{gmd} = \frac{\mu N^2 d_{avg} c_1}{2} (\ln(c_2/\rho) + c_3\rho + c_4\rho^2) \quad (3.1)$$

where L_{gmd} is inductivity of the spiral based on geometric mean distance, μ is magnetic permeability in free space and N is number of turns. d_{avg} is average diameter of the spiral and ρ is the fill ratio, as will be described in Equations (3.2) and (3.3). c_i are layout dependent coefficients, as represented in Table 3.1.

Table 3.1: Coefficients for Equation (3.1) [62].

Layout	c_1	c_2	c_3	c_4
Square	1.27	2.07	0.18	0.13
Hexagonal	1.09	2.23	0.00	0.17
Octagonal	1.07	2.29	0.00	0.19
Circle	1.00	2.46	0.00	0.20

$$d_{avg} = \frac{d_{out} + d_{in}}{2} \quad (3.2)$$

where d_{out} is outer diameter and d_{in} is inner diameter; as well as

$$\rho = \frac{d_{out} - d_{in}}{d_{out} + d_{in}} \quad (3.3)$$

Fill ratio [62] or fill-factor ratio [25] ρ represents how hollow the antenna is. Small fill ratio means the antenna is hollow and $d_{out} \approx d_{in}$, while large fill ratio means the antenna is full and $d_{out} \gg d_{in}$. At the same conditions, the inductance of a full coil antenna is less than a hollow one because the contribution of negative mutual inductance at the center of the coil is more than positive mutual inductance [62]. Fill ratio also defines as the ratio between track width and track spacing [25] of the coil antenna.

3.1.2 Outer Diameter

The outer diameter determines dimension of the antenna, as well as magnetic efficiency of it. For higher self-inductance and better coupling coefficient [95] in antennas, larger diameter is advisable.

Several parameters effect on the size of antennas. Mutual distance d effects directly on the outer diameter of antenna $2r$, while both of them are defining coupling coefficient and operating region of the inductive-coupling channel as $d/2r$ [38].

The optimal radius r_l for a transmitter antenna can be obtained by

$$r_1 = \sqrt{d^2 + r_2^2} \quad (3.4)$$

where r_2 is the given receiver antenna radius and d is mutual distance. For small remote antennas, radius of the base antenna equals about the communication distance [99]. In the case of antenna lamination, if the thickness of laminate layer is significantly less than antenna diameter, the mutual inductance d will increase linearly [95].

Frequency of operation is other significant parameter on antenna diameter. The coil antennas should be much smaller than the wavelength to avoid radiation [99]. For example, for operating frequency of 13.56 MHz, the wavelength is about 23 m that means outer diameter of antenna have to be less than it. Obviously, as the diameter of antenna decrease, the frequency of operation should increase, and vice versa.

Fluctuations of outer diameter can effect on resistance and inductance of coil antenna, as represented in Figure 3.3. By increasing the outer diameter of the antenna, the resistance and inductance of antenna are increasing in the same slope.

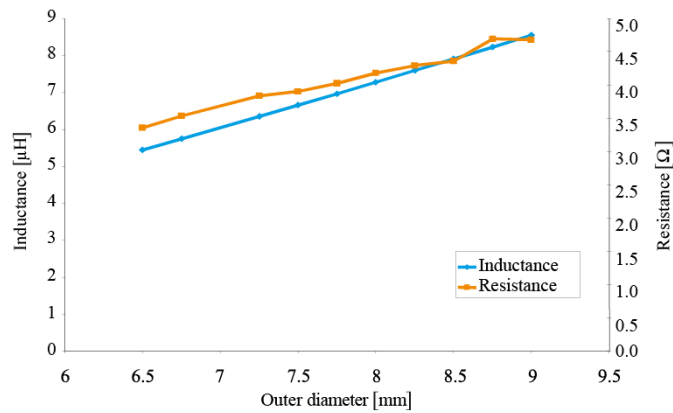


Figure 3.3: Influence of outer diameter of coil antenna on resistance and inductance [26]. By increasing the outer diameter, the resistance and inductance are increasing in the same slope.

In WPT systems, for optimization of coupling between two antennas, the outer diameter of transmitter must be larger than outer diameter of receiver [26].

3.1.3 Inner Diameter

Inner diameter of the coil causes two effects on magnetic behaviors of the antenna. At the beginning, by decreasing of inner diameter, the rate of inductivity and coupling coefficient increases, while at the same time, the flux linkage and coupling coefficient decreases [50]. This phenomenon caused by two types of current directions inside of the spiral traces, as they demonstrated at Figure 3.4.

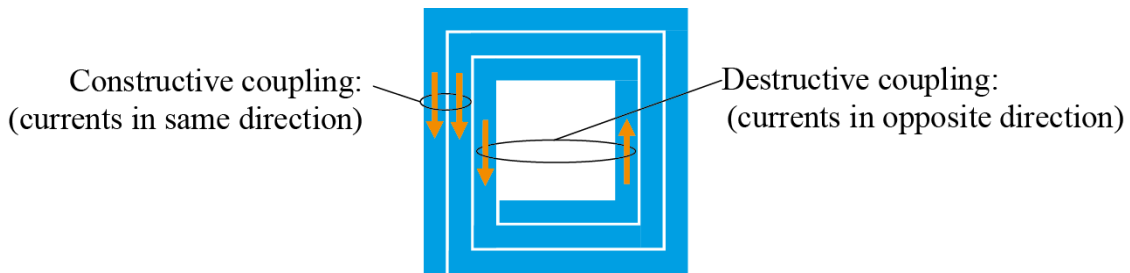


Figure 3.4: Same-directional and contra-directional currents cause to appear positive and negative mutual inductances, as well as constructive coupling and destructive coupling between conductive traces in a spiral coil [22], [42].

The same-directional and contra-directional currents [22] cause to appear positive and negative mutual inductances between conductive lines [42]. Since the total inductance of spiral coil antenna is equal to algebraic sum of self-inductance and mutual inductance, the positive and negative mutual coupling, increases and decreases the value of the total inductance, respectively [22]. Accordingly, an optimum value should be defined for inner diameter of the coil antennas. As an example, Figure 3.5 shows changing the rate of coupling coefficient with inner diameter of the coil, in an experiment [50]. By increasing the inner diameter of antenna to near 10 mm, the coupling coefficient is increasing by the reason of less destructive coupling. The higher values for inner diameter cause to reduce the coupling coefficient because of less generated self-inductance and mutual inductance. In WPT systems, for optimization of coupling between two coil antennas, the inner diameter of transmitter must be smaller than inner diameter of receiver [26].

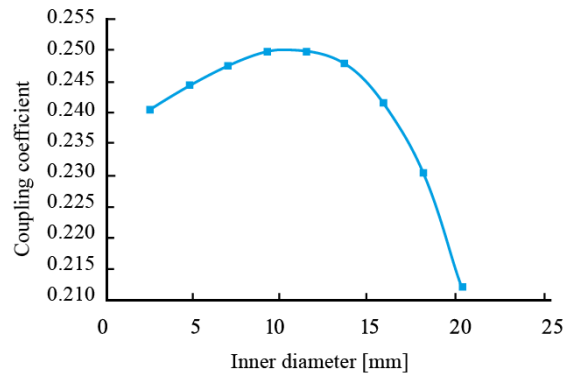


Figure 3.5: Changing the coupling coefficient with inner diameter. The distances between coils is 30 mm, re-drawn from [50]. Increasing the inner diameter of antenna to near 10 mm causes to increase the coupling coefficient by the reason of less destructive coupling. The higher values for inner diameter cause to reduce the coupling coefficient because of less generated self and mutual inductances.

3.1.4 Track Width

With increase in track width, the inductance is decreased [42]. Also, there is a report on the low impact of track width on self-inductance, mutual inductance and leakage inductance [95], but certainly track width can effect on resistance and coupling [26]. Figure 3.6 (a) reveals the relation between track width and resistance, while Figure 3.6 (b) represents the effect of track width on inductivity. By increasing the track width, the resistance and inductance are decreasing.

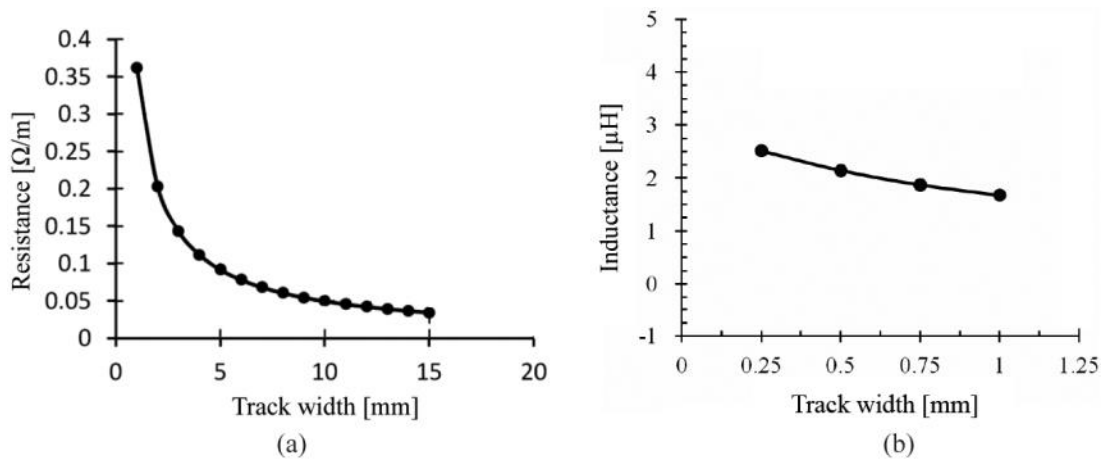


Figure 3.6: (a) The effect of track width on resistivity at 4 MHz frequency. The track thickness is 0.105 mm [19]. (b) The relation between track width and inductance in a four-layer PCB inductor with track gap 0.25 mm and turns number 6 at 13.56 MHz frequency [42]. By increasing the track width, the resistance and inductance are decreasing.

Typical practical integrated spiral inductors are built with track width more than or equal to track spacing because of increasing inter winding magnetic coupling and decreasing the area consumption [62]. The typical achievable track widths by screen printing is limited to the order of 100 μm [96] or more.

3.1.5 Track Spacing

Track space is the gap between conductive traces in a coil antenna. Less track space causes current crowding at inner side of antenna, more AC resistance at higher frequencies [25], and more winding rounds in limited areas. On the other hand, increase in track spacing decreases the value of the inductance (see Figure 3.7 (a)). By increasing the gap between conductive tracks, the mutual coupling and overall inductance decrease [42] (see Figure 3.7 (b)). Increase in track spacing can also decrease the parasitic capacitance [62] and proximity effect losses [26] between conductive traces in coil antennas. For repeatable experiments, straight and clean edges [15] are advisable for track spaces. In calculation of track spacing, the bleed out of ink during printing or firing should take into account, too [35].

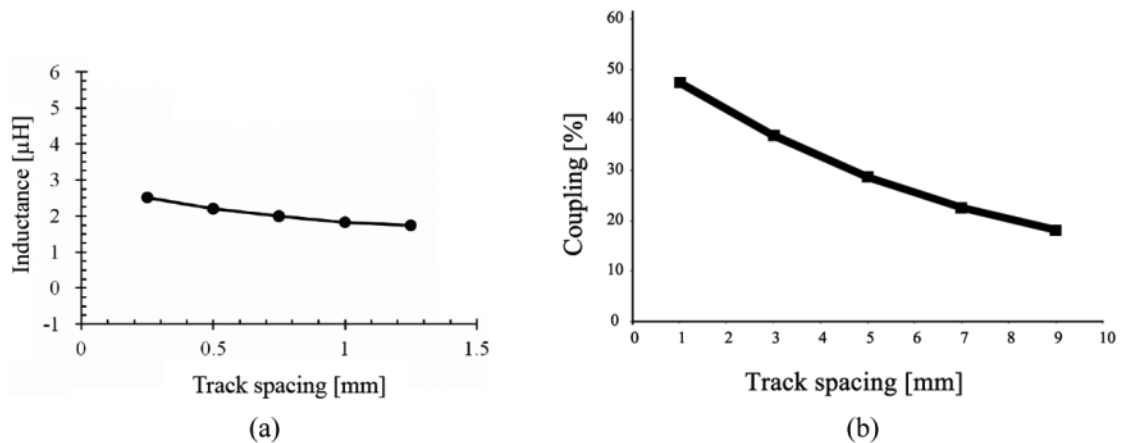


Figure 3.7: (a) Track spacing versus inductance in a four-layer PCB inductor with track gap 0.25 mm and turns number 6 at 13.56 MHz frequency [42]. (b) The relation between track spacing and coupling in PCB spiral coil 10 turns at 5 MHz frequency [26]. By increasing the track spacing, the inductance and coupling are decreasing.

3.1.6 Track Thickness

Track thickness does not influence significantly on inductivity. It can be ignored [62] in inductance calculation. The effect of track thickness is mostly on development of conductivity. For instance, the resistivity of a printed resistor varies inversely with the film thickness [67].

By increasing the bulkiness of conductive traces, ohmic losses decrease in coil antennas. Also, skin effect losses at high frequencies reduces [68], too.

3.1.7 Number of Turns

The inductance of the coil is proportional to the square of turn numbers [99] (see Equation (3.1)). More number of turns in a spiral coil is equal to more length for the antenna. Increasing the length of coil antenna causes to increase the inductance value [42] as well as inter-winding capacitance [53] and parasitic series resistance of the coil. By increasing parasitic series resistance, the value of quality factor decreases dramatically [95]. To approach higher efficiency, minimizing resistance and maximizing the coupling factor [27] are two important key points. Coupling does not depend on the number of turns [99], [27], [26], [95] but minimizing the resistance can be achieved by definition of optimum turn numbers for the coil. Mutual inductance is also depends on the number of turns [99]. Figure 3.8 represents the relation between number of turns and inductance. By increasing the number of turns, the inductance is increasing.

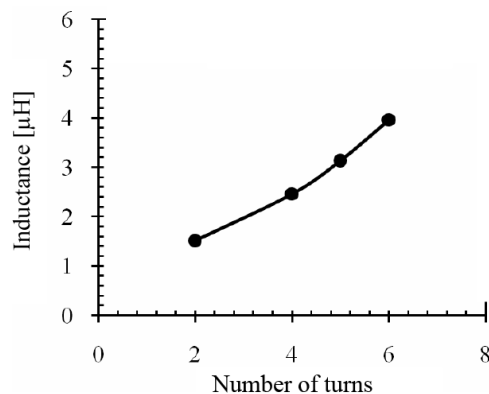


Figure 3.8: Turn numbers versus inductance in a four-layer PCB inductor with track width 0.25 mm and track gap 0.25 mm at 13.56 MHz frequency [42]. By increasing the turns number, the inductance is increasing.

In a spiral antenna, if outer and inner diameters are constant values, the specified inductance of antenna is proportional to turn numbers [26].

3.1.8 Geometrical Design Optimization

To reach an optimal geometrical design, should find a trade-off between coil diameter, resistive loss, and parasitic capacitance. If the diameter is limited, then the only possible variations are track spacing and track width. To keep the coil radius r_{in} fixed, by increasing the track spacing s_0 should reduce the track width w_0 , and vice versa [25]. Figure 3.9 represents the relation between track spacing and track width in spiral coil topology, where the diameter is constant and Δs and Δw are change in track spacing and track width, respectively.

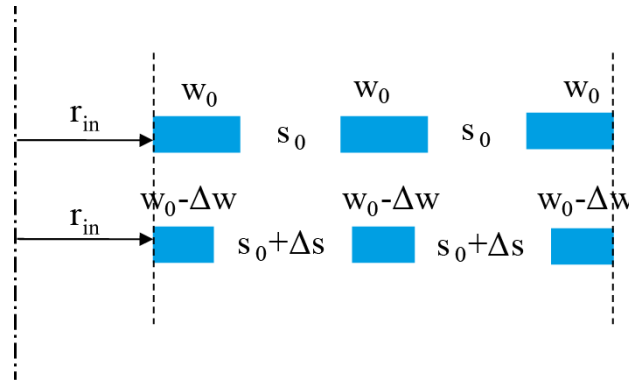


Figure 3.9: Relation between track width w and track spacing s in spiral coil topology, where the diameter r_{in} is constant, Δs is change in track spacing and Δw is change in track width [25].

Because printed tracks are very thin and very wide, skin effect is more important than proximity effect. Therefore, wide and adjacent tracks are better than narrow and separated tracks. The result is minimizing resistance and improving coupling coefficient, simultaneously. To obtain equivalent self-inductance, the number of turns should increase [26].

Measurement pads or signal pads are a part of geometrical design, too. Optimum size for measurement pads is important. They should be big enough to can connect them easily to measurement contacts but not so big that increase parasitic effects [22]. Figure 3.10 shows a pair of measurement pads of an inductor.

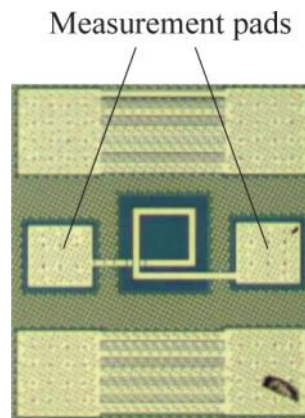


Figure 3.10: The measurement pads of a silicon-on-insulator inductor 0.25 nH [22].

3.2 Concept of Software Workflow for Printed Antennas

General rules in design of thick film microwave circuits can be applicable for printed antennas, too. A critical step in manufacture of thick and thin microwave circuits is fabrication of artwork and masks. The artwork and masks are effective elements on performance, circuit yield, and cost [15]. In preparation of printing artwork should take care about appropriate line width and level of resolution that allow printing the fine lines and spaces [10]. Adjacent thinner lines in compare to thicker ones have more voids and connections [67]. Generally, the minimum value of line width is defined based on screen mesh characteristics. There are some additional parameters that effect on minimum line width, e.g. the printer, substrate, screen, squeegee, ink, and process parameters [67].

There are some difficulties in realization of computer aided designs (CAD) into accurate and usable artwork for microwave layouts [15]. Unfortunately, now, there is not any solution to design an appropriate layout for functional printing and printed electronics, just by application of a single software. The solution is application of several software to make the layout ready for the pre-press process. Definition of a concept for software workflow for printed antennas is the aim of this sub-chapter. The potential challenge on final artwork should be some undesirable influences such as the effect of mesh direction on sharpness quality, the saw tooth effect, the image shift effect, and misregistration of printed layers. Although it is possible to define a mathematical model for simulation of those effects in the artwork, but that is not so simple and accessible.

The effect of mesh direction on sharpness quality

The direction of printed lines on screen can effect on sharpness quality. As Figure 3.11 represents, the edge sharpness of printed lines that are oriented in parallel to the printing direction is higher than printed lines that are oriented transverse to printing direction [34].

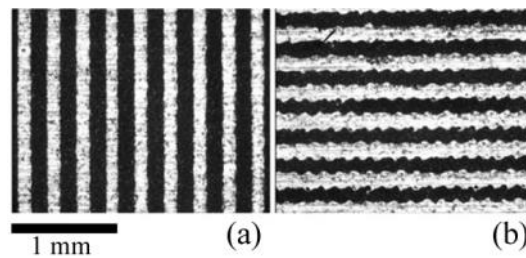


Figure 3.11: Microscopic images of printed silver strain gages (a) In printing direction, and (b) Transverse to printing direction. The line sharpness parallel lines with printing direction is higher than transverse lines to printing direction [34].

Saw tooth effect

Saw tooth effect is other printing challenge that is not considering in CAD software. The mismatch between direction of screen filaments and pattern orientation can cause saw tooth effect. This jagged effect appears on the edge of printed solid lines. As represented in Figure 3.12 and Table 3.2, saw tooth effect can change significantly the values of nominal and real width of the printed fine lines. As the line width becomes smaller, the saw tooth effect increases [77].

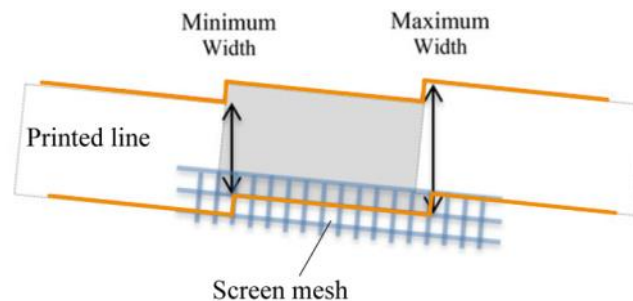


Figure 3.12: Minimum and maximum width of screen printed line, caused by saw tooth effect [77]. Saw tooth effect can change the values of nominal and real width of the printed fine lines.

Table 3.2: The influence of saw tooth effect on minimum and maximum width of screen printed lines, printed with screen mesh 90 and 140 threads per centimeter. As the line width becomes smaller, the saw tooth effect increases [77]. The dash mark indicates that this value is not printable.

Layout width [μm]	Mesh 90 T/cm		Mesh 140 T/cm	
	Minimum [μm]	Maximum [μm]	Minimum [μm]	Maximum [μm]
1000	970	990	980	990
900	860	880	880	890
800	760	780	790	800
700	660	690	680	690
600	530	600	580	600
500	410	500	470	490
400	280	380	370	400
300	180	270	–	–
200	–	–	–	–

Image shift effect

Image shift is other phenomenon that deforms the printed geometry during screen printing process. The elongation of printing screen causes to appear lateral image shift. Figure 3.13 illustrates the image shift effect. More off-contact or snap off between screen and substrate increases the image shift effect [40]. Deformation of screen during printing causes to increase the dimension of printed pattern in compare with the mask pattern.

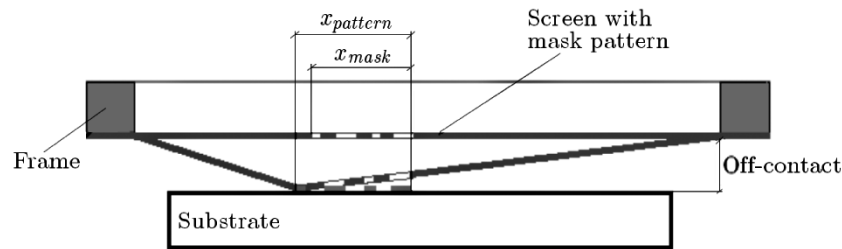


Figure 3.13: Image shift caused by screen elongation [40]. Deformation of screen during printing causes to increase the dimension of printed pattern $x_{pattern}$ in compare with the mask pattern x_{mask} .

Misregistration

Registration of deposited layers is other example of challenges. As illustrated in Figure 3.14, the second ink-layer is deposited on the first ink-layer. The size of patterns in layers and the gap between them should allow small overlaps and misalignments. An idealized cross section of a double-layer thick film represented in Figure 3.14, too [47].

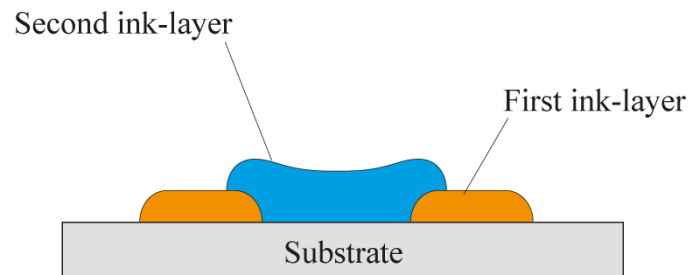


Figure 3.14: An idealized cross section and overlaps of a thick film double-layer [47].

3.2.1 Software Workflow

In graphic industry, the digital artworks are categorized in three types:

- Vector
- Bitmap
- The combination of vector and bitmap

Vector graphics include the graphic elements as mathematical geometries. Vector graphics are resolution-independent and can be modified without losing image quality [3]. They are more useful for drawing the sharp edges and solid areas. For example,

Adobe Illustrator [2] is a vector based software. Figure 3.15 (a) depicts a vector drawing with visual magnification of 3200%.

Bitmap images or raster images include the graphic elements as the pixels. Bitmap images are resolution-dependent and are losing the image quality during modification [3]. They are more useful for halftones and gradient areas. For example, Adobe Photoshop [6] is a bitmap based software. Figure 3.15 (b) depicts a bitmap image with resolution of 300 dots per inch (DPI) and the visual magnification of 3200%.

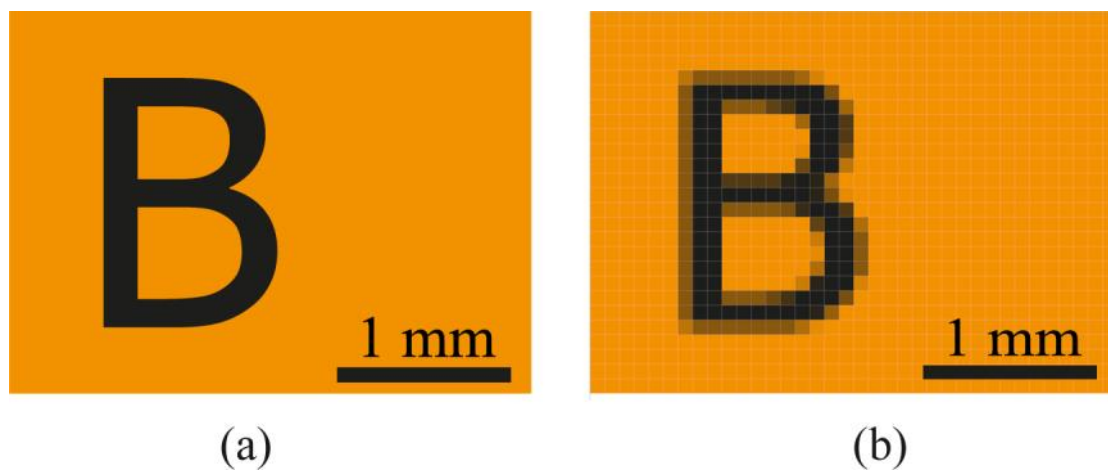


Figure 3.15: (a) A vector drawing, and (b) A bitmap image. The magnification of both of them is 3200%.

Some software like Adobe InDesign [5] can make or modify the artworks that are including vector and bitmap elements together. This type of artworks is more conventional for newspaper layouts and so on.

Usually, the functional printing and printed electronics artworks include the sharp edge elements and solid areas, not the halftones. Therefore, the design of artwork should be done by a vector based software (see Figure 3.16). Application of bitmap software can cause to jag the line edges and change the line width w . The change in w can significantly effect on conductivity and parasitics of the circuit elements, e.g. capacitance C_s , as represented in Figure 3.16 (b).

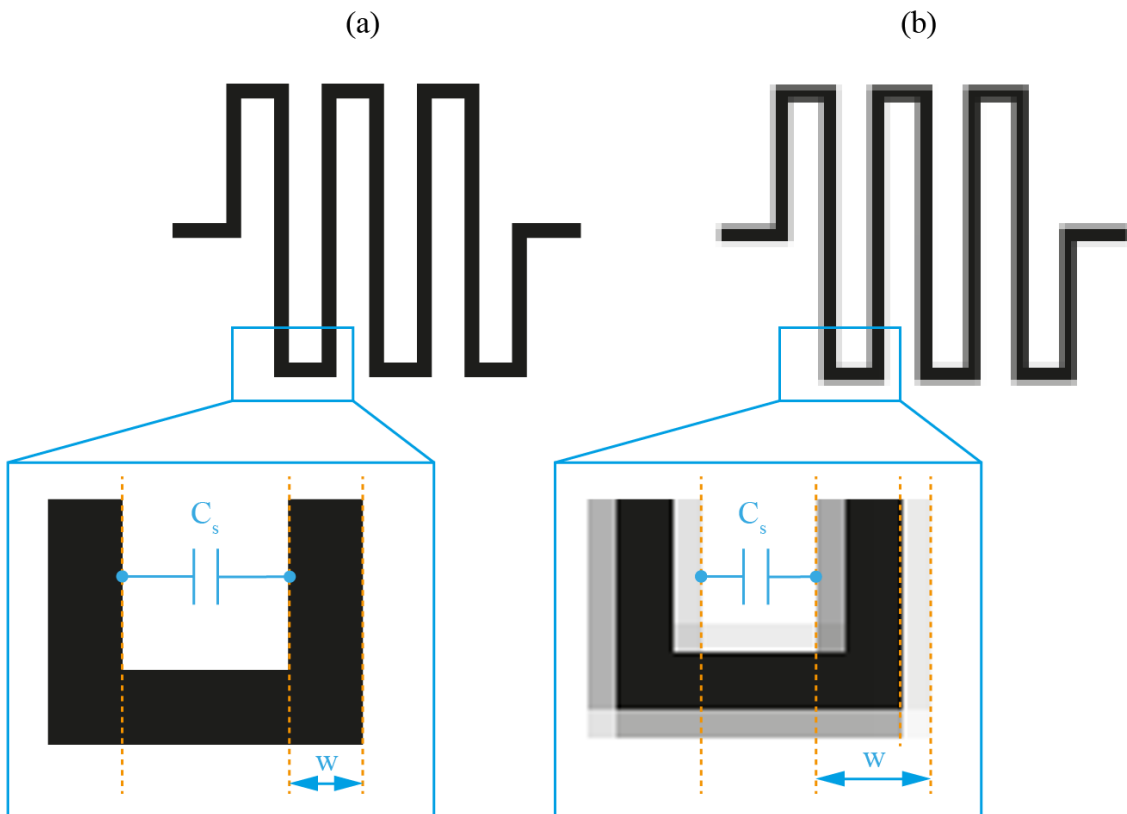


Figure 3.16: The artwork in vector format (a) and bitmap format (b). The sharpness of the lines and the line width w can change in bitmap format. Line width deviations can effect on conductivity, parasitic capacitance C_s , etc.

There is a wide range of vector based software for various purposes of design and engineering. The design tools and facilities, and also the accuracy and tolerances of them are different. For example, Adobe Illustrator [2], Autodesk AutoCAD [13], and Rhinoceros [75] are vector based software, but the first one is suitable for graphic design, the second one is useful for mechanical design, and the third one is appropriate for complicated geometric design.

A challenge on layout design for printed electronics is the accuracy of dimensional values in vector based software (see Figure 3.17 (a)). The dimension of traces and elements must be accurate. In some software, the line width tolerance for small values in the range of micrometer is not reliable. For that reason, it is better to define the outlines of elements Δw equal to 0 and finally fill them with solid colors (see Figure 3.17 (b)). Otherwise, the Δw value can be added to desired dimension w_0 .

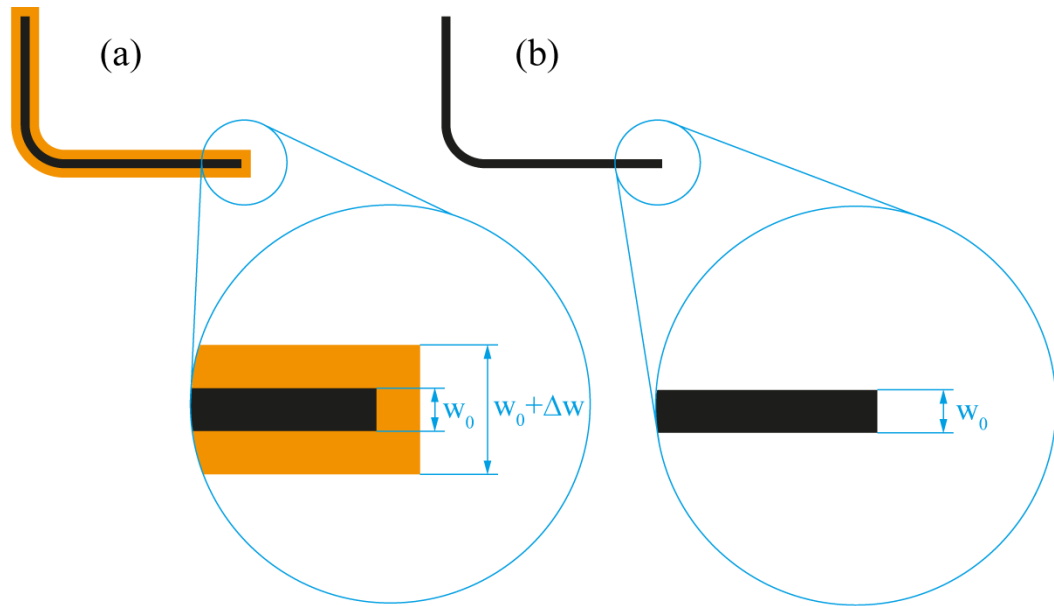


Figure 3.17: The line width of traces in drawing software. (a) Increasing in line width w_0 is changing the value to $w_0 + \Delta w$; and (b) Definition of outlines equal to 0 and filling them with solid color can fix the problem.

The outlines can be defined precisely in Rhinoceros or Autodesk AutoCAD with the line width of 0. Then it should be exported to Adobe Illustrator as a Drawing Interchange Format (DXFTM) [12] file. The DXF file type is professionally documented. DXF files are produced based on American Standard Code for Information Interchange (ASCII). The ASCII based codes cause to easier process on DXF files [30]. The imported DXF file in Illustrator is filled with black color to generate solid areas. The width of outlines should be kept in 0, with no color. Finally, the artwork should be saved as the native format of software (e.g. AI for Adobe Illustrator), or be exported as DXF or Portable Document Format (PDF) [3] file. Using PDF file type is advisable because vector graphics can keep the sharp edges if be saved in PDF [3]. Also, most of prepress service bureaus accept the PDF files for making printing forms. The type of exported PDF file can be normal. Setting the standard on PDF/X is not necessary. Checking the PDF file for prepress is possible in Adobe Acrobat Pro. Figure 3.18 depicts the software workflow process for functional printing and printed electronics artworks.

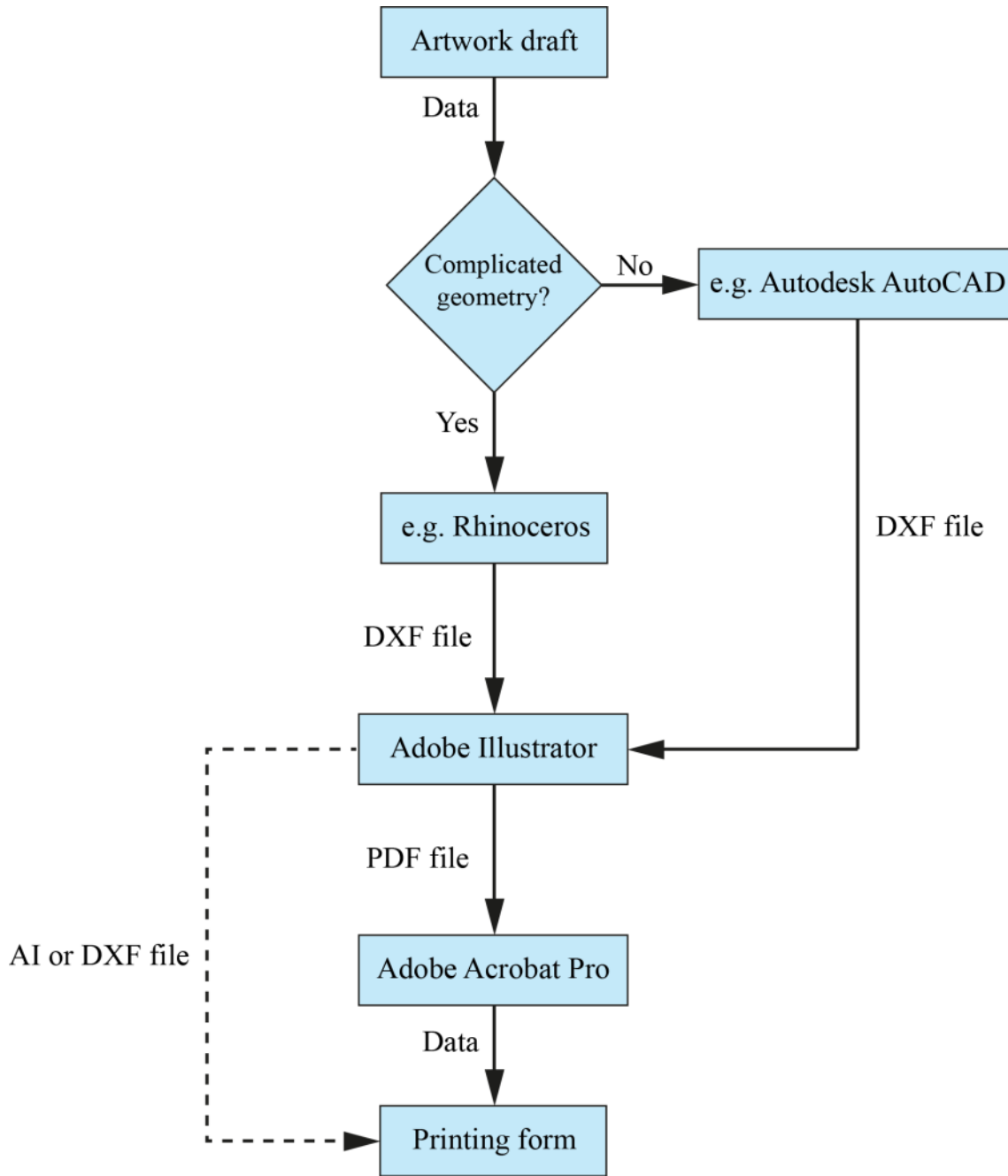


Figure 3.18: The software workflow process for functional printing and printed electronics artworks. Artwork outlines are defined in Rhinoceros or Autodesk AutoCAD, according to level of complexity. The data is exported to Adobe Illustrator as a DXF file. The outlines are filling in Adobe Illustrator to make solid areas. The file can be exposed directly on printing form as an AI or DXF file, or can be exported as a PDF file to be readable with Adobe Acrobat Pro. The advantage of PDF is that most of prepress service bureaus accept this file type.

4 Experimental Setup

The aim of this chapter is to explain the experimental setup for printing the antennas. The first part of chapter represents the parameters and adjustment of experimental setup. That includes layout design and software settings. The next parts are about mesh screen, ink, printing procedure and curing, and the number of printed samples.

The Steps of Printing-experiments of Research

In this research, the variables of printing-experiment are:

- Layout design
- Mesh screen
- Ink
- Measurement of the printed samples

The printing process is *off-contact*, that means there is a gap between screen and substrate. Three layouts are designed for this research: a *Preliminary* layout for practical tests on printing the fine lines, a *Comparative* layout, for comparison of electromagnetic characteristics of the coil antennas, and a *Final* layout for the application of wireless powering. Two types of mesh screens are applied for research: polyester mesh and stainless steel mesh. Polyester mesh is applied in *Preliminary* layout screen, while stainless steel mesh is used in *Comparative* layout and *Final* layout screens. Three types of silver inks are utilized to print conductive traces on substrates. Figure 4.1 shows the steps of printing-experiments of research. Also the measurement of printed samples is taken with a network analyzer (see sub-chapter 2.5).

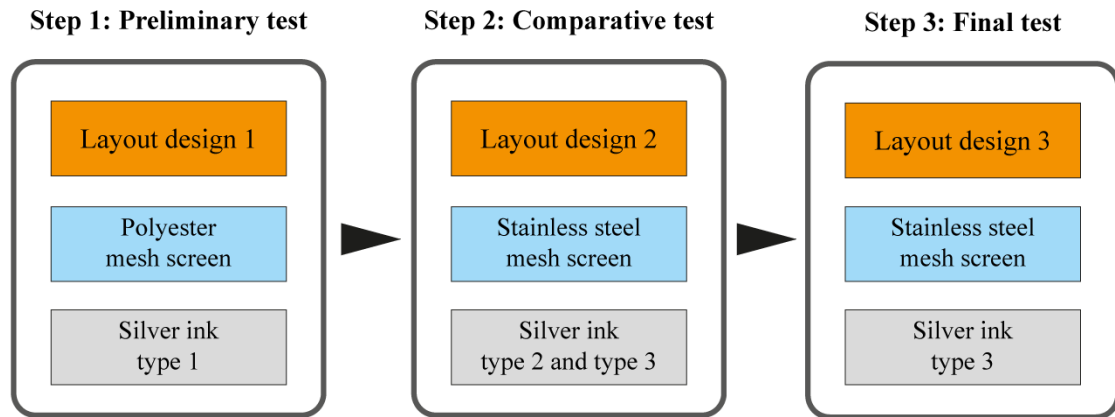


Figure 4.1: The steps of printing-experiments of research.

4.1 Layout design and Software Settings

The first step in printing antennas is design of printing layout. The geometry of antenna should be figured out. A meaningful relation between different geometries helps to can compare the measurement results. Three different layouts are designed for present experiment:

- A *Preliminary* layout for practical tests on printing the fine lines and dimensional characteristics of antennas, including thirteen different samples in the range of 15 to 50 mm.
- A *Comparative* layout to have a comparison between electromagnetic characteristics of different printed antennas, including four different spiral antennas, based on *Preliminary* layout.
- A *Final* layout for utilization in wireless powering, including an 80 mm diameter antenna as the final design.

The goal is to find optimum design for printed antennas.

4.1.1 Preliminary Layout

The most important aim of preliminary test is to find the lowest possible track width and the lowest possible track spacing for spiral coil antennas. The results have been used in next step for *Comparative* layout design.

The *Preliminary* layout contains thirteen circular spiral antennas with different outer diameter, track width, track spacing, and number of turns, as represented in Figure 4.2 and Table 4.1. The geometrical shape and mostly, inner diameter are like the same for all of them.

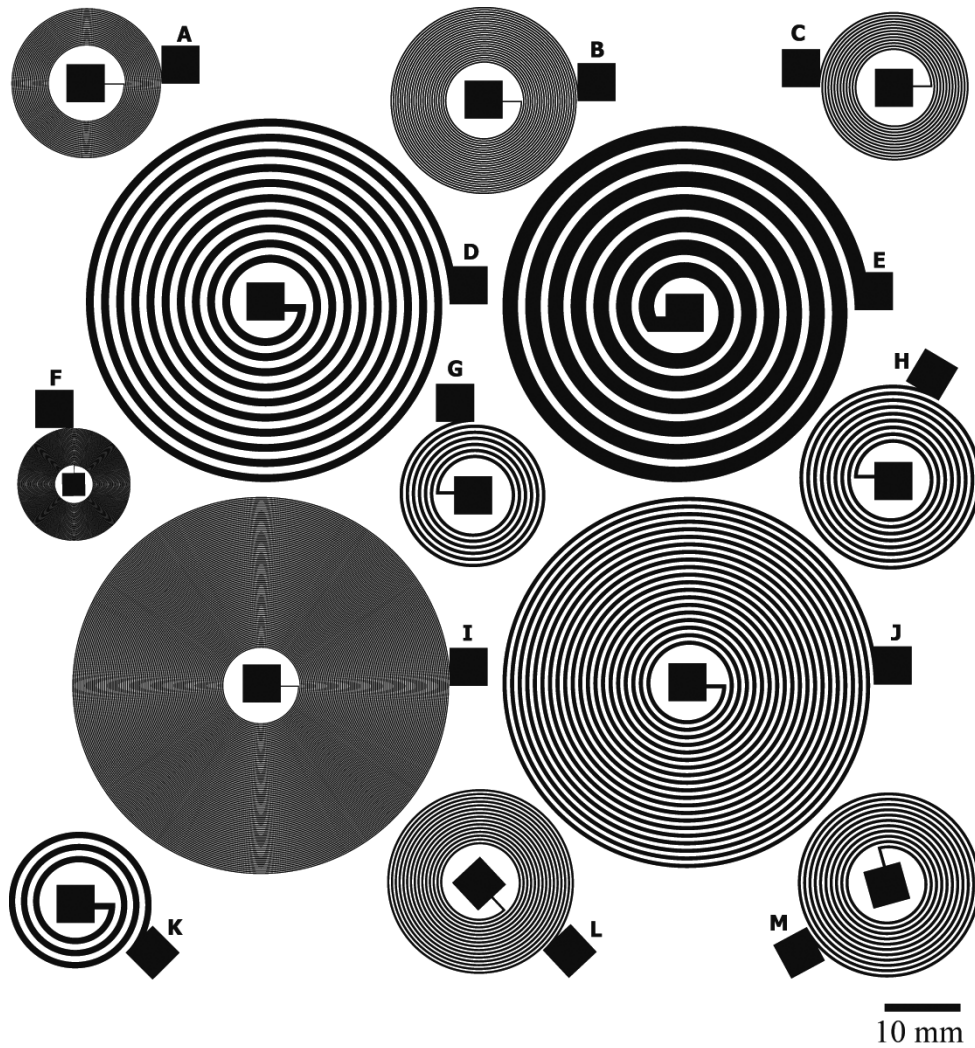


Figure 4.2: Circular spiral antennas included in *Preliminary* layout. Dimensional characteristics of antennas is represented in Table 4.1.

Table 4.1: The dimensional characteristics of antennas included in *Preliminary* layout (see Figure 4.2).

Sample	Inner dia. [mm]	Outer dia. [mm]	Track width [mm]	Track spacing [mm]	Number of turns [~]
A	10	20	0.10	0.10	25
B	10	25	0.15	0.15	25
C	10	20	0.20	0.20	12.5
D	10	50	1.00	1.00	10
E	10	50	2.00	1.00	6.5
F	5	15	0.05	0.05	50
G	10	20	0.40	0.40	6.25
H	10	25	0.45	0.45	8.25
I	10	50	0.10	0.10	100
J	10	50	0.50	0.50	20
K	10	20	0.80	0.80	3.25
L	10	25	0.25	0.25	15
M	10	25	0.35	0.35	10.75

4.1.2 Comparative Layout

A *Comparative* layout is designed for the comparison of different printed antennas. The aim is to compare electromagnetic characteristics and dimensional values of antennas. The results have been used in design of *Final* layout for wireless powering with printed antennas.

The artwork includes four spiral antennas. All of them are circular spirals. The inner diameter, outer diameter, and track spacing in four patterns are like the same. The variables are track width and number of turns. Accordingly, track length and ink covered area can be varied.

The patterns are concentrated at the middle of screen to reach more homogeneity in thickness of deposited ink. Figure 4.3 and Table 4.2 represents the features of *Comparative* layout.

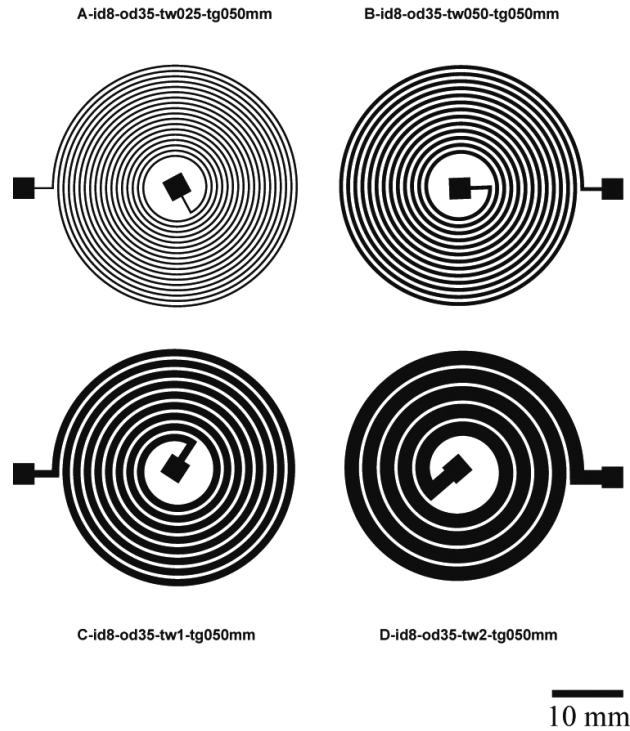


Figure 4.3: Circular spiral antennas included in *Comparative* layout. Dimensional characteristics of antennas is represented in Table 4.2. Every sample is determined with a notation including the category (A-D), and inner diameter (id), outer diameter (od), track width (tw), and track gap (tg), in millimeters.

Table 4.2: Dimensional characteristics of antennas included in *Comparative* layout (see Figure 4.3).

Sample	Inner dia. [mm]	Outer dia. [mm]	Track width [mm]	Track spacing [mm]	Number of turns
A	8	35	0.25	0.50	17.66
B	8	35	0.50	0.50	12.99
C	8	35	1.00	0.50	8.31
D	8	35	2.00	0.50	4.57

As Table 4.2 includes, the track width is doubling in subsequent samples, while the value of track spacing, inner diameter, and outer diameter are constant. Accordingly, the number of turns must be decreased. Therefore, the electromagnetic characteristics of samples can be different.

4.1.3 Final Layout

Final layout includes one antenna. The results of *Comparative* layout are applied in *Final* layout design. The aim is to use it for wireless power transfer. The design is started by definition of outer diameter, track width, track spacing, and number of turns, respectively. That is the reason why the value of inner diameter is not a round number. The outer diameter is 80 mm, while the inner diameter is around 52 mm to make a hollow antenna with small fill ratio. Decreasing the fill ratio can decrease negative mutual inductance, and accordingly, increase the power transfer efficiency by the antenna (see sub-chapter 3.1.3). Figure 4.4, Figure 4.5 and Table 4.3 represents the features of *Final* layout.

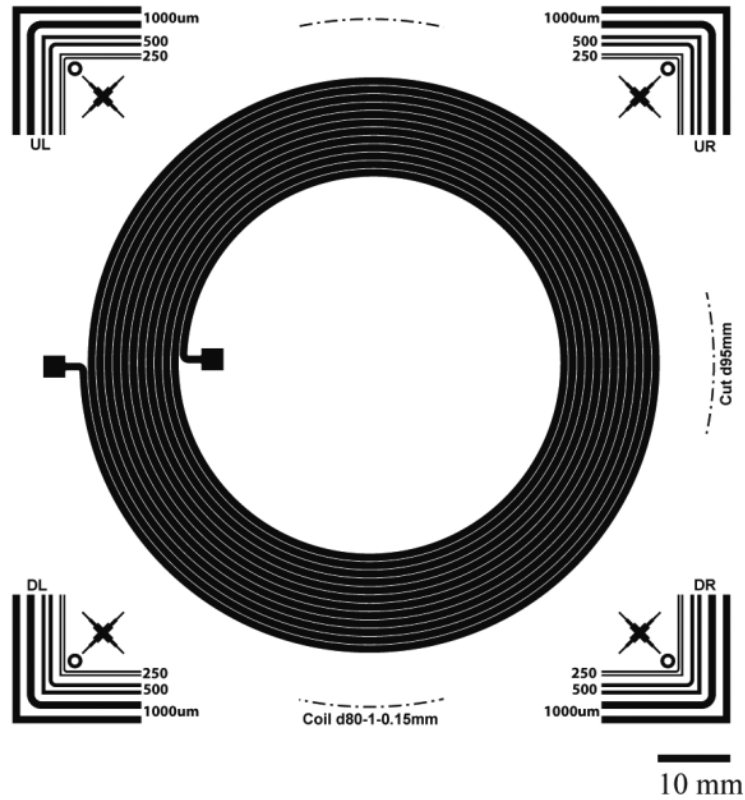


Figure 4.4: Circular spiral antenna included in *Final* layout. Dimensional characteristics of antennas is represented in Table 4.3.

As represented in detail view in Figure 4.5, the corner edges are rounded to develop the electromagnetic functionality of antenna in high frequencies. The guidelines for laser cutting and the perpendicular lines for quality control are added around layout. Center of antenna should be free of guidelines and identification elements, because of electromagnetic effects.

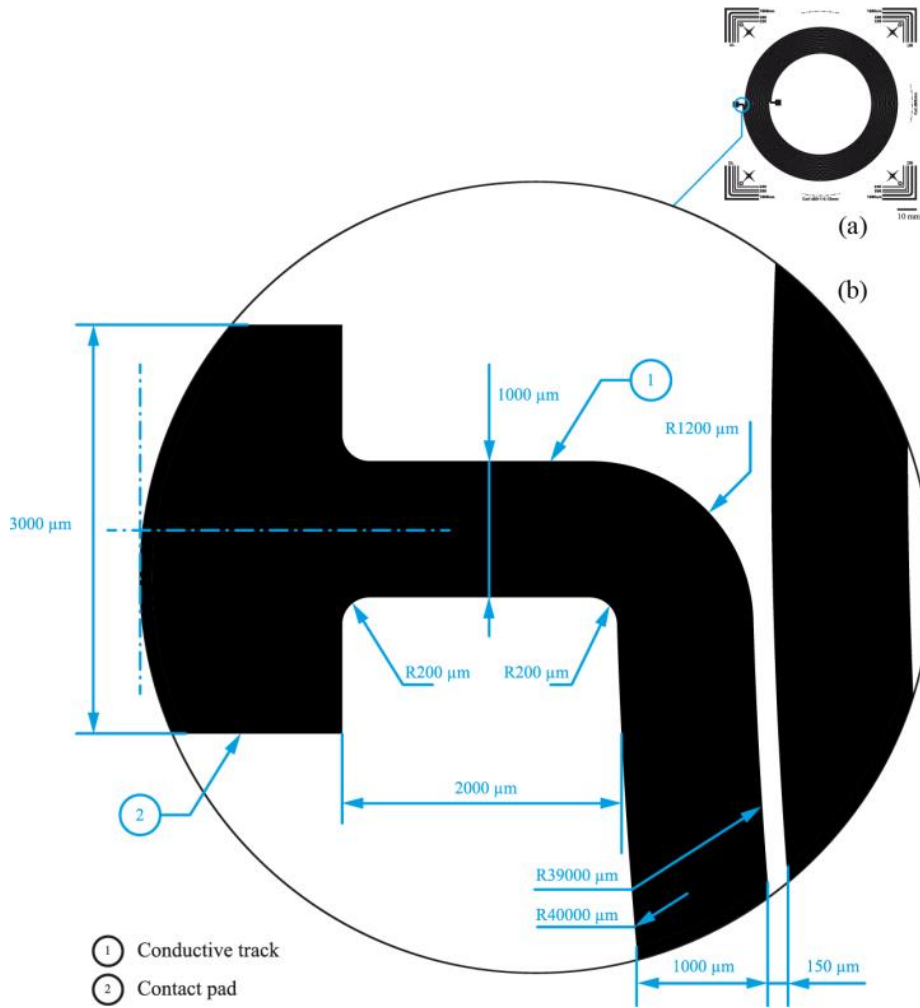


Figure 4.5: Detail view of circular spiral antenna included in *Final* layout. The corner edges are rounded to develop the electromagnetic functionality in high frequencies. The guidelines for laser cutting and the perpendicular lines for quality control are added around layout.

Table 4.3: Dimensional characteristics of antenna included in *Final* layout (see Figure 4.4 and Figure 4.5).

Sample	Inner dia. [mm]	Outer dia. [mm]	Track width [mm]	Track spacing [mm]	Number of turns
<i>Final</i> layout	51.55	80	1	0.15	12

4.1.4 Software Settings

The artworks of *Preliminary* layout and *Comparative* layout are drawn in Rhinoceros Version 5 (developed by Robert McNeel & Associates) [75]. Rhinoceros is an appropriate software for drawing the complicated geometries, e.g. the Archimedean and equiangular spiral curves for antennas, as explained in sub-chapter 2.3. The interface of Rhinoceros software is represented in Figure 4.6.

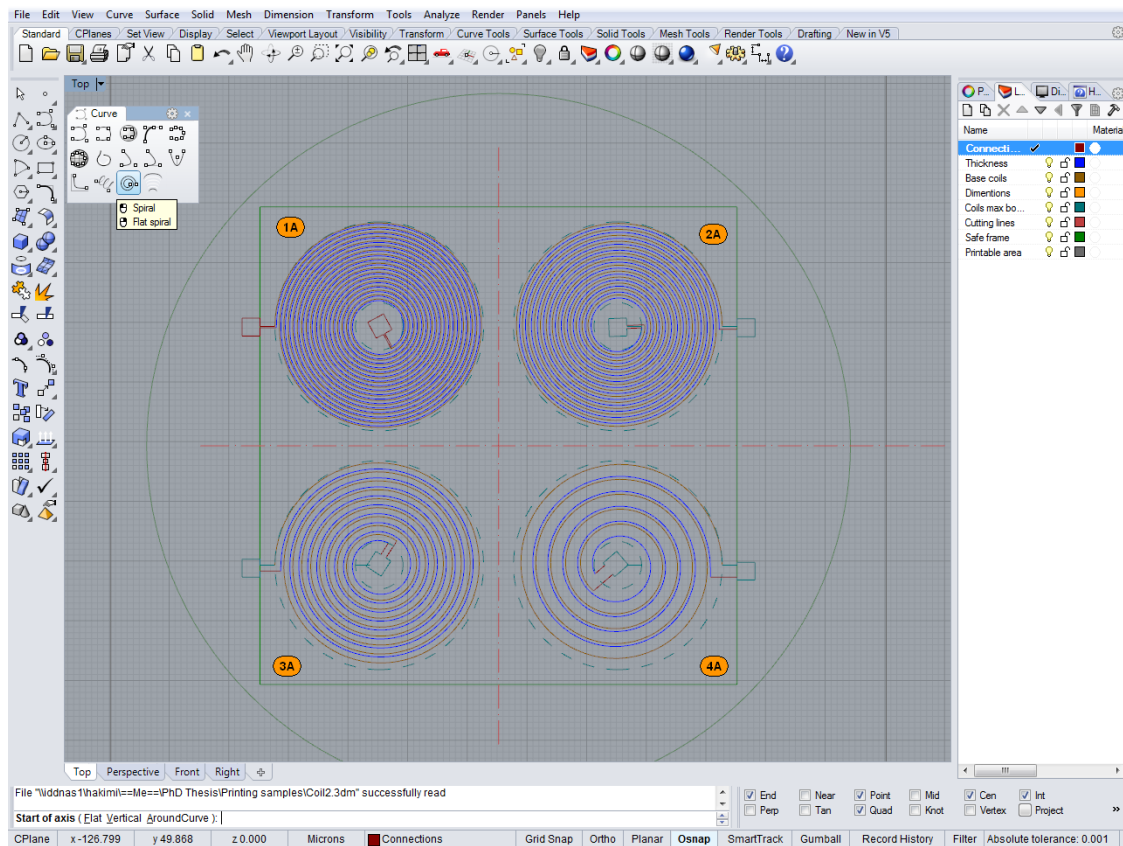


Figure 4.6: The interface of Rhinoceros software. The software is appropriate for complicated geometric design, e.g. the Archimedean and equiangular spiral curves for antennas.

The *Final* layout is simpler than *Preliminary* and *Comparative* layouts. The artwork of *Final* layout is drawn in Autodesk AutoCAD 2015 (developed by Autodesk Incorporation) [13]. The software is suitable for technical drawings. The interface of Autodesk AutoCAD software is represented in Figure 4.7.

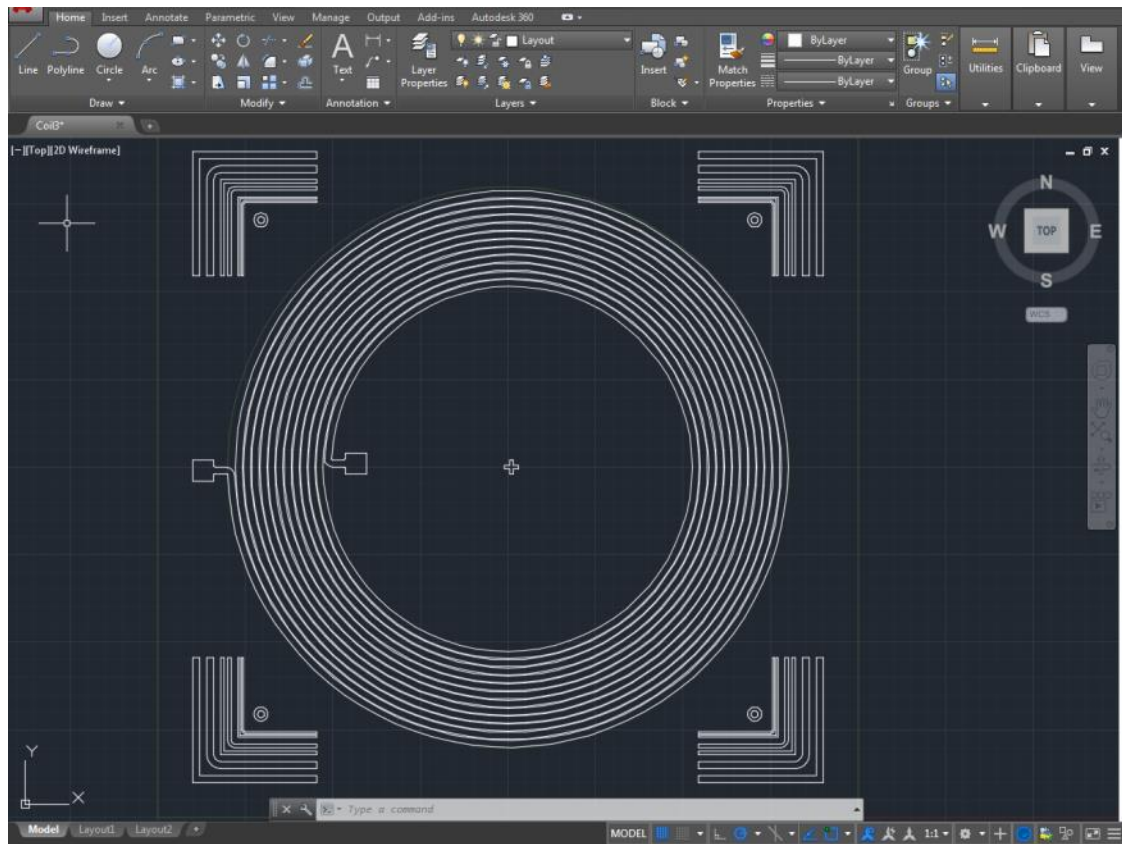


Figure 4.7: The interface of Autodesk AutoCAD software. The software is appropriate for technical drawings.

Every printing area is defined by its outlines. In both of the cases, including the application of Rhinoceros or Autodesk AutoCAD, the line width or the thickness of the lines are defined 0, to be sure that the dimensions of area will not be expanded or contracted in final artwork. Figure 4.8 represents the outlines of printing area.

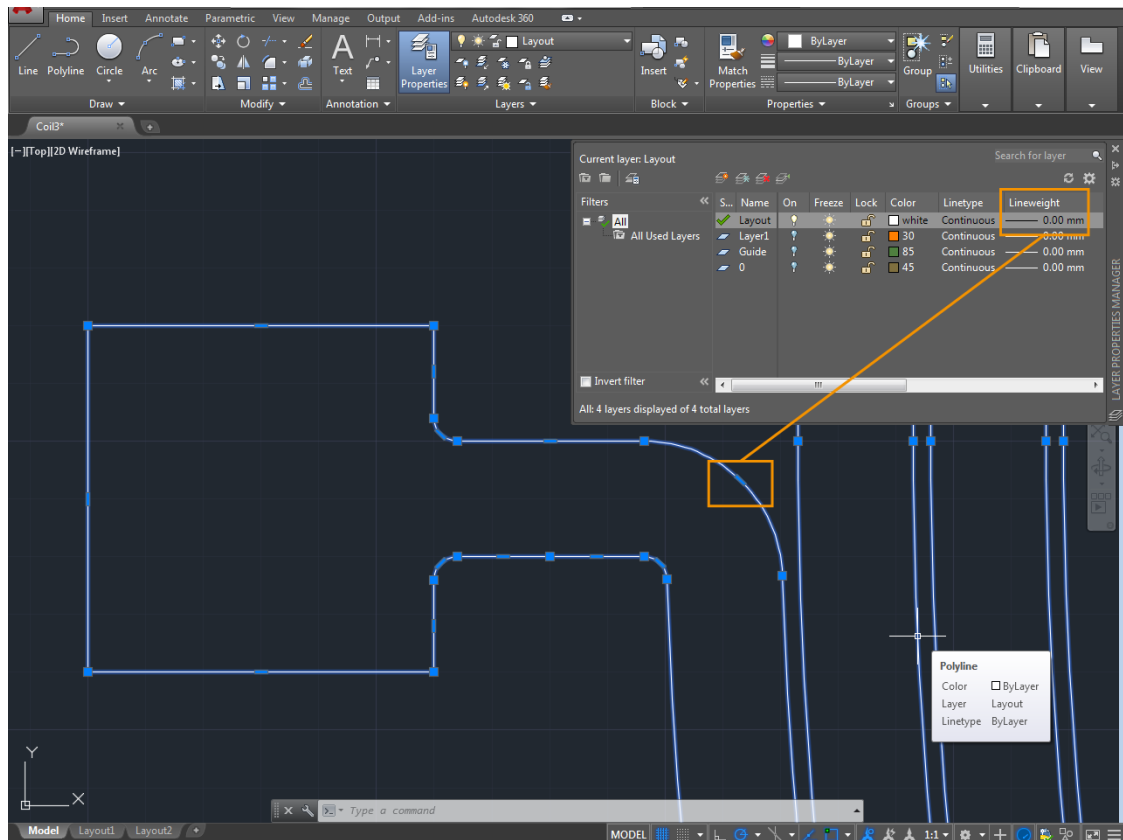


Figure 4.8: Every area is defined by its outlines. The thickness of outlines are defined 0 in drawing software to be sure that the dimensions of area will not be expanded or contracted in final artwork.

The Rhinoceros or Autodesk AutoCAD data is exporting as a DXF file to Adobe Illustrator CS5 (developed by Adobe Systems Incorporated) [2]. The document color mode is defined as grayscale or as process color (cyan, magenta, yellow, and black (CMYK)). On the top side of the software interface, the Fill color shows the color that is filling inside of closed outlines. The Stroke color shows the color of closed outlines. The Stroke weight shows the line width of closed outlines. At the beginning, the Fill color and Stroke color boxes are empty, and the Stroke weight of the line is 0, as represented in Figure 4.9.

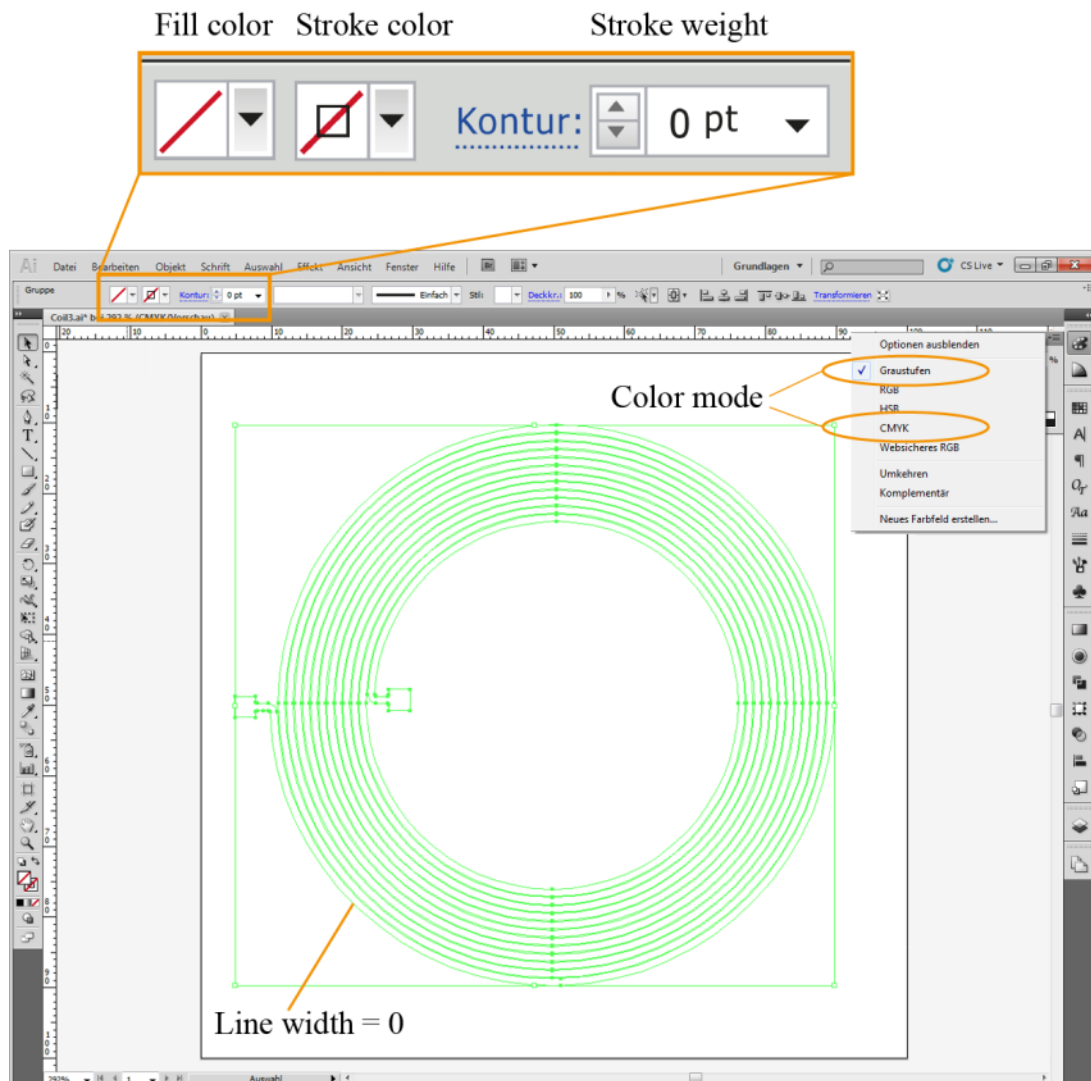


Figure 4.9: The interface of Adobe Illustrator software. The DXF file is imported to Adobe Illustrator. The document color mode is defined as grayscale or CMYK. The Fill color shows the color that is filling inside of closed outlines. The Stroke color shows the color of closed outlines. The Stroke weight shows the line width of closed outlines. At the beginning, the Fill color and Stroke color boxes are empty, and the Stroke weight of the line is 0.

At the next step, the Fill color is changed to black. If the color mode is Grayscale, the black should be 100% and if the color mode is CMYK, the C, M, and Y should be 0% and the black 100%. The Stroke color stays empty, and the Stroke weight stays on 0, as represented in Figure 4.10.

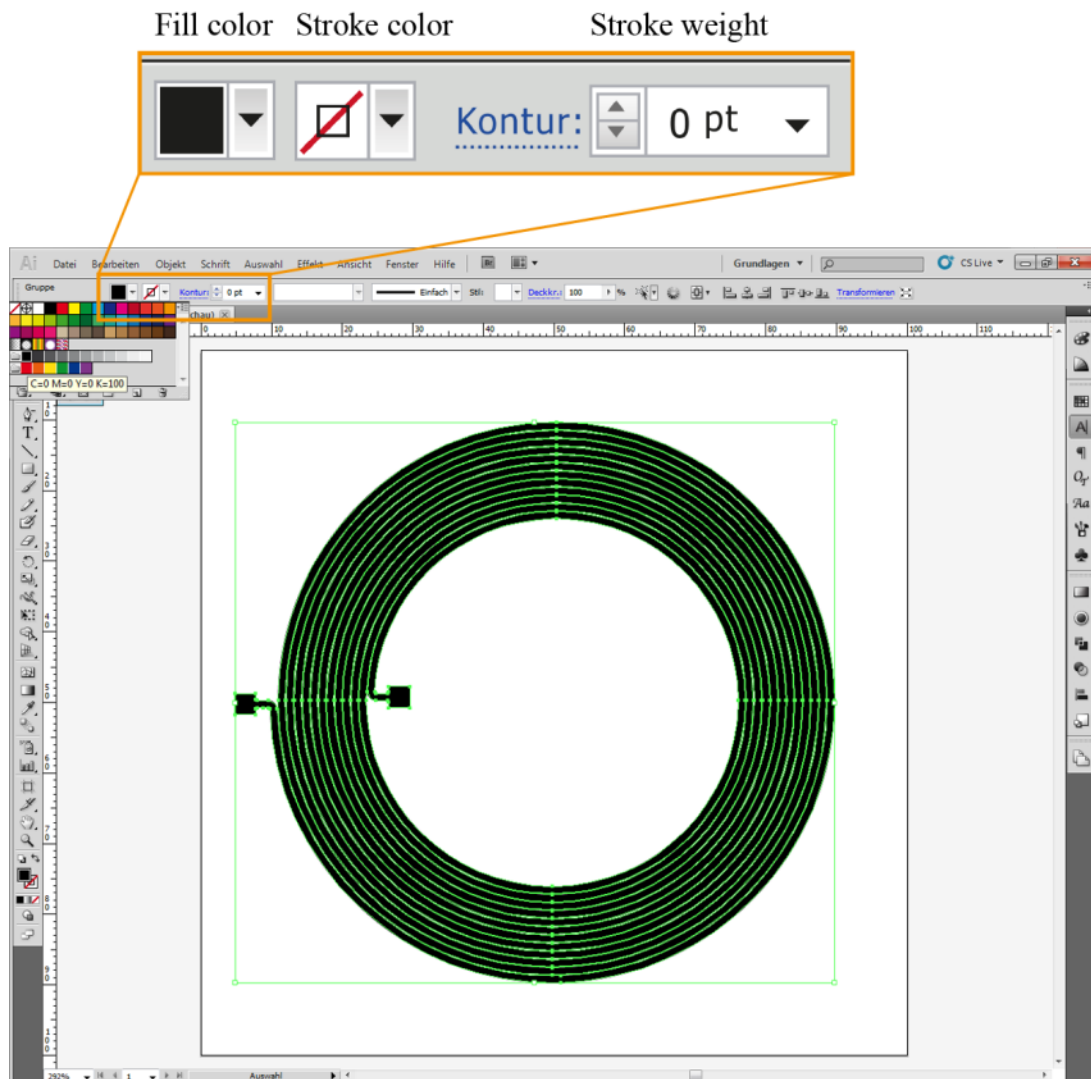


Figure 4.10: The Fill color is changed to black, the Stroke color stays empty, and the Stroke weight stays on 0.

By the done settings, can be assured that the dimensions of printing area in the artwork are not expanded or contracted, as showed in Figure 4.11.

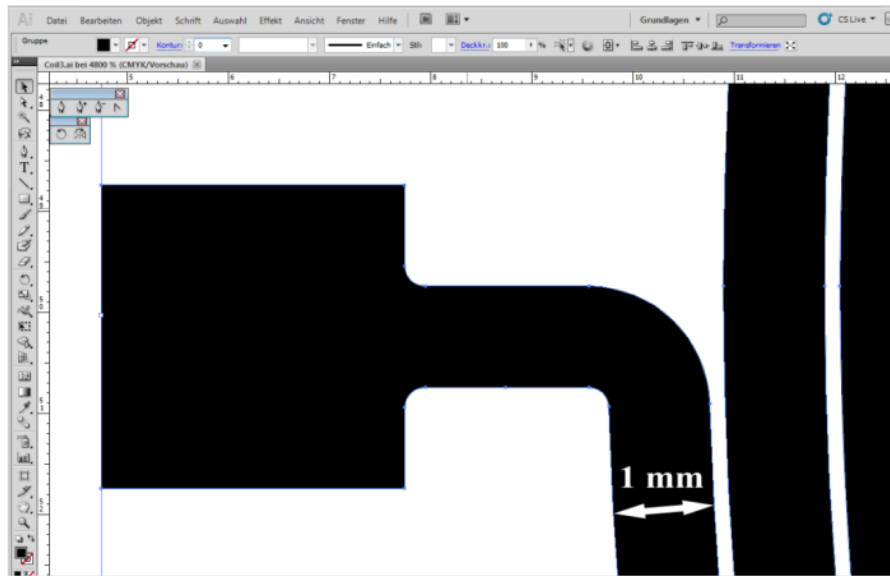


Figure 4.11: The printing area of the artwork in accurate dimensions.

Finally, the artwork is exporting as a PDF file. For setting up the PDF, the Adobe Illustrator file should be saved by using one of the versions of the Adobe Acrobat Pro (developed by Adobe Systems Incorporated) [4] as a printer for Adobe Illustrator software. The output settings are definable, as represented in Figure 4.12.

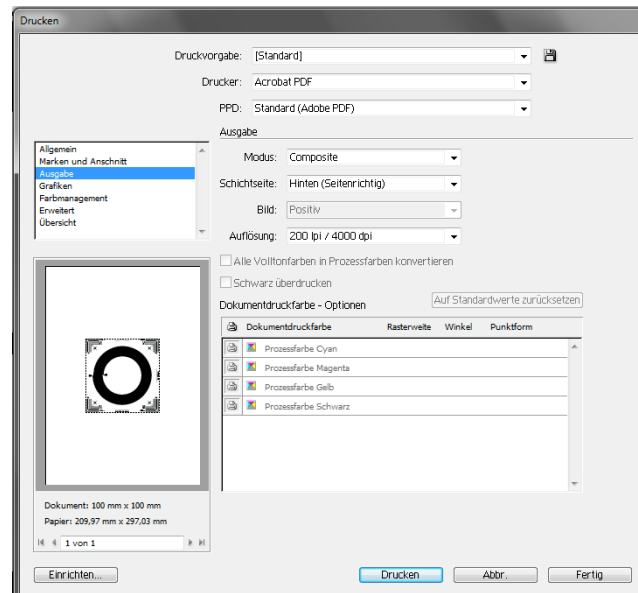


Figure 4.12: The settings of the PDF file can be defined in printer settings of the Adobe Illustrator software. One of the versions of the Adobe Acrobat Pro should be selected as the printer. The output settings are definable here.

The PDF file is checked in Adobe Acrobat software. In the panel of Output preview from the software (Figure 4.13), the black channel should be included the artwork and the other channels cyan, magenta, and yellow must be empty. The printing form is generated from black channel.

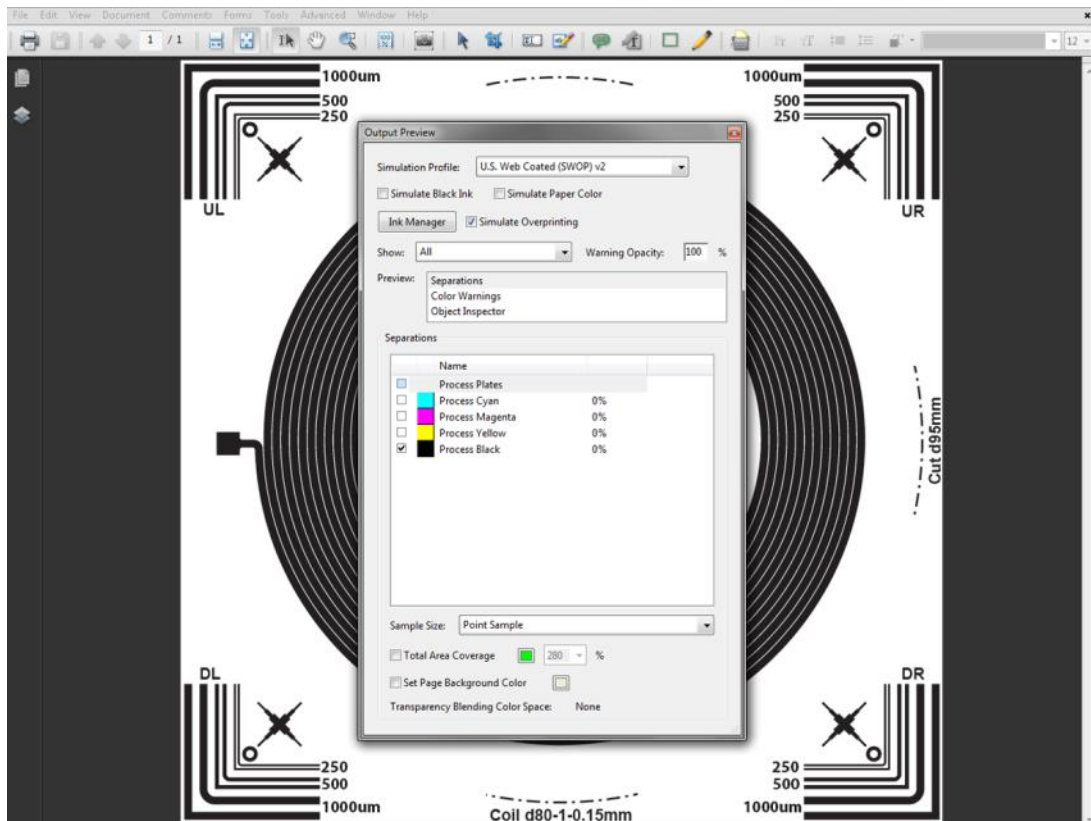


Figure 4.13: Preview of the file in Adobe Acrobat software. The black channel should be included the artwork and the other channels cyan, magenta, and yellow must be empty.

4.2 Mesh Screen

In present work, two types of mesh screens are utilized: polyester mesh and stainless steel mesh. Polyester mesh screen is used for *Preliminary* layout. Stainless steel mesh screen is used for *Comparative* and *Final* layouts.

A *Preliminary* test is done with polyester mesh screen because of availability and affordability. The samples for this part of experiment are printed by application of polyester screen monofilament SEFAR[®] PET 1500 [82] with mesh number 180 per cm, and thread diameter 27 μm . The aim is finding potential printing in conductive tracks of

spiral antennas. The mesh number 180 per cm is normally acceptable for printing small details, but there are some problems with transferring high-viscosity silver inks in fine lines. Additionally, the film thickness of printed inks is relatively low. Decreasing in ink thickness caused to decrease conductivity and accordingly, the power efficiency of the antennas.

The *Comparative* layout and *Final* layout are made from stainless steel mesh screen for the reason of ink thickness development on substrate. The samples are printed by application of stainless steel screen Gallus [29] with mesh number 63 per cm, and thread diameter 36 μm . The mesh number of 63 per cm, in compare to mesh number 180 per cm in *Preliminary* test, is an acceptable number for increasing the film thickness of printed inks. Although there are some limits on fine line deposition. An experimental test on *Final* layout with stainless steel screen 63 per cm approved that the values less than 150 μm for track spacing can increase the risk of ink bleed out and short circuits in printed antennas. Figure 4.14 shows the screens of *Comparative* layout and *Final* layout.

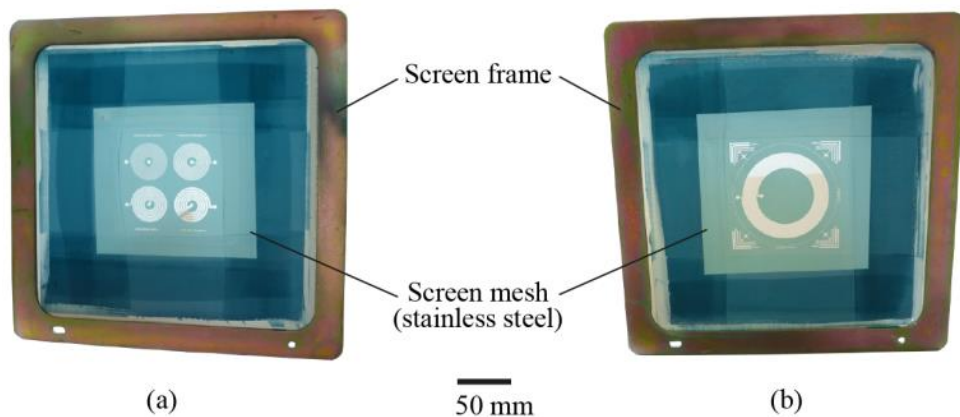


Figure 4.14: Stainless steel mesh screens of the printed antennas with mesh number 63 per cm, and thread diameter 36 μm from Gallus [29]. (a) *Comparative* layout, and (b) *Final* layout.

4.3 Ink

In this research, three types of silver inks are utilized for printing the samples:

- Silver ink *NCS-500AG* from Nicomatic [64]
- Silver ink *SunTronic™ PTF Silver CXT-0644* from Sun Chemical [90]
- Silver ink *Acheson Electrodag PF-050* from Henkel [37]

Silver ink NCS-500AG is used in *Preliminary* test with polyester screen. That is a polymer thick film conductor ink contains silver. Its volume resistivity is $\leq 0.5 \times 10^{-4}$ $\Omega/\text{sq cm}$ with solids content 65%. The printed line thickness of ink with polyester screen 270 mesh (presumably in inches) is 5 ± 1 microns. The curing conditions are 120 °C for 2-3 minutes, or 115 °C for 3-5 minutes [64]. Because of low conductivity achieved by NCS-500AG, this ink would not be used in further layouts. The data sheet of the ink is included in Appendix A2.

Silver ink CXT-0644 is used for printing the *Comparative* layout with a stainless steel mesh screen. That is a conductive ink with silver pigments and thermoplastic binder. Its volume resistivity after curing in 150 °C for 30 minutes is $< 2.5 \times 10^{-5}$ Ω/cm , with solids content 82-85% at 120 °C. Fine resolution < 100 microns can be achieved by the ink. The curing conditions are 120-200 °C for 2-30 minutes. In present work, 3% solvent ER-SOLV04 is mixed with the ink for better printability [90]. The relative conductivity and printability of CXT-0644 is not so good to be used for printing the *Final* layout. The data sheet of the ink is included in Appendix A3.

Silver ink PF-050 is used for printing the *Comparative* layout and *Final* layout with stainless steel mesh screens. It is a thermoplastic base ink with silver type filler. Its volume resistivity after curing is < 0.01 $\Omega/\text{sq/mil}$, with solids content 68.5% for uncured material. Recommended Thickness of screen printed ink after drying is 7.5 to 12.5 μm . The curing conditions are 121 °C for 15 minutes or 140 °C for 3 minutes [37]. The data sheet of the ink is included in Appendix A4.

4.4 Printing Procedure and Curing

The type of printing process is off-contact. All of the samples are printed with a screen printing machine Kammann-K15Q SL at IDD (Institut für Druckmaschinen und Druckverfahren, TUD). Kammann-K15Q SL is a laboratory printer with motor driven squeegee and cross table 300 mm x 200 mm high accuracy ± 0.01 mm. The maximum printing area is 150 mm x 150 mm [48]. The screen printing machine that is used for printing the samples is represented in Figure 4.15.



Figure 4.15: Screen printing machine Kammann-K15Q SL at IDD, that applied for printing the samples.

The *Preliminary* layout is printed by application of silver ink NCS-500AG. The printing screen is polyester mesh monofilament with mesh number 180 per cm and thread diameter 27 μm . The printing setting is pressure 5 bar, speed 0.50 m/s, printing length 130 mm, snap-off 2 mm, squeegee angle 75 degrees, blade type sharp edge and Shore hardness 90°A.

The *Comparative* layout is printed by application of two types of silver inks: CXT-0644 and PF-050, as described in previous part. CXT-0644 is mixed with 3% solvent ER-SOLV04 for better printability. The printing screen is stainless steel screen with mesh number 63 per cm and thread diameter 36 μm for both of inks. The printing setting for ink CXT-0644 is pressure 6 bars and speed 0.40 m/s, while for PF-050 is pressure 5 bars and speed 0.50 m/s. Other settings for both of them are like the same: printing length 130 mm, snap-off 2 mm, squeegee angle 75 degrees, blade type round edge with Shore hardness 75°A.

The number of samples in *Comparative* layout is decreased to four patterns. The samples are concentrated at the middle of screen for the reason of more homogeneity in

film thickness of the ink. Figure 4.16 shows the maximum printing area of the screen and the occupied area by the antennas.

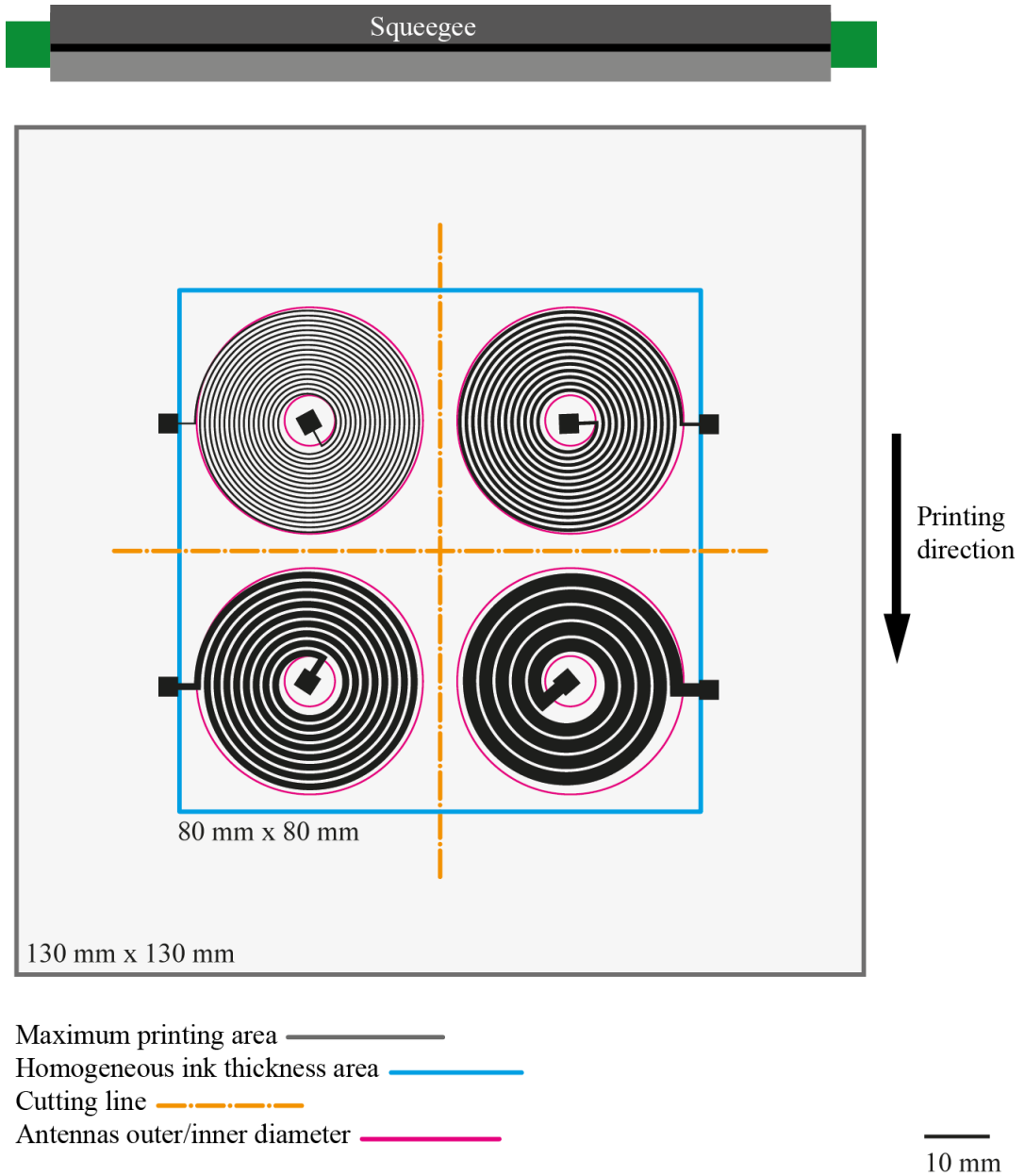


Figure 4.16: Better ink thickness homogeneity is observed inside blue border. Maximum printing area, inner diameter, and outer diameter of the antennas are represented, too. The dashed lines show the cutting paths for separation of samples after curing.

The *Final* layout is printed by application of silver ink Acheson Electrodag PF-050. The printing screen is stainless steel with mesh number 63 per cm and thread diameter 36

μm for both of inks. The printing setting is pressure 5 bar, speed 0.50 m/s, printing length 130 mm, snap-off 2 mm, squeegee angle 75 degrees, blade type round edge with Shore hardness 75°A.

In present experiment, all samples are printed on transparent films made of biaxially oriented polyethylene terephthalate (PET). The PET films are Hostaphan® GN 4600 with one side treated [61]. The data sheet of the substrate is included in Appendix A5.

After drying printed samples in room temperature, they are cured in electric oven with hot air circulation. The curing conditions of silver ink NCS-500AG is 115 °C for 5 minutes, CXT-0644 is 150 °C for 30 minutes, and PF-050 is 121 °C for 15 minutes.

Figure 4.17 shows the image of antennas after curing.

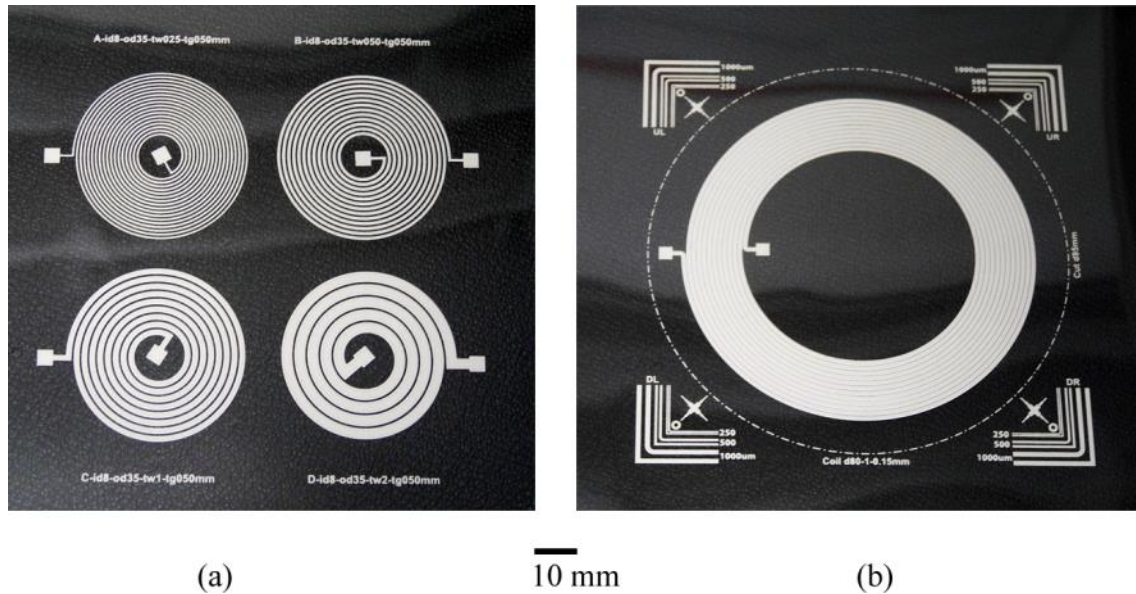


Figure 4.17: Printed samples of the antennas, (a) *Comparative* layout, and (b) *Final* layout. The samples placed on dark background to achieve a higher contrast in photography.

4.5 Experiments

Practical part of present research includes printing the antennas. As mentioned previously in Figure 4.1, the variables of experiment are:

- Layout
- Screen
- Ink

Three layouts are designed for this research:

- *Preliminary* layout
- *Comparative* layout
- *Final* layout

Two types of mesh screens are applied for printing the layouts:

- Polyester mesh
- Stainless steel mesh

Three screens are made for printing the layouts:

- Polyester mesh (for *Preliminary* layout)
- Stainless steel mesh (for *Comparative* layout)
- Stainless steel mesh (for *Final* layout)

Three types of conductive silver inks are used for printing the layouts:

- NCS-500AG from Nicomatic
- CXT-0644 from Sun Chemical
- PF-050 from Henkel

Four printing experiments are done with conductive silver inks:

- NCS-500AG (for *Preliminary* layout)
- CXT-0644 Chemical (for *Comparative* layout)
- PF-050 (for *Comparative* layout)
- PF-050 (for *Final* layout)

Table 4.4 represents number of experiments based on variables and the relation between them. The number of printed samples for every experiment is 20.

Table 4.4: Number of experiments

Layout	Screen	Ink	Number of printed samples
<i>Preliminary</i>	Polyester	NCS-500AG	20
<i>Comparative</i>	Stainless steel	CXT-0644	20
<i>Comparative</i>	Stainless steel	PF-050	20
<i>Final</i>	Stainless steel	PF-050	20

5 Electrical Characterization

This chapter aims to explain the electrical measurement setup that has been applied for characterization of printed antennas. The chapter includes two parts: setup definition, and categorization of printed samples for measurement.

5.1 Setup Definition

In present research, a network analyzer E5061B Agilent Technologies is applied for measurement and characterization of printed antennas. Figure 5.1 shows the instrument. That is an ultimate general-purpose network analyzer and covers the frequency ranges of 5 Hz to 3 GHz.

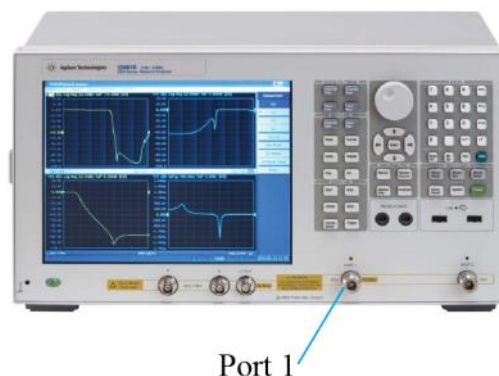


Figure 5.1: Network analyzer Agilent E5061B that is used for measurement and characterization of printed antennas [7]. The test port 1 is used for measurements.

Measurement and characterization of printed antennas are done with reflection method (see sub-chapter 2.5). The printed samples are connected to the port 1 of network analyzer. The frequency is swept from 100 Hz to 40 MHz with intermediate frequency bandwidth (IFBW) 30 kHz. For most of the samples, the first resonance frequency is appeared in this range of frequency. The reflection parameters are plotted on display including magnitude and phase angle of impedance spectrum, in relation to frequency. The inductance, resistance, and parasitic capacitance of printed antennas are calculated

based on a relevant equivalent RLC model (see sub-chapter 2.4.4). Figure 5.2 demonstrates the schematic diagram of measurement setup.

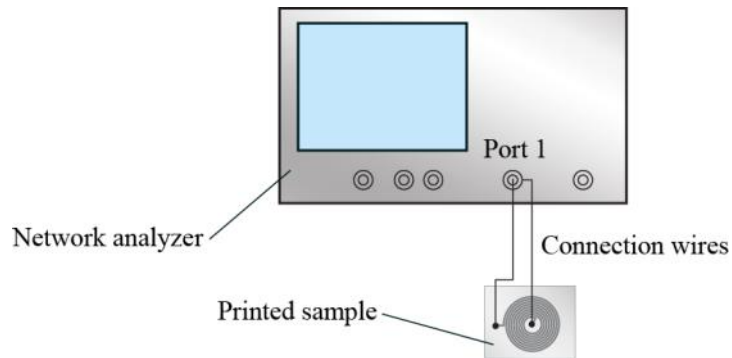


Figure 5.2: Schematic diagram of measurement setup. The printed samples are connected with connection wires to the port 1 of network analyzer.

Setting of Lumped RLC Model

Network analyzer E5061B can provide five types of equivalent circuit models, as represented in Figure 5.3. These models can be used for calculation of RLC approximate values based on measurement data. Model *A* can be applied for inductors with high core loss. Model *B* is mostly useful to analyze general inductors and resistors. Model *C* is suited for resistors with high resistance, as well as model *D* for capacitors. Model *E* can be used for resonators and oscillators [8]. In present work, model *B* is applied for characterization of printed antennas. *C* is parasitic capacitance, *L* is inductance, and *R* is loss resistance.

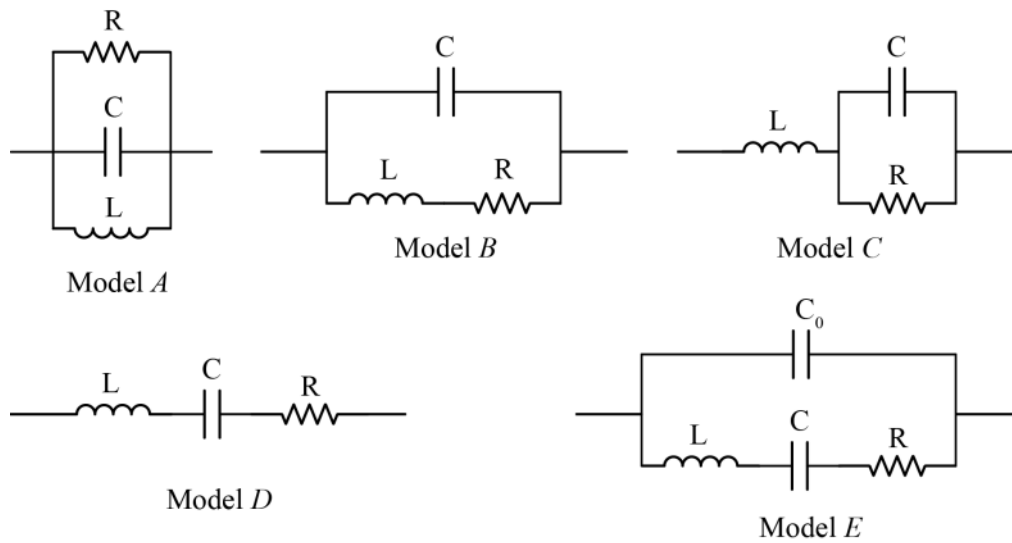


Figure 5.3: Equivalent circuit models for calculation of RLC approximate values in network analyzer. Model A, B, C, D, and E can be applied for high core loss inductors, general inductors, high resistance resistors, capacitors, and resonators, respectively [8]. In present work, model B is used for characterization of printed antennas.

The measurement parameter of model B is based on absolute value of impedance and phase ($|Z|-\theta$). The $|Z|$ at vertical axis is logarithmic while θ at vertical axis is linear. The sweep type is logarithmic [8]. Figure 5.3 represents the equivalent RLC model B that is used for characterization of printed antennas.

5.2 Categorization of Printed Samples for Measurement

The samples of *Preliminary* layout are excluded from measurements because of low conductivity achieved by the ink.

The samples of *Comparative* and *Final* layouts are included in measurements. The goal of measurement is characterization of printed samples and comparison between them. During the text, the samples of *Comparative* layout are indicated with A to D. Figure 5.4 and Table 5.1 represents the dimensional characteristics of the antennas that are included in measurements.

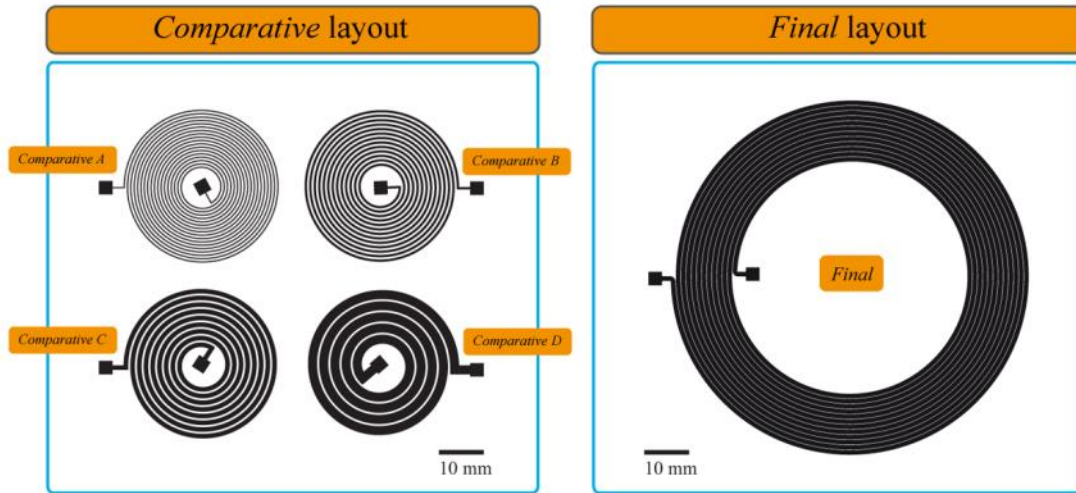


Figure 5.4: Geometric view of the antennas that are included in measurements: *Comparative A*, *Comparative B*, *Comparative C*, *Comparative D*, and *Final*. The dimensional characteristics of antennas is represented in Table 5.1.

Table 5.1: Dimensional characteristics of the antennas that are included in measurements: *Comparative A*, *Comparative B*, *Comparative C*, *Comparative D*, and *Final*. Geometric view of the antennas is showed in Figure 5.4.

Sample	Inner dia. [mm]	Outer dia. [mm]	Track width [mm]	Track spacing [mm]	Number of turns
<i>Comparative A</i>	8	35	0.25	0.50	17.66
<i>Comparative B</i>	8	35	0.50	0.50	12.99
<i>Comparative C</i>	8	35	1.00	0.50	8.31
<i>Comparative D</i>	8	35	2.00	0.50	4.57
<i>Final</i>	51.55	80	1	0.15	12

A reliable result on efficiency, optimal frequency and so on can be achieved by something like five samples per coil [99]. The number of measured samples is four for cases *Comparative A*, *Comparative B*, *Comparative C*, *Comparative D*, and *Final* layouts, with PF-050 ink. Because of some difficulties in printing the CXT-0644 ink, especially in ink transferring from screen to substrate, the number of acceptable printed

samples is limited to three for cases *Comparative C* and *Comparative D*. In addition, there is no acceptable sample for case *Comparative A* and *B*. Table 5.2 represents the number of measured samples for different layouts and inks.

Table 5.2: The number of measured samples for each part of experiment

Printed sample	Screen	Ink	Number of measured samples
<i>Comparative A</i>	Stainless steel	CXT-0644	Not printable
<i>Comparative B</i>			Not reliable for measurement
<i>Comparative C</i>			3
<i>Comparative D</i>			3
<i>Comparative A</i>		PF-050	4
<i>Comparative B</i>			4
<i>Comparative C</i>			4
<i>Comparative D</i>			4
<i>Final</i>			4

6 Results and Discussion

This chapter includes the measurement results of printed antennas. The results and discussion are represented in microscopic controlling and electrical characterization of printed antennas.

The printed samples are categorized in three different groups:

- The *Comparative* group that printed with CXT-0644 ink and includes *C* and *D* patterns. Pattern *A* is not printable with this ink. The printed samples of pattern *B* are not reliable for measurement.
- The *Comparative* group that printed with PF-050 ink and includes *A*, *B*, *C*, and *D* patterns.
- The *Final* group that printed with PF-050 ink and includes just one pattern.

The number of measured samples for first group is three, and for second and third groups is four. One sample from each group is selected to be compared with the samples of other groups. The unique sample of each group is selected based on inductance value. The inductance value of selected samples are the closest value to average inductance value of group.

The data list of all measured samples is included in Appendix A1.

6.1 Microscopic Controlling of Ink Thickness and Line Width Deviations

Although the printed samples looks good visually, but the magnified view of them shows some defects in the edges and on the surface of conductive traces, as represented in Figure 6.1. These effects can influence on efficiency of printed antennas e.g. by decreasing the track spacing and increasing the parasitic capacitance between tracks.

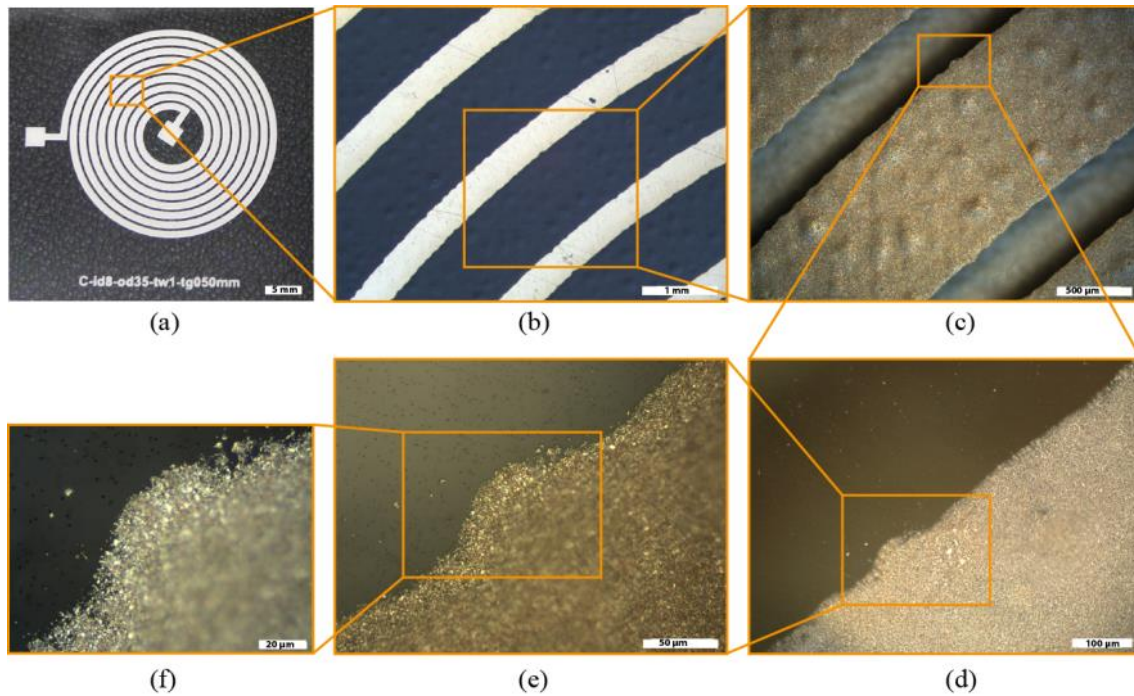


Figure 6.1: (a) The photograph, and (b-f) The microscopic view of layout *Comparative C*, printed with silver ink CXT-0644 on PET substrate. The image magnification is increasing from (b) to (f) respectively.

Deposition of silver ink on substrate contains some defected parts that can influence on efficiency of printed antennas.

The track width and track gap of some printed samples are measured by the application of a Leica DM4000 M microscope [52] (lenses ranging from 2.5x to 100x), and the Leica Application Suite software [51]. Figure 6.2 shows the microscopic image of printed samples, including *Comparative C* (Figure 6.2 (a)) and *Comparative D* (Figure 6.2 (b)), both of them printed with silver ink CXT-0644; and also *Comparative A* (Figure 6.2 (c)), *Comparative B* (Figure 6.2 (d)), *Comparative C* (Figure 6.2 (e)), *Comparative D* (Figure 6.2 (f)), and the *Final* (Figure 6.2 (g)) that all of them printed with silver ink PF-050. Table 6.1 contains the nominal and measured track width and track gap of printed samples that represented in Figure 6.2 (a-g). The measured sizes of track width and track gap of printed samples are more and less than nominal size of them, respectively.

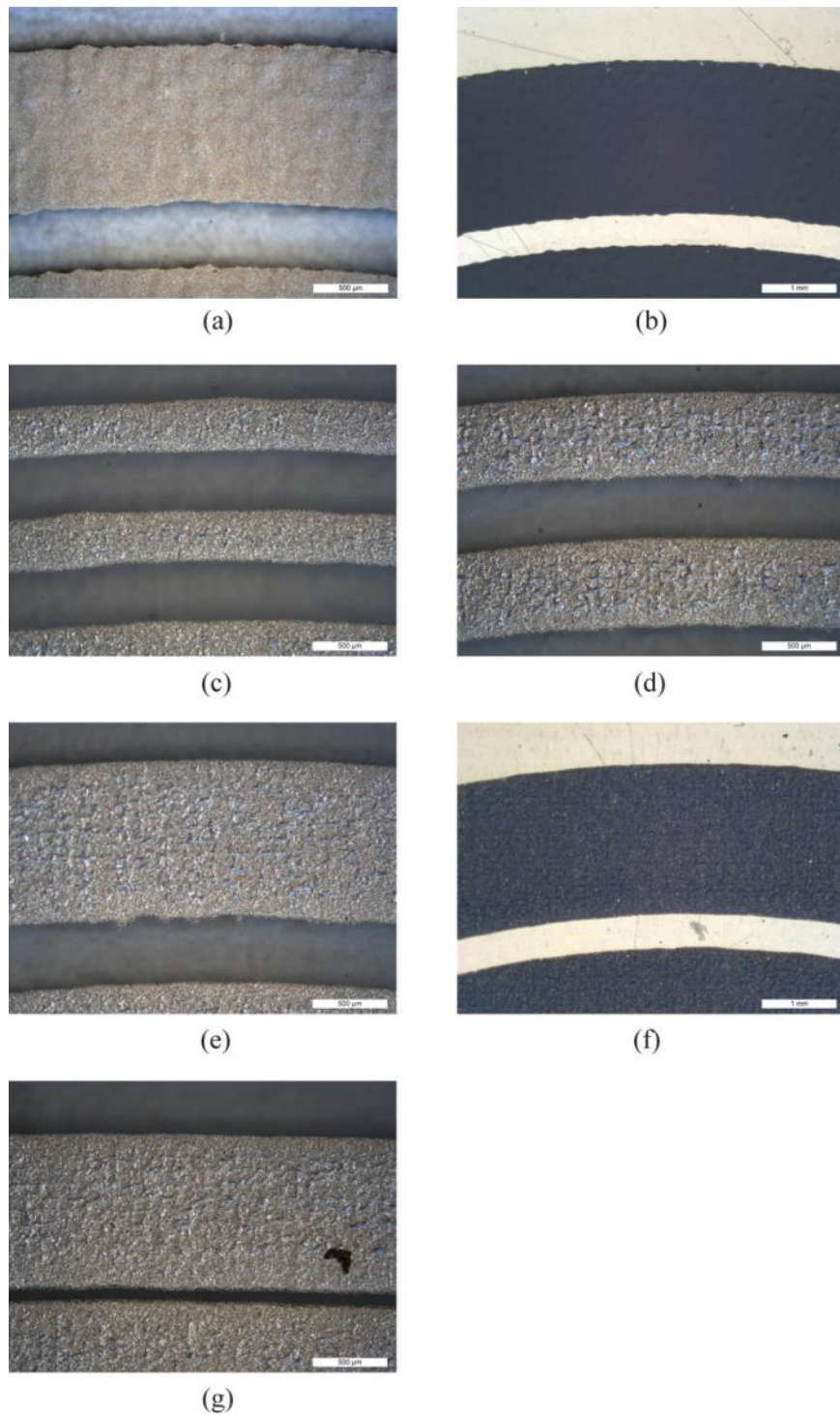


Figure 6.2: The microscopic image of printed samples: (a) *Comparative C* (silver ink CXT-0644), (b) *Comparative D* (silver ink CXT-0644), (c) *Comparative A* (silver ink PF-050), (d) *Comparative B* (silver ink PF-050), (e) *Comparative C* (silver ink PF-050), (f) *Comparative D* (silver ink PF-050), (g) *Final* (silver ink PF-050). The nominal and measured track width and track gap of printed samples represented in Table 6.1.

Table 6.1: The nominal size and measured size of track width and track gap of printed samples that represented in Figure 6.2, including *Comparative C* (Figure 6.2 (a)) and *Comparative D* (Figure 6.2 (b)), both of them printed with silver ink CXT-0644, and also *Comparative A* (Figure 6.2 (c)), *Comparative B* (Figure 6.2 (d)), *Comparative C* (Figure 6.2 (e)), *Comparative D* (Figure 6.2 (f)), and the *Final* (Figure 6.2 (g)) that all of them printed with silver ink PF-050. The measured size of printed samples is done with Leica Application Suite software [51]. The measured sizes of track width and track gap of printed samples are more and less than nominal size of them, respectively.

Ink	Printed sample	Nominal size		Measured size	
		Track width [μm]	Track gap [μm]	Track width [μm]	Track gap [μm]
CXT-0644	<i>Comparative C</i>	1000	500	1043.83	439.32
	<i>Comparative D</i>	2000	500	2059.80	425.33
PF-050	<i>Comparative A</i>	250	500	340.09	399.81
	<i>Comparative B</i>	500	500	550.89	424.94
	<i>Comparative C</i>	1000	500	1041.30	445.02
	<i>Comparative D</i>	2000	500	2014.64	447.02
	<i>Final</i>	1000	150	1035.27	72.75

Figure 6.3 shows one of the printed samples with silver ink CXT-0644. The most conventional disorders of printed samples with silver ink CXT-0644 are included in this figure and indicated with the numbers of 1 to 7. The numbers 1 and 2 show the pinholes on the cured ink area. In some cases, there are some discontinuous areas of the ink at the edges of printed tracks, as indicated with numbers 3 and 4. The number 5 zone shows several peaks that are repeated all around the area of printed ink. The white lines depict tangent lines of the peaks. The angle of white lines is near 45° . That is equal to screen mesh angle. The effect can be caused by transferring the ink through the mesh during printing. The numbers 6 and 7 indicate the jagged edges of printed tracks. The two arc shaped white lines show the limits of one of the jagged edges.

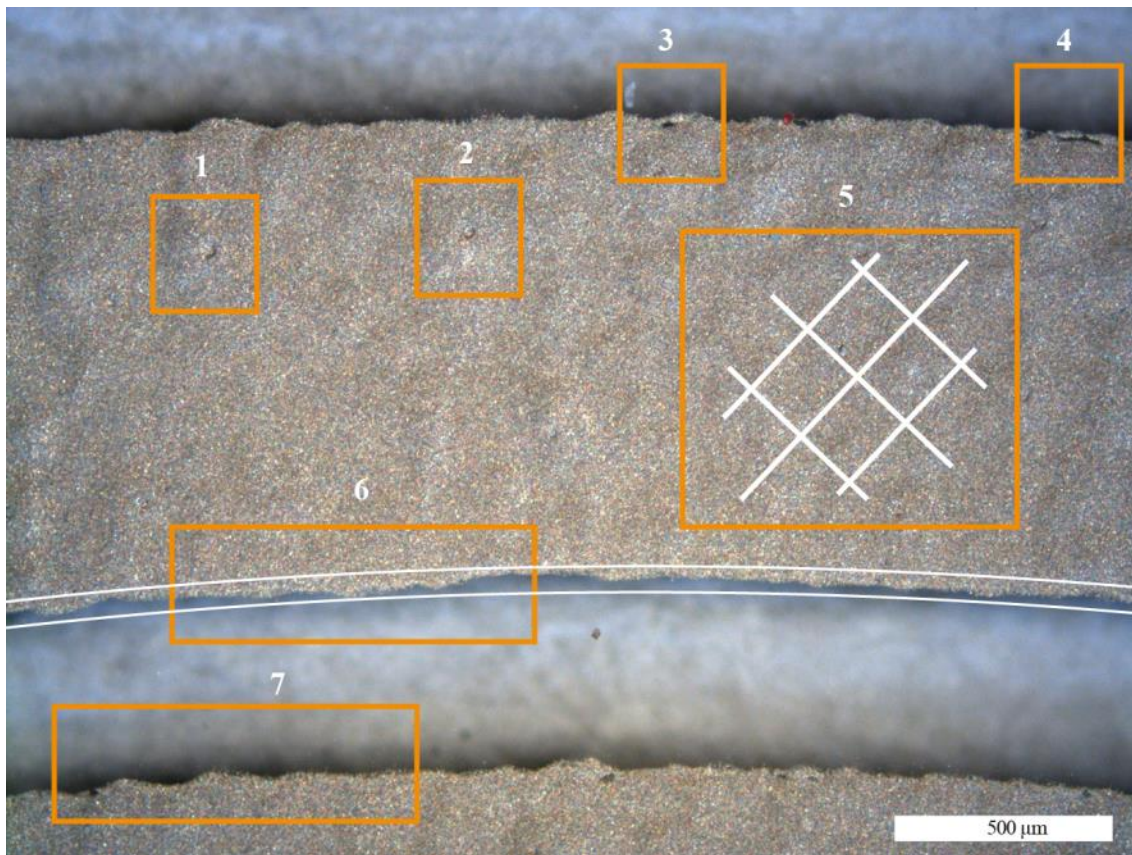


Figure 6.3: The most conventional disorders of printed samples with silver ink CXT-0644. The numbers 1 and 2 show the pinholes. The numbers 3 and 4 indicate discontinuous areas of the ink at the edges of printed tracks. The number 5 zone shows several peaks on ink area. The white lines depict tangent lines of the peaks. The numbers 6 and 7 indicate the jagged edges of printed tracks. The two arc shaped white lines show the limits of the jagged edge.

Figure 6.4 shows one of the printed samples with silver ink PF-050. The most conventional disorders of printed samples with silver ink PF-050 are included in this figure and indicated with number 1 and arc shaped white lines. The number 1 zone shows several peaks that are repeated all around the ink area. The white lines demonstrate the tangent lines of the peaks. As mentioned before about Figure 6.3, the angle of white lines is near 45° and that is equal to screen mesh angle. The effect can be caused by transferring the ink through the mesh. The two arc shaped white lines show the limits of jagged edge of the track. In rare cases, the non-inked areas are available in printed samples, as indicated with number 2.

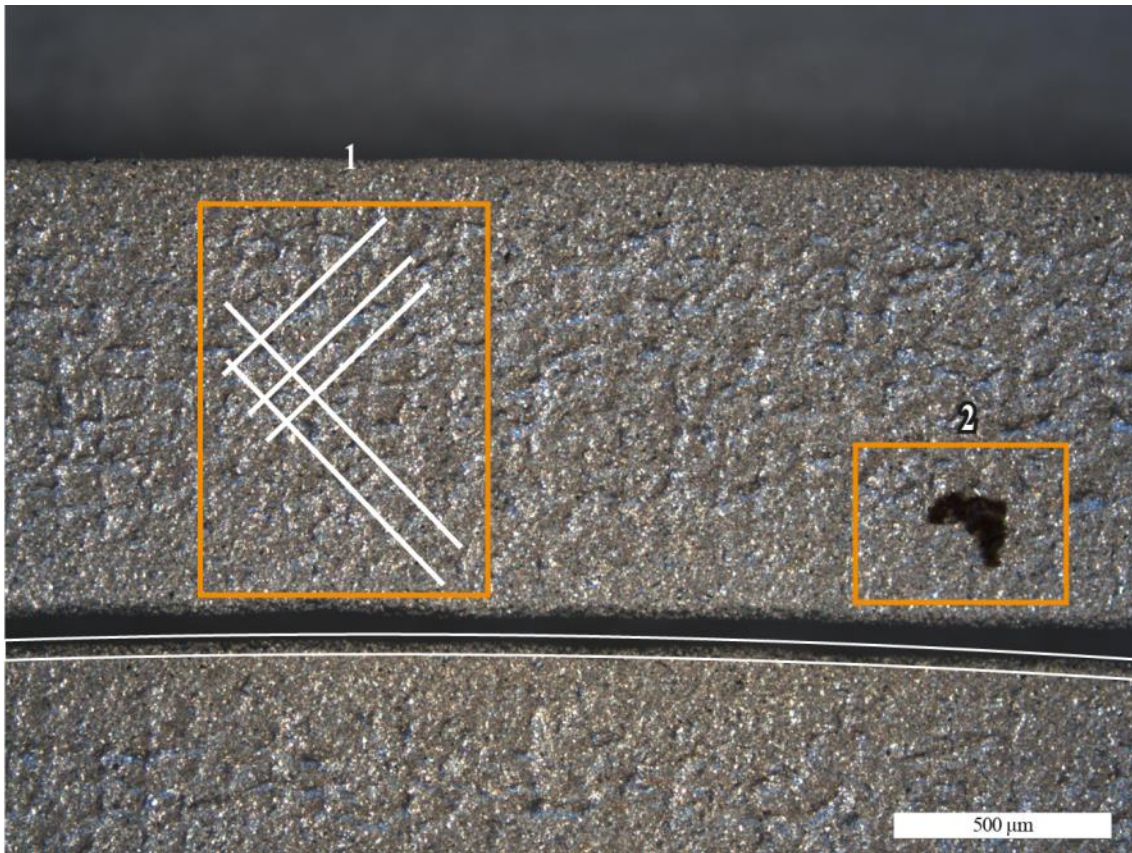


Figure 6.4: The most conventional disorders of printed samples with silver ink PF-050. The number 1 zone shows several peaks on ink area. The white lines depict tangent lines of the peaks. The two arc shaped white lines show the limits of jagged edge of the track. Number 2 indicates a non-inked area on printed sample.

To have a better view on the height deviation and the thickness of printed ink on substrate, the confocal microscopy measurement is applied on one of the printed samples by the application of a Sensofar PLu Neox microscope [83]. Figure 6.5 (a) shows a normal microscopic view of *Final* layout, printed with silver ink PF-050. Figure 6.5 (b) and Figure 6.5 (c) show the three dimensional view of printed silver ink PF-050 on PET substrate. The color spectrum from blue to red shows the minimum to maximum height, respectively. The height of printed ink is increasing steadily at the edges.

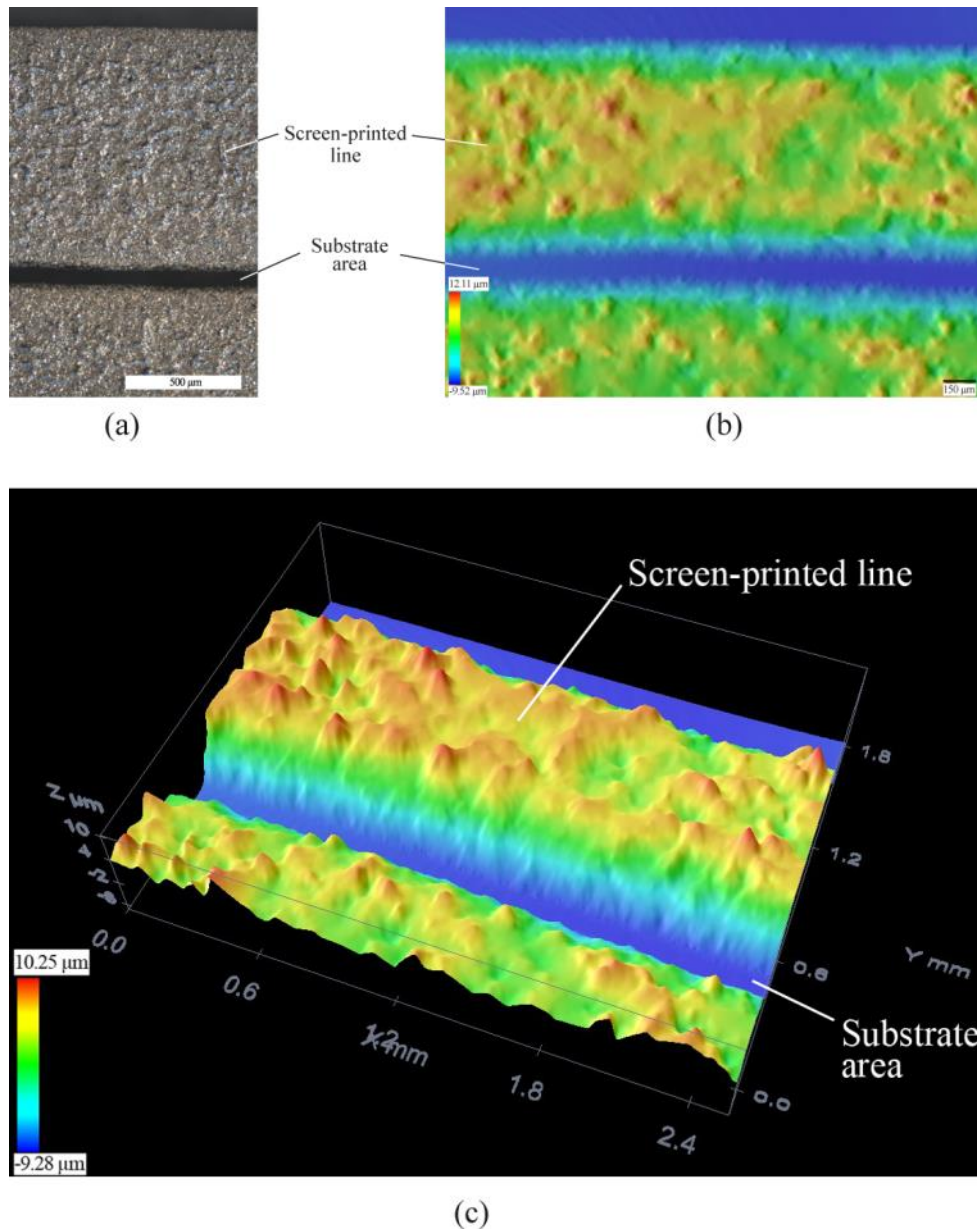


Figure 6.5: (a) Normal microscopic view of *Final* layout, printed with silver ink PF-050. (b) and (c) The confocal microscopy measurement of printed silver ink PF-050 on PET substrate. The color spectrum from blue to red shows the minimum to maximum height, respectively. The height of printed ink is increasing steadily at the edges.

The height deviation of printed sample (*Final* layout, printed with silver ink PF-050) is represented in Figure 6.6 and Table 6.2. The table contains the height value of 5 different points of printed sample. The average value, maximum, minimum, and standard deviation of measured sample points are 13.34 μm, 14.23 μm, 12.66 μm, and 0.64 μm, respectively.

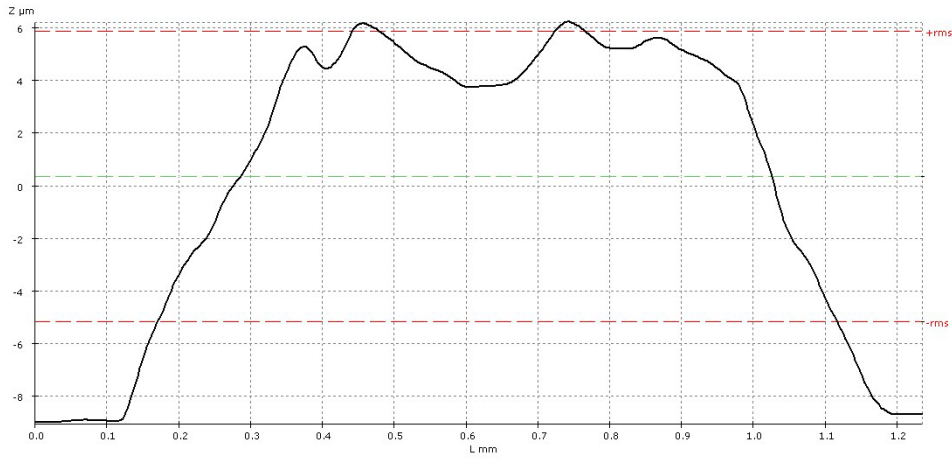


Figure 6.6: The height deviation of printed sample (*Final* layout, printed with silver ink PF-050). The horizontal axis represents the track width L value in mm, and the vertical axis shows the height of printed ink Z in μm .

Table 6.2: The height value of 5 different points of printed sample (*Final* layout, printed with silver ink PF-050) that represented in Figure 6.6. The average value, maximum, minimum, and standard deviation of measured sample points are included in table, too.

Measured sample points	Ink thickness				
	dz [μm]	Average dz [μm]	Maximum dz [μm]	Minimum dz [μm]	Standard deviation dz [μm]
Sample point 1	13.94	13.34	14.23	12.66	0.64
Sample point 2	12.66				
Sample point 3	14.23				
Sample point 4	13.17				
Sample point 5	12.71				

6.2 The Influence of Design, Ink and Mesh Screen on Electrical Characteristics

In this part, the electric characteristics of printed antennas is represented, including impedance, AC and DC resistance, parasitic capacitance, inductance, frequency of resonance, quality factor, and figure-of-merit.

6.2.1 Impedance

For characterization of printed antennas, the impedance spectrum of samples is plotted based on polar form. The plots are produced by importing the comma separated values (CSV) data files from network analyzer to DIAdem 14.0.0 software (developed by National Instruments) [63]. The magnitude and phase angle of impedance spectrum, versus frequency represented in Figure 6.7 - Figure 6.15. The range of frequency is 100 Hz to 40 MHz with IFBW 30 kHz. The frequency of resonance indicated with a vertical narrow line in plots.

The Figure 6.7 and Figure 6.8 include the impedance magnitude and phase angle of *Comparative C* and *Comparative D*. Both of them are printed with CXT-0644 ink. Layout *A* is not printable with this ink, and the layout *B* samples are not reliable for measurement.

The upper diagram in Figure 6.7 shows that by increasing the frequency in layout *C*, the impedance magnitude is increased to reach to the peak level at resonance frequency. At the same level of frequency, the phase angle of impedance is reduced to 0° as depicted in lower diagram. After resonance frequency, the phase angle is decreasing because of capacitive reactance [9]. As represented in Figure 6.8, by increasing the frequency in layout *D*, the magnitude and phase angle of impedance are increasing although the resonance frequency does not appear in this range of frequency.

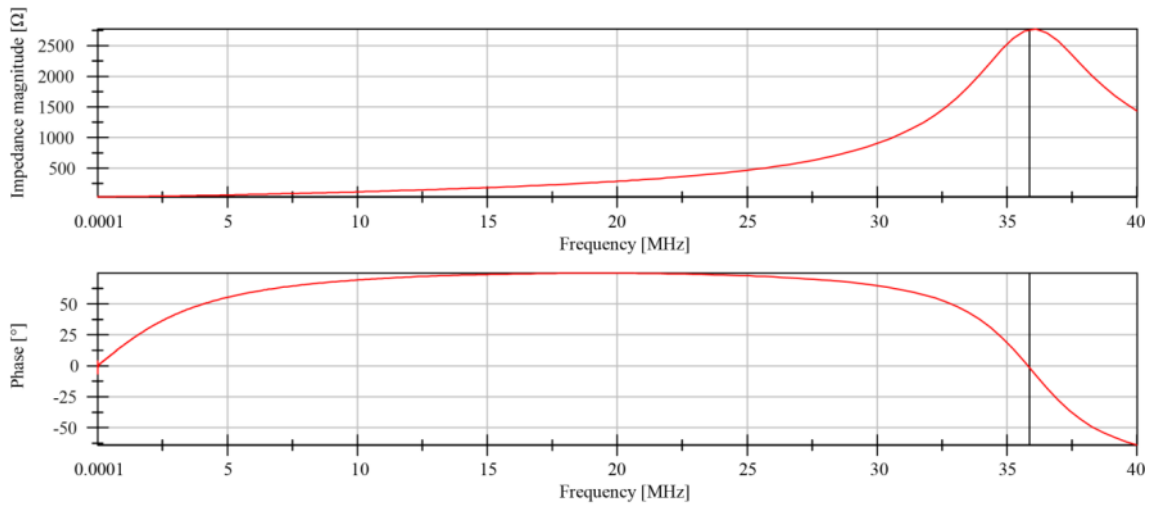


Figure 6.7: The measured impedance magnitude and phase angle of *Comparative C* with ink CXT-0644. The vertical narrow line indicates resonance frequency.

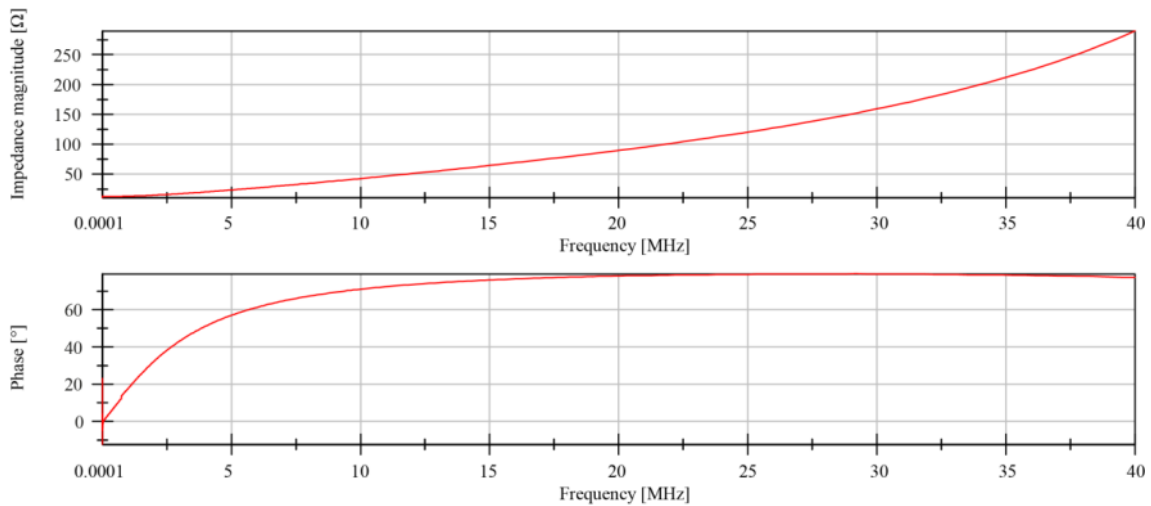


Figure 6.8: The measured impedance magnitude and phase angle of printed sample *Comparative D* with ink CXT-0644.

The Figure 6.9 - Figure 6.12 include the impedance magnitude and phase angle of *Comparative A, B, C, and D* that are printed with PF-050 ink. By increasing the track width and decreasing the number of turns in *A* to *D*, the resonance frequency increasing significantly. As well as previous samples, by increasing the frequency, the impedance magnitude is increased. The resonance frequency of samples *A, B, and C* is included in this range of frequency. The maximum impedance appears in resonance frequency while the phase angle is decreased to 0° . After resonance frequency, the impedance and

phase angle are decreasing. As depicted in Figure 6.12, frequency development in layout *D* increases the magnitude and phase angle of impedance. The resonance frequency of layout *D* is not contained in this range of frequency.

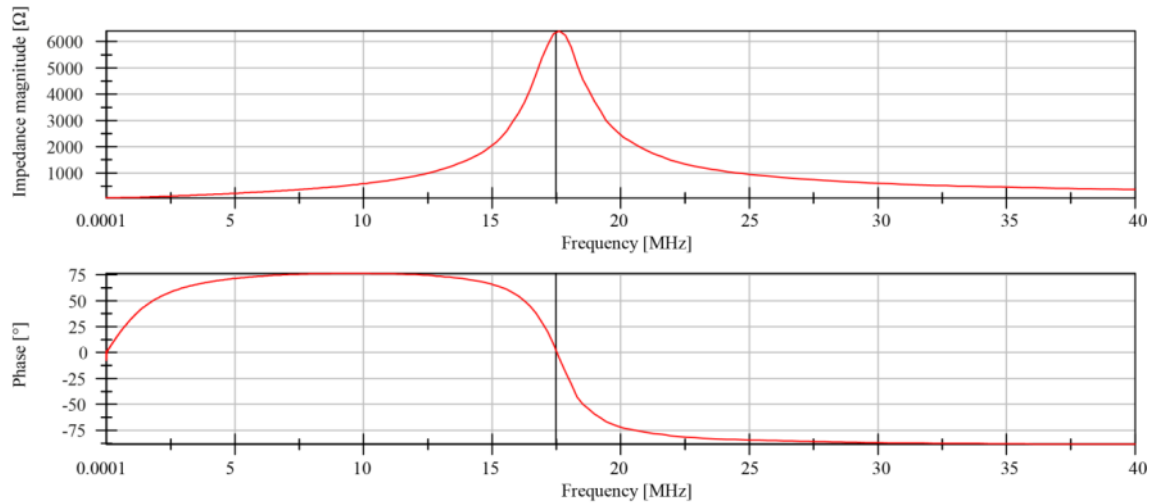


Figure 6.9: The measured impedance magnitude and phase angle of printed sample *Comparative A* with ink PF-050.

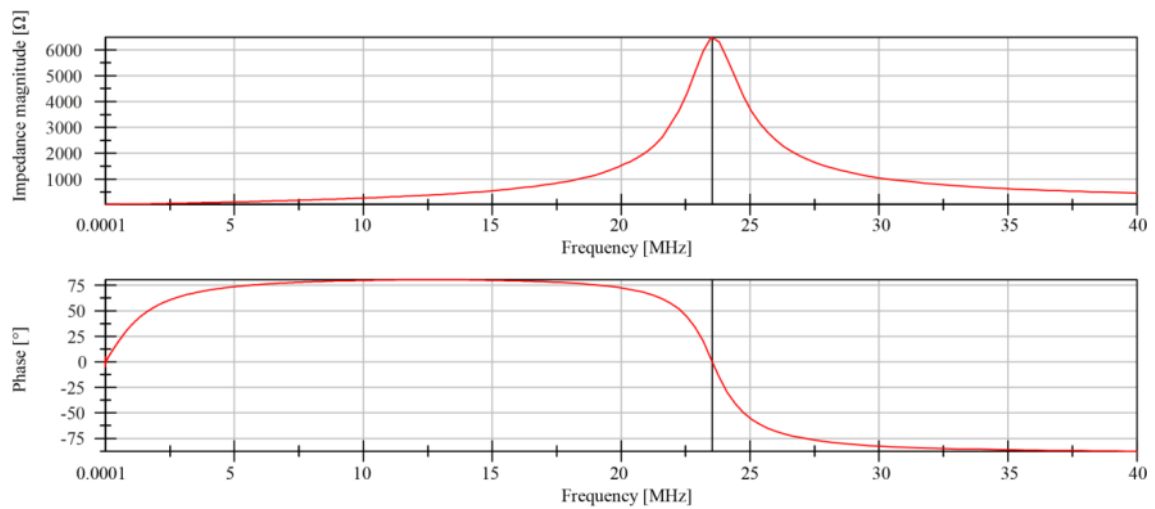


Figure 6.10: The measured impedance magnitude and phase angle of printed sample *Comparative B* with ink PF-050.

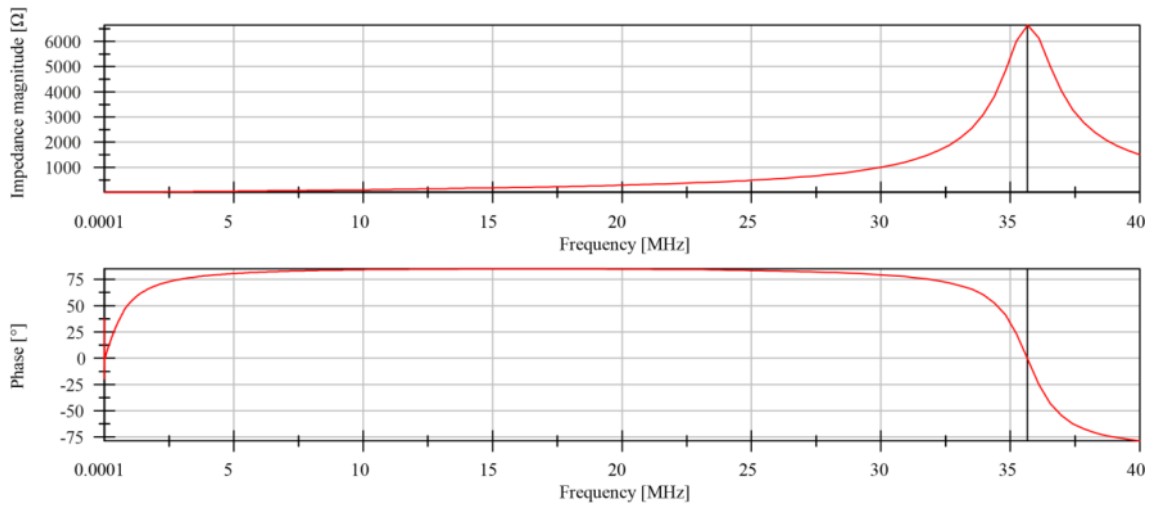


Figure 6.11: The measured impedance magnitude and phase angle of printed sample *Comparative C* with ink PF-050.

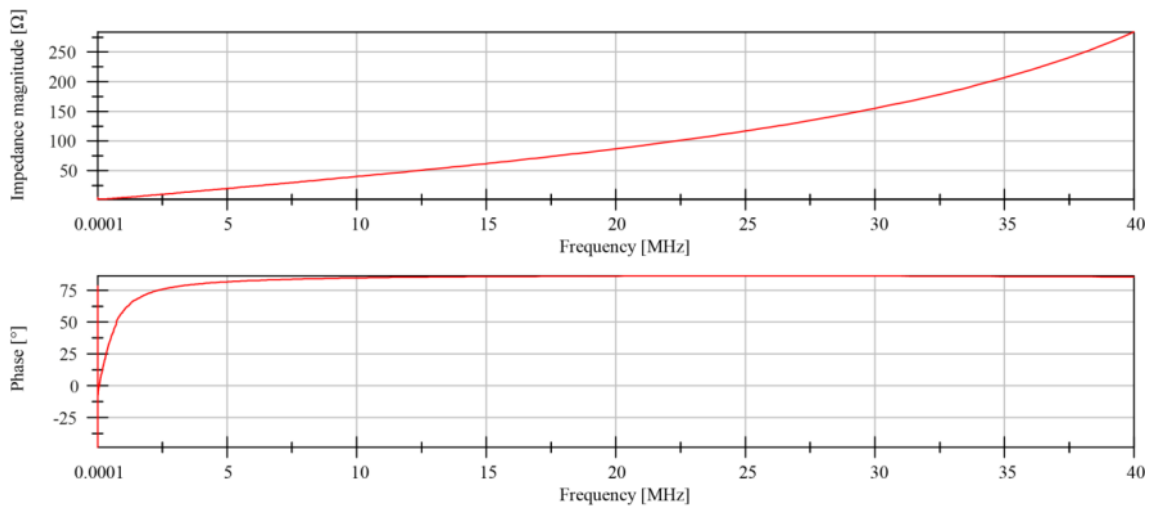


Figure 6.12: The measured impedance magnitude and phase angle of printed sample *Comparative D* with ink PF-050.

The comparison between two samples of layout *C* that are printed with different inks shows that the resonance frequency is almost equal while the impedance value is significantly changed by the type of ink. As represented in Figure 6.13 the impedance magnitude of printed antenna with ink PF-050 (lower image) is relatively more than ink CXT-0644 (upper image). Also the phase angle of printed samples with ink PF-050 exceeds to higher angle compare to ink CXT-0644. The means the printed antennas with ink PF-050 are more similar to pure inductors (Figure 6.14).

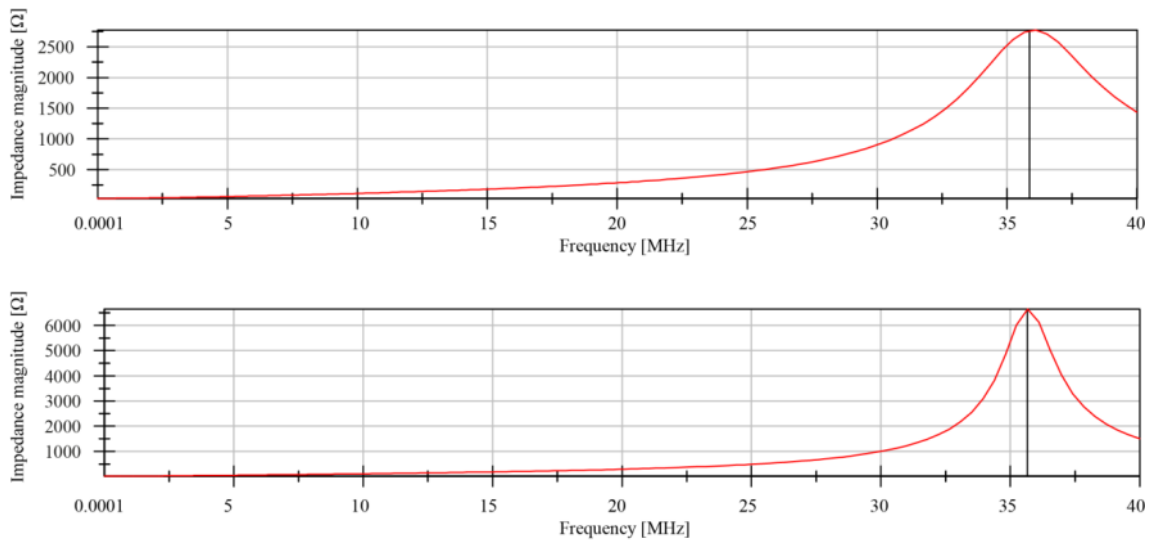


Figure 6.13: The measured impedance magnitude of *Comparative C* with ink CXT-0644 (upper image) and ink PF-050 (lower image). The vertical narrow line indicates resonance frequency.

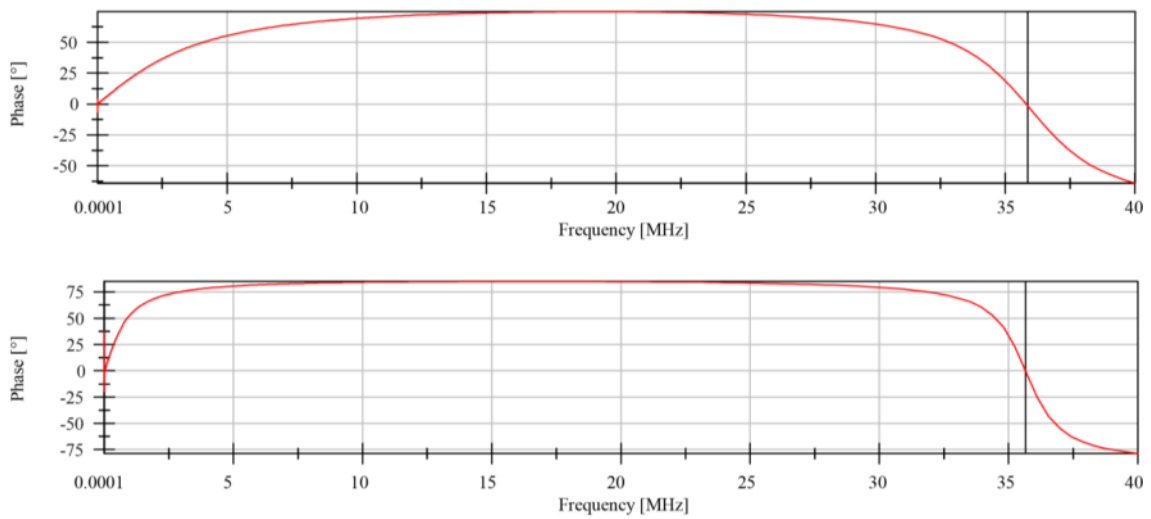


Figure 6.14: The measured phase angle of *Comparative C* with ink CXT-0644 (upper image) and ink PF-050 (lower image). The vertical narrow line indicates resonance frequency.

Figure 6.15 shows the impedance magnitude and phase angle of *Final* layout that printed with PF-050 ink. The phase angle does not exceed 90° in this sample, too. The impedance magnitude of this layout is higher than *Comparative* layout samples *A-D* that are printed with the same ink. Also, the resonance frequency is lower than other samples.

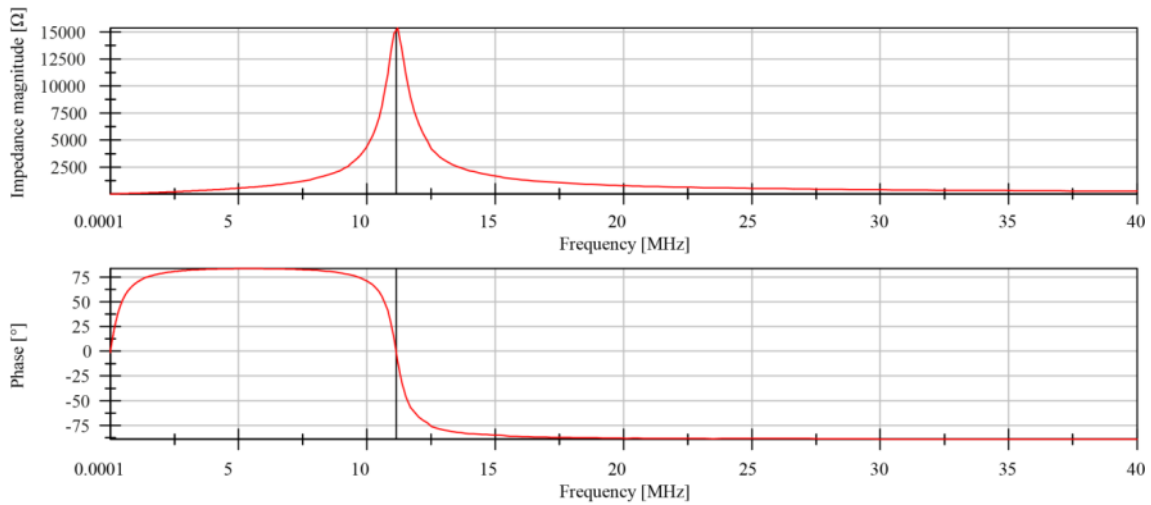


Figure 6.15: The measured impedance magnitude and phase angle of printed sample *Final* with ink PF-050.

6.2.2 AC Resistance

The AC resistance of samples is calculated by application of Equation (2.11), based on measured impedance of printed samples that represented in sub-chapter 6.2.1. The AC resistance in relation to frequency represented in Figure 6.16 to Figure 6.25. The plots are produced by importing the calculated data to DIAdem 14.0.0 software. The range of frequency is 100 Hz to 40 MHz with IFBW 30 kHz. The frequency of resonance indicated with a vertical narrow line in plots.

The Figure 6.16 and Figure 6.17 show the calculated AC resistance of *Comparative C* and *Comparative D*. Both of them are printed with CXT-0644 ink. Layout *A* is not printable with this ink, and the layout *B* samples are not reliable for measurement.

As depicted in Figure 6.16 and Figure 6.17, by increasing frequency, the AC resistance is increasing until the resonance frequency. This development of resistance can be caused by skin effect or proximity effect. The AC resistance is decreasing with the frequencies that are higher than resonance frequency that maybe caused by capacitive behavior of printed antennas, as mentioned in previous part the sub-chapter 6.2.1 for the impedance value. Layout *D* does not exceed resonance frequency (see Figure 6.17).

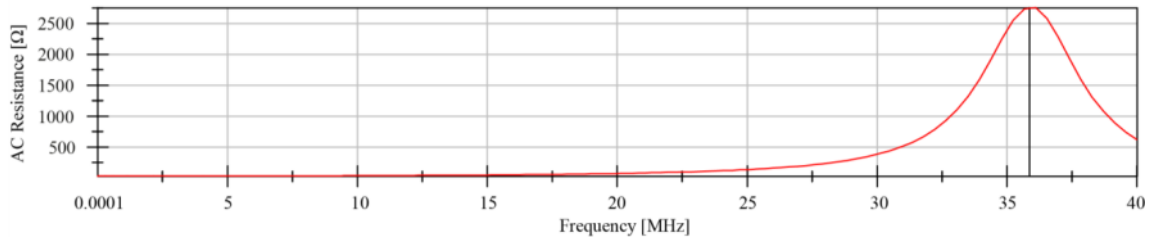


Figure 6.16: The calculated AC resistance of printed sample *Comparative C* with ink CXT-0644.

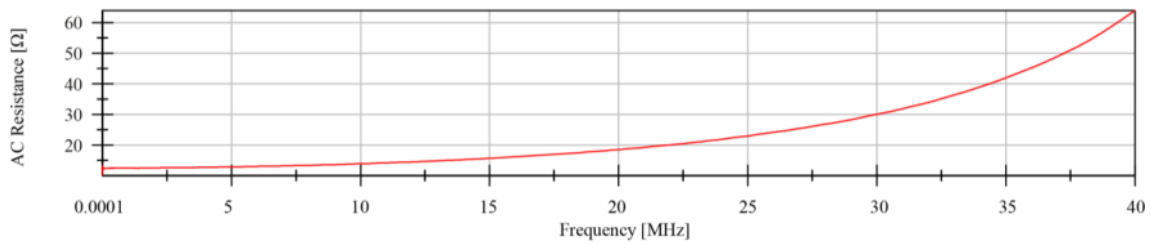


Figure 6.17: The calculated AC resistance of printed sample *Comparative D* with ink CXT-0644.

The Figure 6.18 to Figure 6.21 show the calculated AC resistance of *Comparative A*, *B*, *C*, and *D* that are printed with PF-050 ink. Like previous samples, by increasing the frequency, the AC resistance is increased. The resonance frequency of samples *A*, *B*, and *C* is included in this range of frequency. The maximum AC resistance appears in resonance frequency and then starts to decrease. As represented in Figure 6.21, frequency development in layout *D* increases the resistance while the resonance frequency of layout *D* is not included in this range of frequency.

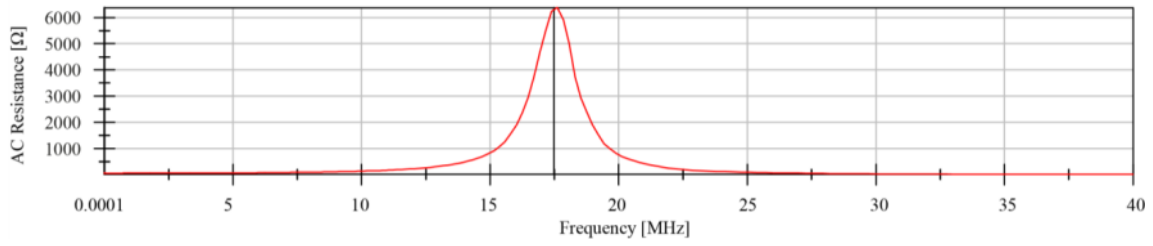


Figure 6.18: The calculated AC resistance of printed sample *Comparative A* with ink PF-050.

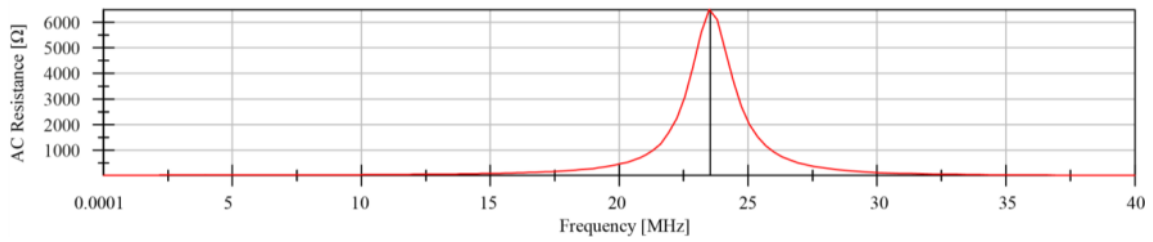


Figure 6.19: The calculated AC resistance of printed sample *Comparative B* with ink PF-050.

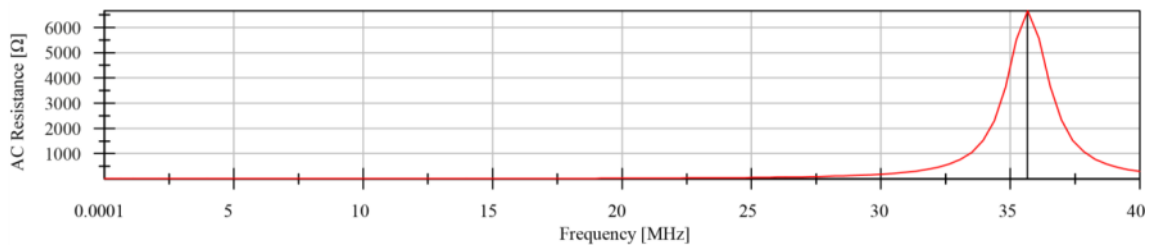


Figure 6.20: The calculated AC resistance of printed sample *Comparative C* with ink PF-050.

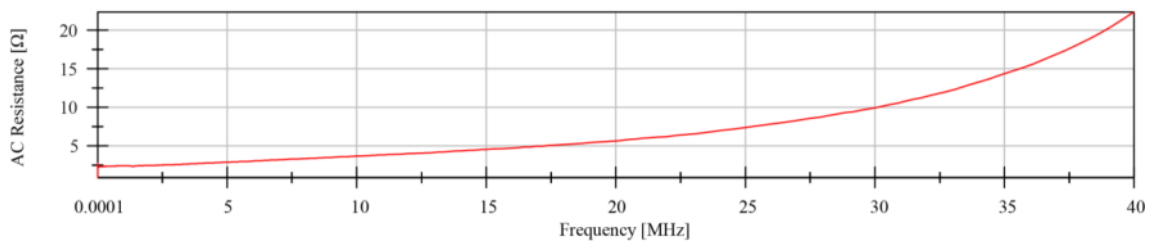


Figure 6.21: The calculated AC resistance of printed sample *Comparative D* with ink PF-050.

The calculated AC resistance of *Final* layout that printed with PF-050 ink is represented in Figure 6.22.

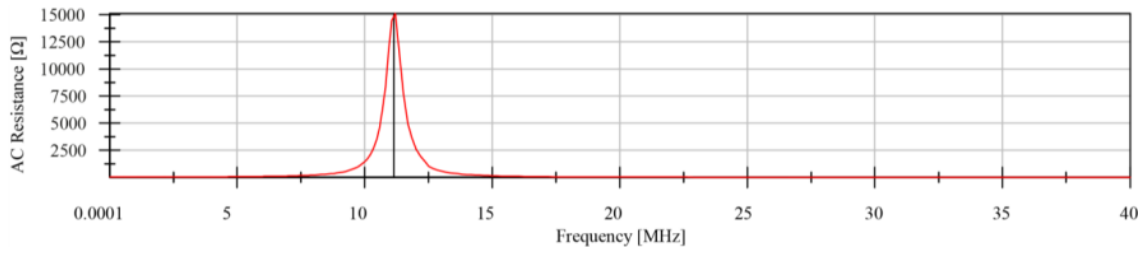


Figure 6.22: The calculated AC resistance of printed sample *Final* with ink PF-050.

Table 6.3 represents the maximum AC resistance of printed samples in frequency range 100 Hz to 40 MHz, and at resonance frequency.

Table 6.3: Maximum AC resistance of printed samples in frequency range 100 Hz to 40 MHz, and at resonance frequency.

Ink	Printed sample	Maximum AC resistance in 100 Hz to 40 MHz [Ω]	AC resistance at resonance frequency [Ω]	Resonance frequency [MHz]
CXT-0644	<i>Comparative C</i>	2751.42	2751.42	36.08
	<i>Comparative D</i>	63.92	Out of range	58.83
PF-050	<i>Comparative A</i>	6374.77	6374.77	17.57
	<i>Comparative B</i>	6482.38	6482.38	23.65
	<i>Comparative C</i>	6648.03	6648.03	35.72
	<i>Comparative D</i>	22.36	Out of range	58.83
	<i>Final</i>	15100	15100	11.20

As demonstrated in Figure 6.23 and Figure 6.24, the AC resistance of one layout that printed with two types of the ink can change significantly versus frequency.

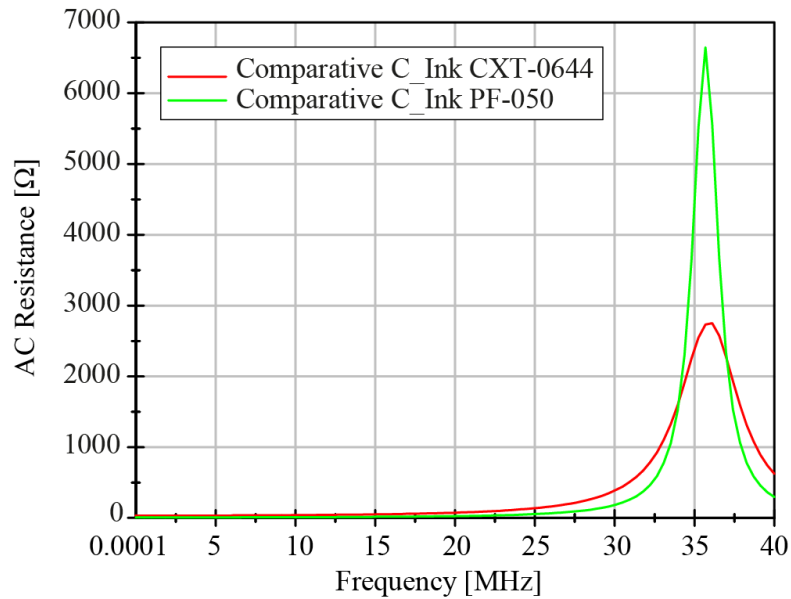


Figure 6.23: Comparison between the calculated AC resistances of printed samples *Comparative C* with two types of inks: ink PF-050 and ink CXT-0644.

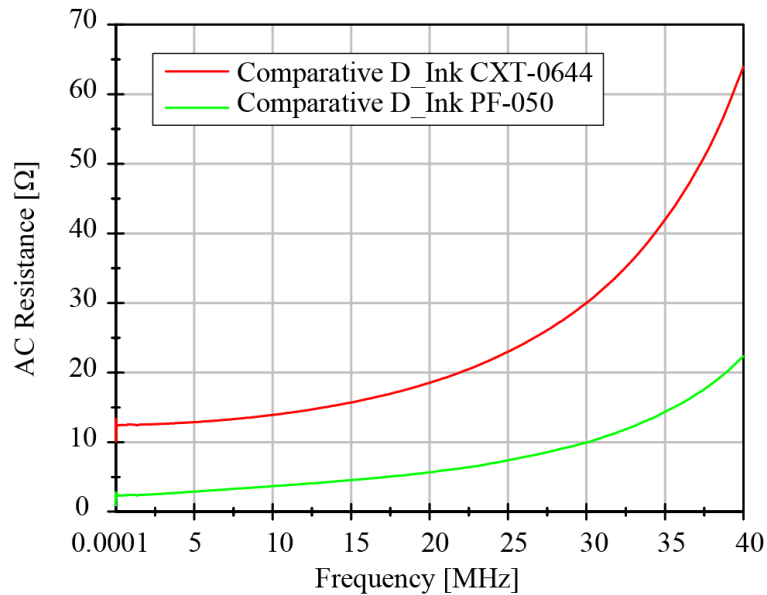


Figure 6.24: Comparison between the calculated AC resistances of printed samples *Comparative D* with two types of inks: ink PF-050 and ink CXT-0644.

Generally, in printed lines, the skin effect is more important than proximity effect [26], but according to Figure 6.25 and Table 6.4 the proximity effect can be stronger than skin effect. Figure 6.25 shows the calculated AC resistance versus frequency for different layouts that printed with the same type of the ink. Considering the track

spacing of the antennas at Table 6.4, by decreasing the gap between traces from *Comparative* layouts (0.5 mm) to *Final* layout (0.15 mm), the AC resistance is increasing (see Figure 6.25), while increasing in track length from 309.93 mm to 1193.49 mm in *Comparative* layouts *D-A* is not increasing the resistivity significantly. That means in printed samples, the proximity effect can be more effective than skin effect.

Table 6.4: Geometrical dimensions of printed samples represented in Figure 6.25. The track width, track gap, and track length are nominal dimensions and are measured with CAD software.

Ink	Printed sample	Track width [mm]	Track gap [mm]	Track length [mm]
PF-050	<i>Comparative A</i>	0.25	0.5	1193.49
	<i>Comparative B</i>	0.5	0.5	877.95
	<i>Comparative C</i>	1	0.5	562.52
	<i>Comparative D</i>	2	0.5	309.93
	<i>Final</i>	1	0.15	2477.63

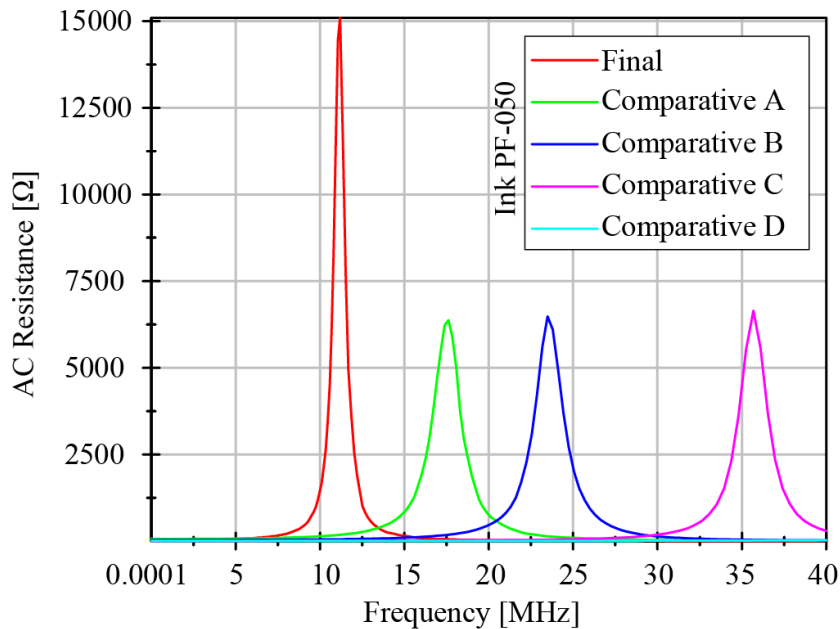


Figure 6.25: Comparison between calculated AC resistance of printed samples *Comparative A, B, C, D,* and *Final* with ink PF-050. Geometrical dimensions of printed samples is represented in Table 6.4.

6.2.3 DC Resistance

DC resistance of printed antennas is measured by application of a conventional multimeter. The measured data is very close to resistance values that are calculated by network analyzer based on equivalent RLC model (see Figure 5.3). Table 6.5 represents the measured DC resistance values for different printed antennas. Assume that the ink thickness is a constant value for all printed samples, by the application of Equation (2.8), the comparative DC conductivity can be represented as the last column of Table 6.5. The ratio of track length to track width can be significant, too.

Table 6.5: Track length, track width, the ratio of track length to track width, the measured DC resistance, and comparative DC conductivity of *Comparative A, B, C, D*, and *Final* with ink PF-050 and ink CXT-0644. The track length and track width are nominal dimensions and are measured with CAD software.

Ink	Printed sample	Geometrical dimensions			DC resistance [Ω]	Comparative DC conductivity
		Track length [mm]	Track width [mm]	Ratio of track length to track width		
CXT-0644	<i>Comparative C</i>	562.52	1	562.52	31.3	17.97
	<i>Comparative D</i>	309.93	2	154.965	9.7	15.98
PF-050	<i>Comparative A</i>	1193.49	0.25	4773.96	60.1	79.43
	<i>Comparative B</i>	877.95	0.5	1755.9	22.4	78.39
	<i>Comparative C</i>	562.52	1	562.52	7.6	74.02
	<i>Comparative D</i>	309.93	2	154.965	2.5	61.99
	<i>Final</i>	2477.63	1	2477.63	35.1	70.59

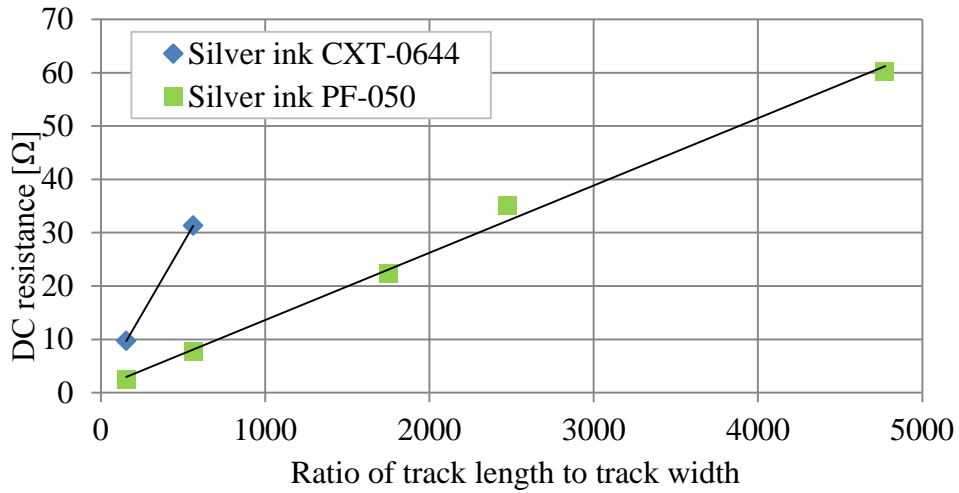


Figure 6.26: Ratio of track length to track width versus measured DC resistance for different inks and layouts. The black line shows the linear trend line of the variable points.

Figure 6.26 shows the ratio of track length to track width versus measured DC resistance. By increasing the value of this ratio, the DC resistance is increasing. Rate of the changes can be different for various inks. The slope of trend line for printed samples with CXT-0644 ink is more than PF-050 ink. Figure 6.27 depicts the effect of track length to track width ratio on comparative DC conductivity. Assume that ink film thickness is constant for all printed samples, the conductivity of PF-050 ink is more than CXT-0644 ink. Geometrical dimensions of printed samples represented in Table 6.5.

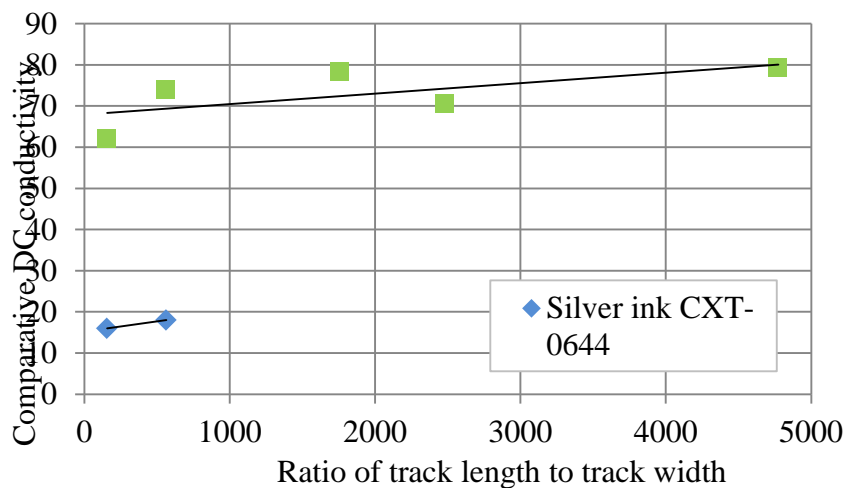


Figure 6.27: Ratio of track length to track width versus comparative DC conductivity for different inks and layouts. The black line shows the linear trend line of the variable points.

6.2.4 Parasitic Capacitance

The parasitic capacitance of samples is calculated by network analyzer, based on equivalent RLC model (see Figure 5.3). Table 6.6 represents the parasitic capacitance, track width, track spacing, track length, and number of turns for different printed antennas. The track length and track spacing are nominal dimensions and are measured with CAD software.

Table 6.6: The calculated parasitic capacitance, track width, track spacing, track length, and turn numbers of *Comparative A, B, C, D*, and *Final* with ink PF-050 and ink CXT-0644. The track length and track spacing are nominal dimensions and are measured with CAD software.

Ink	Printed sample	Parasitic capacitance [pF]	Geometrical dimensions		
			Number of turns	Track length [mm]	Track spacing [mm]
CXT-0644	<i>Comparative C</i>	12.73	8.31	562.52	0.5
	<i>Comparative D</i>	11.99	4.57	309.93	0.5
PF-050	<i>Comparative A</i>	13.22	17.66	1193.49	0.5
	<i>Comparative B</i>	12.77	12.99	877.95	0.5
	<i>Comparative C</i>	12.66	8.31	562.52	0.5
	<i>Comparative D</i>	12.07	4.57	309.93	0.5
	<i>Final</i>	14	12	2477.63	0.15

By increasing the turn numbers of antenna, the parasitic capacitance increases rapidly [53], [35]. Figure 6.28 (upper) shows the relation between parasitic capacitance and number of turns in various printed samples. Application of track length instead of turn numbers can be significant too (Figure 6.28 (lower)).

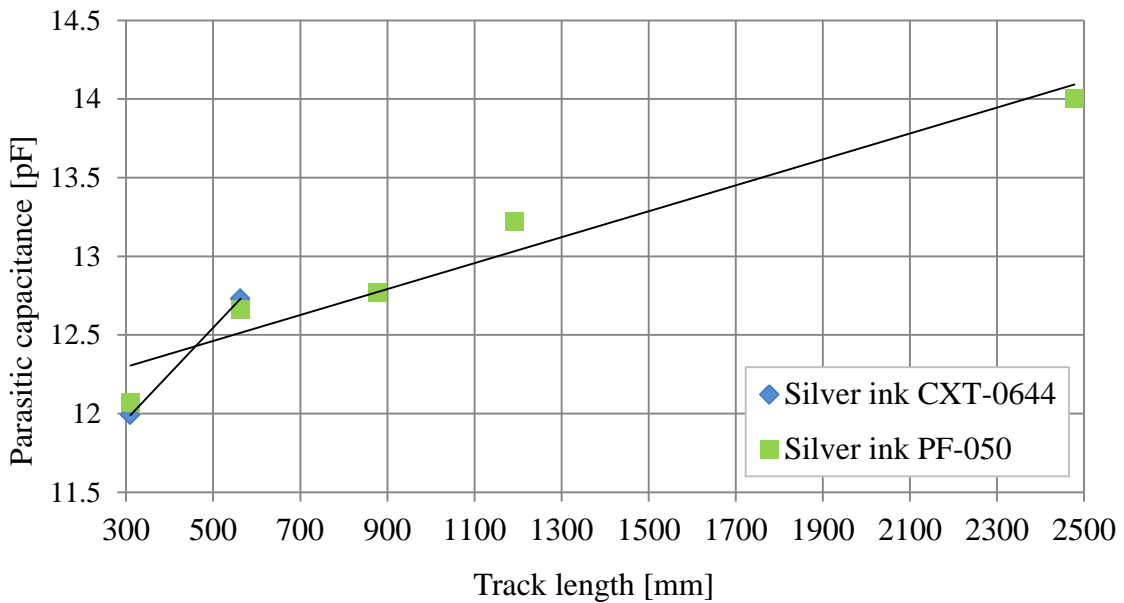
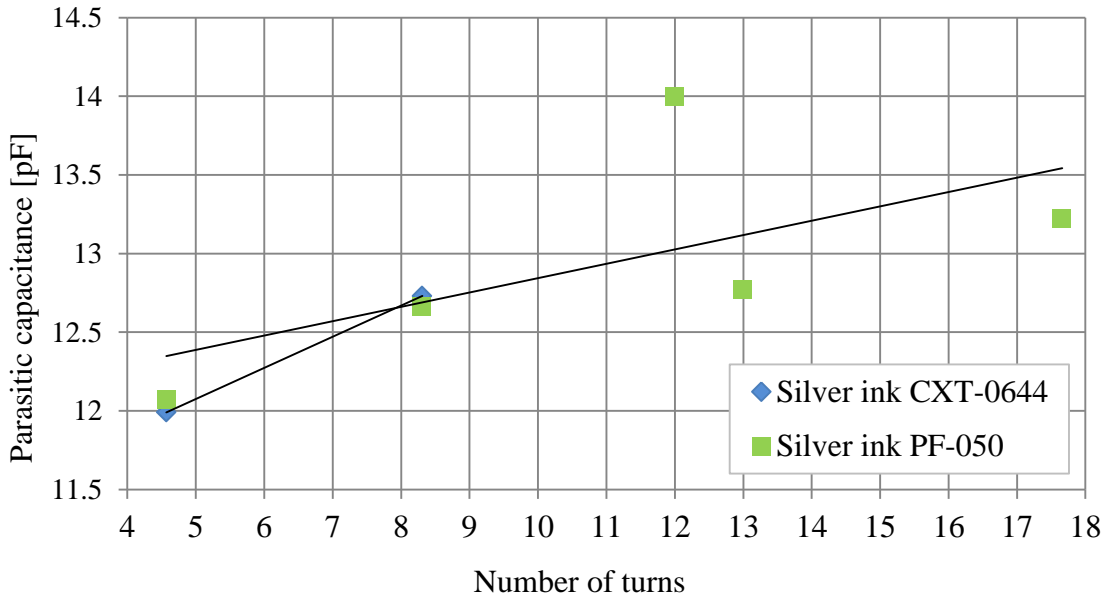


Figure 6.28: The calculated parasitic capacitance versus number of turns for different inks and layouts, and parasitic capacitance versus track length for different inks and layouts. Track spacing is 0.5 mm for all *Comparative* layouts. Track spacing for *Final* layout is 0.15 mm. The black line shows the linear trend line of the variable points.

6.2.5 Inductance

The inductance of printed samples is calculated by network analyzer, based on equivalent RLC model (see Figure 5.3). Table 6.9 represents the inductance value, track width, track spacing, and track length for different printed antennas. The outer diameter, inner diameter, track width, track spacing, track length and ink area are nominal dimensions and are measured with CAD software.

Table 6.7: The calculated inductance, and nominal outer diameter, inner diameter, track width, track spacing, track length, number of turns, and ink area of *Comparative A, B, C, D*, and *Final* with ink PF-050 and ink CXT-0644. The outer and inner diameter, track width, spacing, length and ink area are nominal dimensions and are measured with CAD software.

Ink	Printed sample	Inductance [μH]	DC resistance [Ω]	Geometrical dimensions						
				Outer dia. [mm]	Inner dia. [mm]	Track width [mm]	Track spacing [mm]	Track length [mm]	Number of turns	Ink area [mm^2]
CXT-0644	<i>Comparative C</i>	1.53	31.3	35	8	1	0.5	562.52	8.31	562.52
	<i>Comparative D</i>	0.611	9.7	35	8	2	0.5	309.93	4.57	619.85
PF-050	<i>Comparative A</i>	6.21	60.1	35	8	0.25	0.5	1193.49	17.66	298.31
	<i>Comparative B</i>	3.55	22.4	35	8	0.5	0.5	877.95	12.99	438.96
	<i>Comparative C</i>	1.57	7.6	35	8	1	0.5	562.52	8.31	562.52
	<i>Comparative D</i>	0.607	2.5	35	8	2	0.5	309.93	4.57	619.85
	<i>Final</i>	14.44	35.1	80	51.55	1	0.15	2477.63	12	2477.66

By increasing the number of turns, the inductance of printed samples are increasing (Figure 6.29 (a)). Also development of track length can improve the inductance value (Figure 6.29 (b)). Generally, increasing the ink area and track width can decrease the inductance of printed samples, as represented in Figure 6.29 (c) and (d).

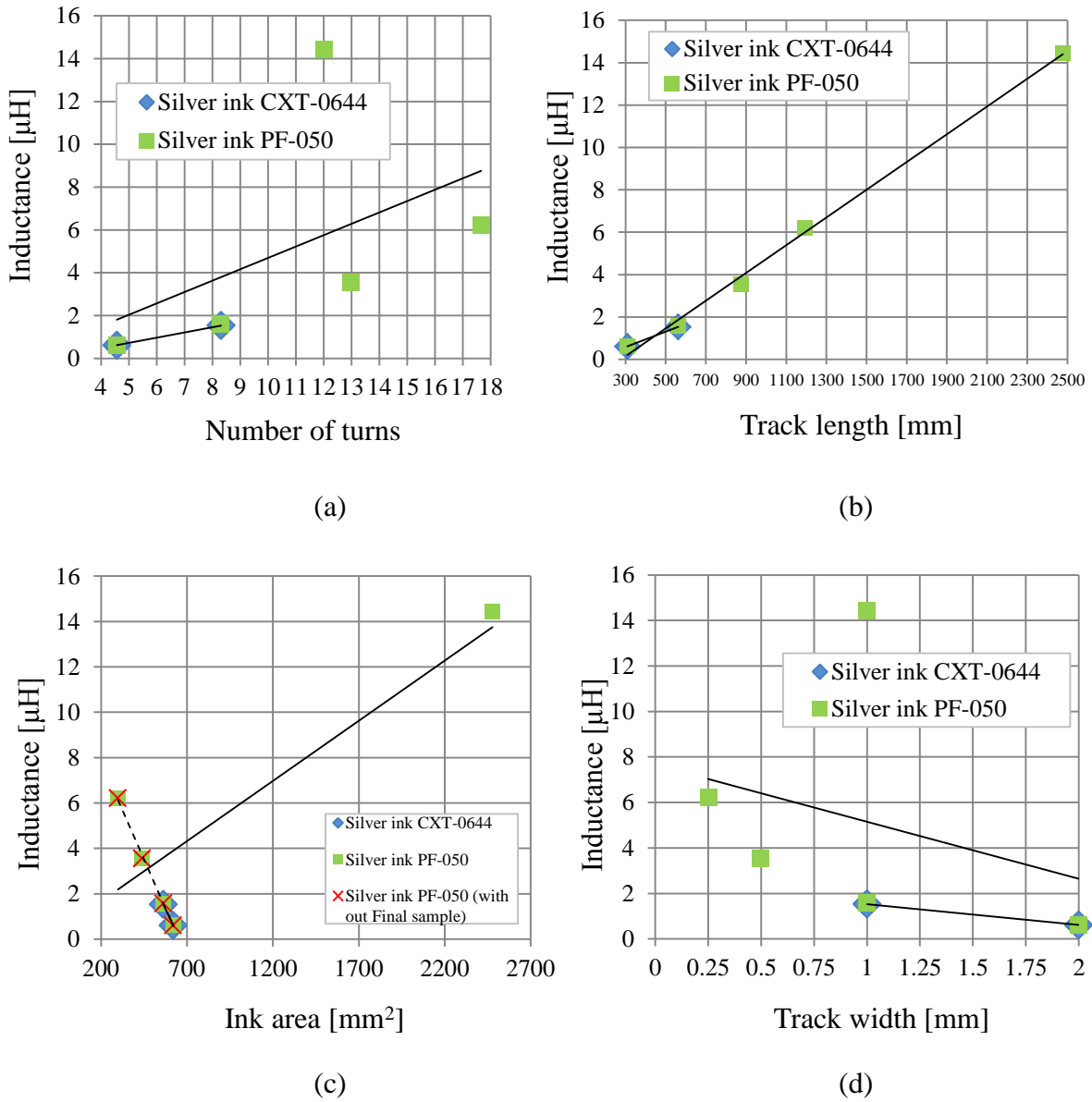


Figure 6.29: (a) Number of turns versus calculated inductance, (b) track length versus calculated inductance (c) printed ink area versus calculated inductance, and (d) track width versus calculated inductance for different layouts and inks. Geometrical dimensions of the antennas are represented in Table 6.7. The values of track length, printed ink area, track width are nominal and calculated with CAD software. The black lines show the linear trend line of the variable points.

6.2.6 Frequency of Resonance

The resonant frequency of printed antennas is calculated by application of Equation (2.21), based on calculated inductance and parasitic capacitance of samples that represented in 6.2.5 and 6.2.4 parts.

Table 6.8 expresses the resonant frequency values for different printed antennas. Generally, by increasing the resonant frequency in a sample, the inductance, and parasitic capacitance decreasing.

Table 6.8: The calculated resonant frequency values of *Comparative A, B, C, D*, and *Final* with ink PF-050 and ink CXT-0644, based on calculated inductance and parasitic capacitance.

Ink	Printed sample	Frequency of resonance [MHz]	Inductance [μH]	Parasitic capacitance [pF]
CXT-0644	<i>Comparative C</i>	36.08	1.53	12.73
	<i>Comparative D</i>	58.83	0.611	11.99
PF-050	<i>Comparative A</i>	17.57	6.21	13.22
	<i>Comparative B</i>	23.65	3.55	12.77
	<i>Comparative C</i>	35.72	1.57	12.66
	<i>Comparative D</i>	58.83	0.607	12.07
	<i>Final</i>	11.20	14.44	14

6.2.7 Quality Factor

The quality factor is calculated by Equation (2.25). The R_L value is defined as the value of series resistance R_s in equivalent RLC model of printed antennas (see Figure 5.3). R_s is extracted from impedance at phase angle 0° [9], as represented in Table 6.9. The values of resonant frequency and inductance are expressed in 6.2.6 and 6.2.5 parts. Table 6.9 expresses the calculated quality factor of different printed antennas.

Table 6.9: The calculated quality factor, frequency, inductance, and resistance of *Comparative A, B, C, D*, and *Final* with ink PF-050 and ink CXT-0644.

Ink	Printed sample	Quality factor	Quality parameters		
			Frequency [MHz]	Inductance [μ H]	Resistance [Ω]
CXT-0644	<i>Comparative C</i>	11.95	36.08	1.53	29.00
	<i>Comparative D</i>	20.60	58.83	0.611	10.96
PF-050	<i>Comparative A</i>	12.97	17.57	6.21	52.82
	<i>Comparative B</i>	19.59	23.65	3.55	26.91
	<i>Comparative C</i>	51.19	35.72	1.57	6.88
	<i>Comparative D</i>	135.09	58.83	0.607	1.66
	<i>Final</i>	29.23	11.20	14.44	34.75

The quality factor of *Comparative* layouts A-D with PF-050 ink is increasing from A to D, as well as the quality factor of *Comparative* layouts C and D with CXT-0644 ink. The quality factor of *Comparative D* with PF-050 ink is significantly higher than the same layout with CXT-0644 ink. This effect is caused by lower resistance of PF-050 ink. As discussed previously in sub-chapter 6.2.2, the resistivity of *Final* layout is relatively high, because of proximity effect losses. As represented in Table 6.9, the high resistive losses of *Final* layout decreases the quality factor of the antenna significantly.

Typical quality factor of copper or silver coils is in the range of 50 to 100 for centimeter-size coreless solenoids, as well as 100 to 200 for cored ones. The quality factor value will be decreased into 10 to 20 for millimeter-size printed coils [99]. The quality factor values of 27 to 60 for PCB inductors is reported by Islam et al. [42]. The quality factor of printed coil antennas in present work (Table 6.9) compare to conventional values [99] and state of the art works [42] is represented is Figure 6.30.

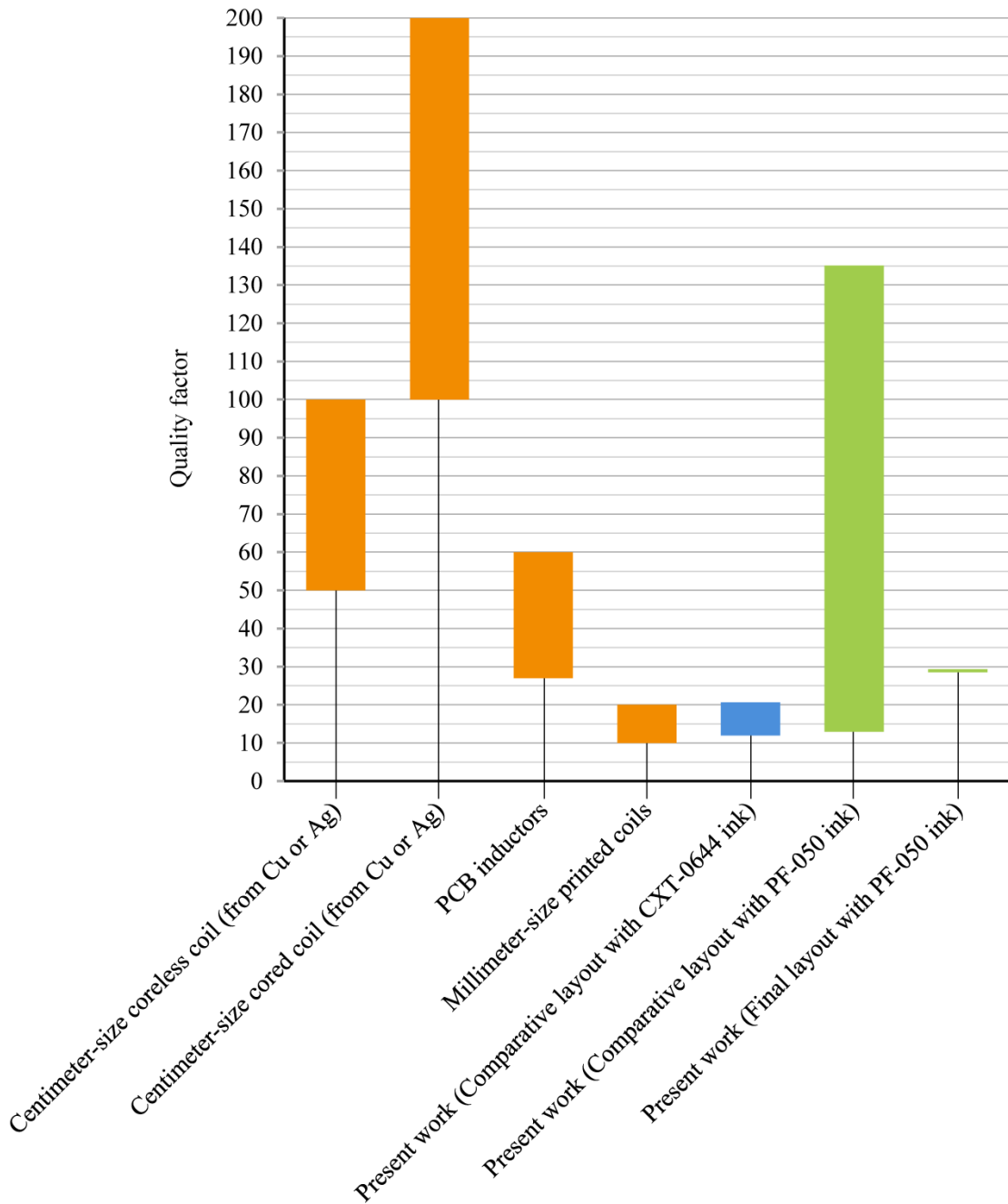


Figure 6.30: The calculated quality factor of printed coil antennas in present work compare to conventional values [99] and state of the art works [42]. The indicator of *Final* layout in diagram is just one point.

Although the quality factor can represents an overview on the efficiency of the antennas but that is not a sufficient value in cases that the geometry of the antennas are defined by different values.

6.2.8 Figure-of-merit

The FOM of samples is calculated by application of Equation (2.26) based on the values of calculated inductance, quality factor at resonance frequency, and area. The value of overall area A_O is substituted with occupied area by the ink on substrate A_I . This value can indicate the rate of ink-consumption for each pattern. Figure 6.31 shows the overall area and ink area of an antenna. The values of inductance, quality factor at resonance frequency, and ink area are included in Table 6.10.

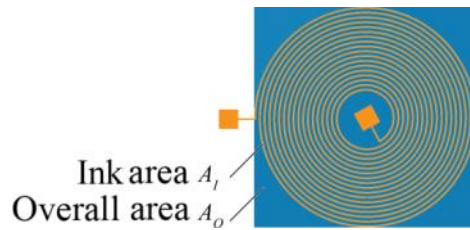


Figure 6.31: The overall area A_O (blue part) and ink area A_I (orange part) in an antenna layout.

Table 6.10: The calculated values of FOM, quality factor at resonance frequency, inductance, and area for *Comparative A, B, C, D, and Final* with ink PF-050 and ink CXT-0644. The overall area and ink area are nominal dimensions and are measured with CAD software.

Ink	Printed sample	Inductance L [nH]	Quality factor Q	Overall area A_O [mm ²]	Ink area A_I [mm ²]	FOM overall area FOM_O [nH/mm ²]	FOM ink area FOM_I [nH/mm ²]
CXT-0644	<i>Comparative C</i>	1530	11.95	1147.55	562.52	15.93	32.50
	<i>Comparative D</i>	611	20.60	1097.36	619.85	11.47	20.31
PF-050	<i>Comparative A</i>	6210	12.97	1185.95	298.31	67.91	270
	<i>Comparative B</i>	3550	19.59	1173.08	438.96	59.28	158.43
	<i>Comparative C</i>	1570	51.19	1147.55	562.52	70.03	142.87
	<i>Comparative D</i>	607	135.09	1097.36	619.85	74.72	132.29
	<i>Final</i>	14440	29.23	6352.58	2477.66	66.44	170.35

The FOM of some state of the art works in PCB inductor design [42] in compare to present work are represented in Table 6.11. The FOM is based on overall area.

Table 6.11: Inductance, maximum quality factor, overall area, and FOM of state of the art works in PCB inductor design [42] in compare to present work.

Different works		Inductance [nH]	Q_{\max}	Overall area [mm ²]	FOM overall area [nH/mm ²]	
PCB samples	Islam et al. [42]	3958.8	27	100	1068.88	
	Masuch et al. [58]	273	42	25	459.73	
	Jow et al. [46]	510	60	100	306.00	
	Peters et al. [70]	4013	44	2484	71.14	
Present work (printed samples)	Ink CXT-0644	<i>Comparative C</i>	1530	11.95	1147.55	15.93
		<i>Comparative D</i>	611	20.60	1097.36	11.47
	Ink PF-050	<i>Comparative A</i>	6210	12.97	1185.95	67.91
		<i>Comparative B</i>	3550	19.59	1173.08	59.28
		<i>Comparative C</i>	1570	51.19	1147.55	70.03
		<i>Comparative D</i>	607	135.09	1097.36	74.72
		<i>Final</i>	14440	29.23	6352.58	66.44

Figure 6.32 gives a comparison between FOM of printed antennas in present research and those are included in Table 6.11. The FOM is based on overall area of the samples. The FOM of printed antennas are extremely less than PCB samples. Considering the high resistive losses of conductive inks, the FOM value of printed antennas is not so high.

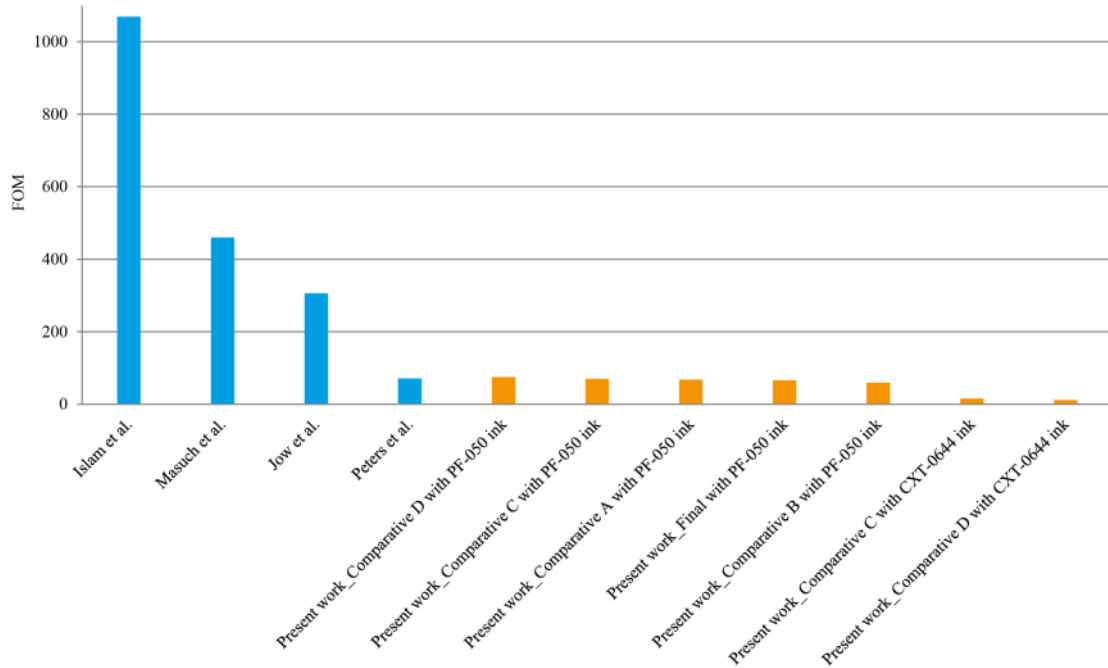


Figure 6.32: Comparison between FOM of printed antennas in present research and other works included in Table 6.11. The FOM is based on overall area of the samples.

The FOM ranking of printed antennas in present research based on ink area is represented in Table 6.12.

Table 6.12: FOM ranking of printed antennas in this research based on ink area.

Printed sample		FOM ink area [nH/mm^2]
Ink PF-050	<i>Comparative A</i>	270
	<i>Final</i>	170.35
	<i>Comparative B</i>	158.43
	<i>Comparative C</i>	142.87
	<i>Comparative D</i>	132.29
Ink CXT-0644	<i>Comparative C</i>	32.50
	<i>Comparative D</i>	20.31

7 Application of Printed Antennas in Demonstrator

A demonstrator is made to show the functionality of printed antennas in a wireless powering product. The *Final* layout is applied for wireless powering in the demonstrator (Figure 7.1 (a)). The sample is printed with stainless steel mesh and *PF-050* ink. The structure of the demonstrator is made from a pair of plexiglass parts that are cutted by the laser in circular shape. The printed antenna as a receiver antenna is embedded between these two clear parts. By application of a PCB board, four LEDs and a rectifier capacitor are inserted at the middle part of circular structure. Figure 7.1 (b) shows the demonstrator and included parts, and Figure 7.1 (c) represents the electronics schematic.

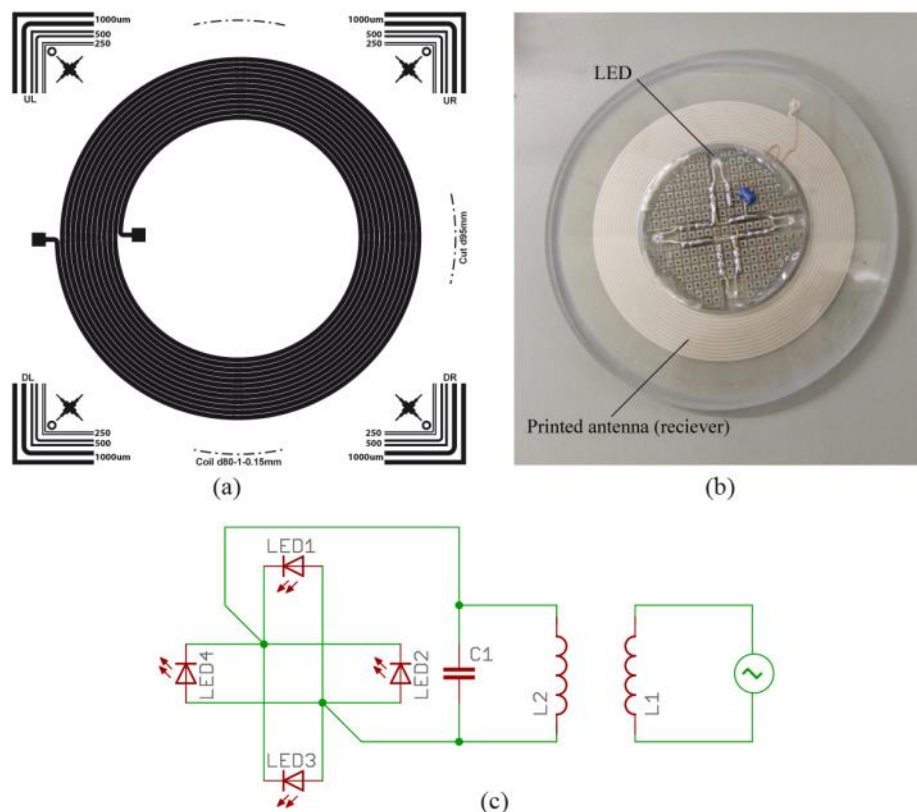


Figure 7.1: (a) The *Final* layout that is applied for wireless powering in the demonstrator; (b) The demonstrator and included parts; and (c) the schematic of electronic circuit board, where *LED 1-4* are LEDs, C_1 is rectifier capacitor, L_2 is printed receiver antenna, and L_1 is printed transmitter antenna. The electronics schematic is drawn by the application of EAGLE software Version 7.2.0 Light Edition [16].

The transmitter antenna is like the same as receiver antenna. The transmitter antenna is connected to a function generator that is emitting a sinusoidal wave [99] with frequency 1 MHz and amplitude 7 V. The signal is amplified with an amplifier. The LEDs is lighting with maximum distance 50 mm between transmitter and receiver antennas. The input voltage is 30 V DC, the maximum current is 400 mA, and the transmitted power is 0.2 watts. Figure 7.2 represents the demonstrator.

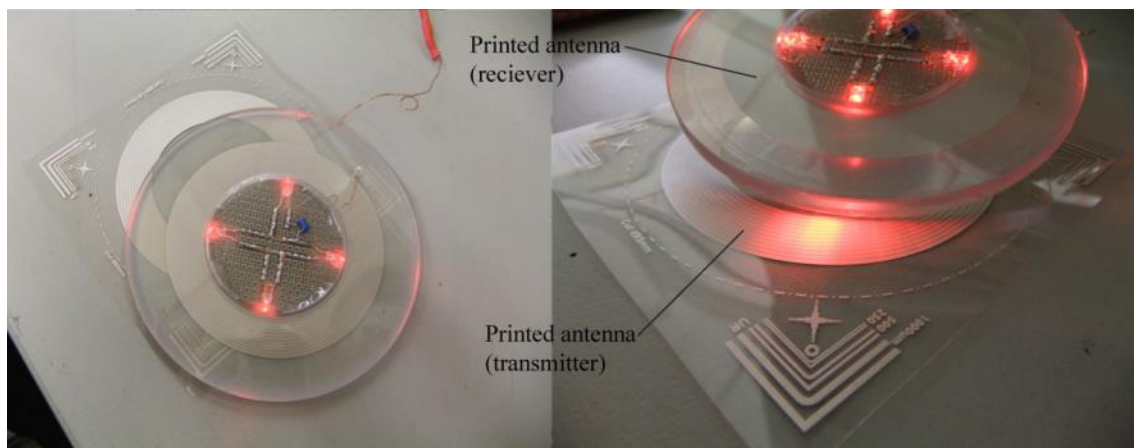


Figure 7.2: Wireless power transfer via printed antennas.

The demonstrator could be developed for lighting a packaging as depicted in Figure 7.3.

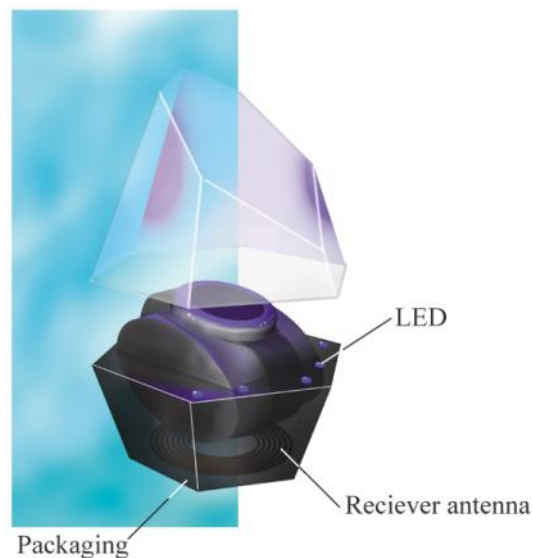


Figure 7.3: A concept design based on represented demonstrator. The LEDs are applied for lighting inside the packaging.

Design of new products based on wireless powering printed antennas can be interesting for some reasons. Novel designs can be fabricated fast with less logistics prices. The volume of production is adjustable. The production is relatively green. Flexibility and combination with ergonomic user interfaces are additional advantages [54]. The potential applications of printed antennas can be in a wide variety of products. Figure 7.4 depicts a concept design based on wireless powering with printed antennas. The packaging in the shelf with a printed antenna can receive the inductive power from other antenna that embedded in the shelf structure and represent a dynamic graphic.

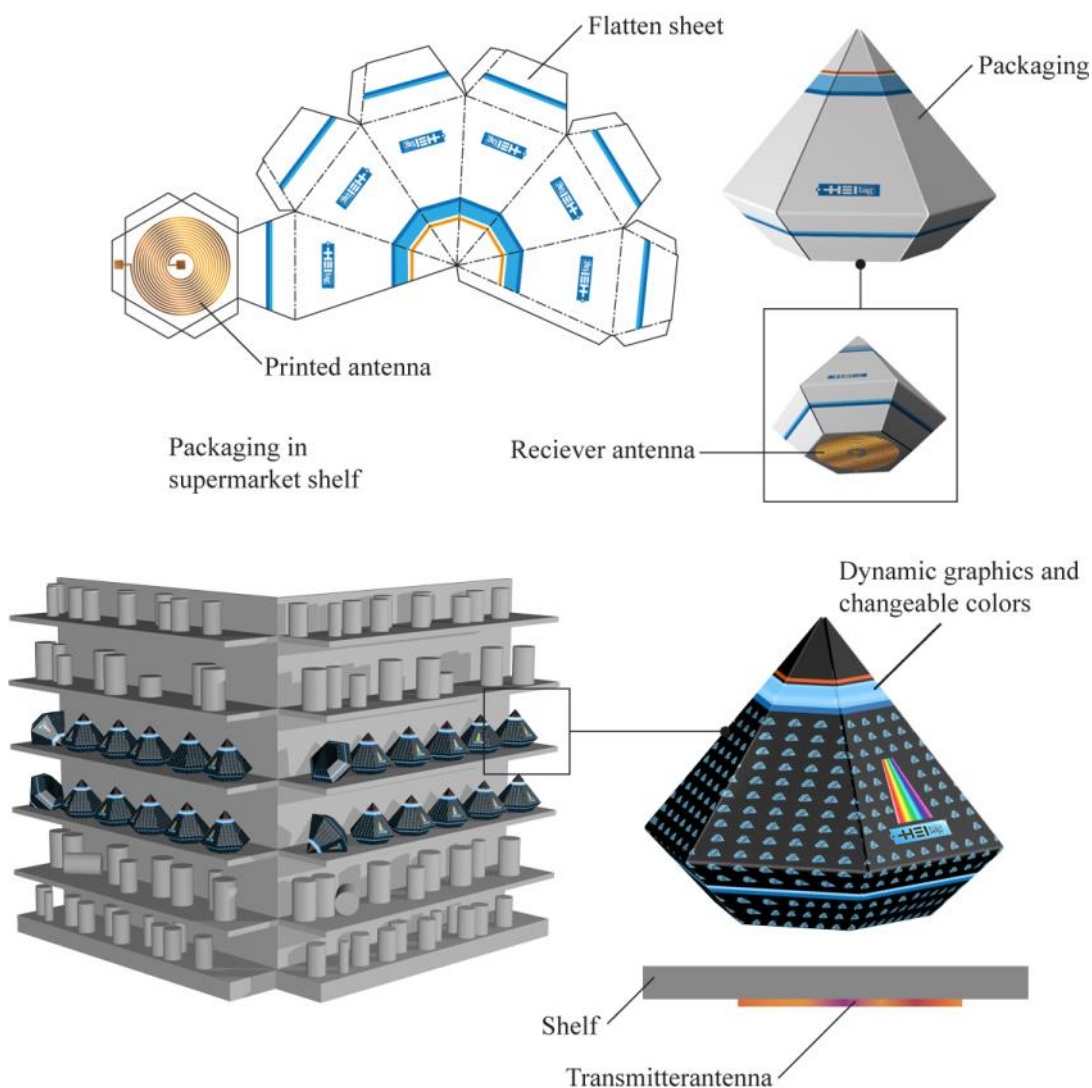


Figure 7.4: A concept design based on wireless powering with printed antennas: The printed antenna on packaging receives the inductive power from the shelf. The color of packaging can change based on received power or data.

The usage of printed antennas can be developed by optimization of power link. Application of larger transmitters with more number of turns can decrease operating frequency and improve power efficiency [66].

8 Conclusion and Outlook

Feasibility study on wireless powering via printed antennas is the scientific goal of the thesis. It is absolutely essential to answer some major questions: Is it possible to apply printed antennas for transferring the power? If the answer is yes, how can identify the efficiency rate of printed antennas? How can optimize the geometrical design of printed antennas for higher efficiency? How much is the efficiency status of printed antennas in compare with conventional ones, e.g. PCB antennas?

The scientific goal of the thesis reached during the research. The experimental results show that screen-printed antennas can be applied for wireless powering. That means the transmitter and receiver printed antennas transfer the power, wirelessly. A screen-printed antenna that is applied in a demonstrator shows the functionality of printed antenna, practically.

The screen printing technique is applied for printing the samples. Screen printing is a reliable, repeatable and affordable technique. In addition, the thickness of deposited ink by screen printing is relatively higher than other printing techniques that caused to decrease the resistance losses of printed antennas. Three layouts are designed for printing the antennas: *Preliminary* layout, *Comparative* layout, and *Final* layout. The *Preliminary* layout is utilized for practical tests on fine line printing and dimensional characteristics of antennas. The *Comparative* layout is applied for comparison between electromagnetic characteristics of antennas. The *Final* layout is used in wireless powering. Two types of mesh screens (polyester and stainless steel) and three types of conductive silver inks (NCS-500AG Nicomatic, CXT-0644 Sun Chemical, and Acheson Electrodag PF-050 Henkel) are applied. All samples are printed on PET substrates. To identify the efficiency rate of printed antennas, a network analyzer is applied. The characterization of printed antennas is done based on reflection method by network analyzer. The printed antennas are probed to port 1 of network analyzer and the frequency is swept from 100 Hz to 40 MHz. The first resonance frequency of most of printed samples is included in this range. The reflection parameters including magnitude and phase angle of impedance spectrum are plotted. The inductance, resistance, and parasitic capacitance are calculated based on equivalent RLC model. The quality factor

and figure-of-merit (FOM) of printed antennas are calculated based on prevalent equations. Nevertheless, what are the most important parameters that effect on optimization of geometrical design of the printed antennas and the efficiency of them? By increasing the frequency, the impedance magnitude of printed samples is increased. At resonance frequency, the magnitude of impedance reached to maximum level and the phase angle of impedance is reduced to 0° . The phase angle is decreased after resonance frequency. The phase angle did not exceed 90° in all of the samples. By increasing the track width and decreasing the number of turns in printed samples, the resonance frequency improved extremely. Application of different inks significantly changed the impedance value of printed samples, while the resonance frequency did not change. The AC resistance of printed samples increased until the resonance frequency, and then decreased. It can change considerably for different types of the inks. In printed samples, the proximity-effect-losses can be more effective than skin-effect. The ratio of track length to track width can be significant for DC resistance comparison. The DC resistance is increasing with this ratio. The trend line slope of printed samples with CXT-0644 ink, in compare with PF-050 ink, is more. By increasing the track length or turn numbers of printed spirals, the parasitic capacitance is increasing in the range of several picofarads. By increasing the number of turns or track length of printed antennas, the inductance is increasing. Generally, increasing the ink area and track width can decrease the inductance of printed samples. The inductance of printed samples with different inks is in the range of 0.607 to 14.44 μH . The quality factor and FOM are conventional factors to compare the power efficiency of different antennas. The quality factor of layouts is developing from *A* to *D* layouts. The resistive losses strongly effect on the quality factor. The range of quality factor of printed samples with different inks is from 11.95 to 135.09, while typical quality factor of copper or silver coils is in the range of 50 to 100 for centimeter-size coreless solenoids, as well as 100 to 200 for cored ones. The quality factor value will be decreased into 10 to 20 for millimeter-size printed coils. The quality factor values of 27 to 60 for PCB inductors is reported.

The FOM is defined based on inductance, quality factor, and overall area of the antenna. FOM of printed antennas in present research is in the range of 11.47 nH/mm^2 to 74.72 nH/mm^2 . In compared with other works, the FOM values of printed antennas are obviously less than PCB antennas. Some FOM reported values of PCB antennas are 71.14 nH/mm^2 , 306.00 nH/mm^2 , 459.73 nH/mm^2 , and 1068.88 nH/mm^2 , while the FOM

values of printed antennas in present research are 11.47 nH/mm², 15.93 nH/mm², 59.28 nH/mm², 66.44 nH/mm², 67.91 nH/mm², 70.03 nH/mm², and 74.72 nH/mm². The high resistive losses of conductive inks is the major reason. The conductive ink includes a set of conductive particles, polymer binder, solvent, and some additives. After curing the ink in high temperature, the conductive particles are joined together and make a porous structure. Other parts of the ink are evaporated or remained as non-conductive materials. That is the reason that why the conductivity of printed ink is less than metal sheets that laminated on PCBs.

In present work, the overall area in FOM equation is substituted with ink area. The ink area can represent the total dimension of printed antennas, as well as the rate of ink consumption. The FOM ranking of printed antennas is represented based on ink area. In present research, that is in the range of 20.31 nH/mm² to 270 nH/mm². The range of The *Comparative layout A* (270 nH/mm²), the *Final layout* (170.35 nH/mm²), and *Comparative layout B* (158.43 nH/mm²) are the highest ones. All of them are printed with PF-050 ink and screen mesh stainless steel. Calculation of FOM based on ink area is not possible for other works out of present research, because there is no access to the details of their geometrical data. Representation of FOM based on ink area can be a useful index for comparison of antenna efficiency versus ink consumption.

The *Final layout* is applied for wireless powering in a demonstrator. That is a hallow antenna with less fill-ratio and more mutual coupling. In summary, the application of printed antennas in wireless powering is possible, but the efficiency of them is less than conventional antennas e.g. PCB antennas.

A concept for software workflow for design of printed antennas is represented. The geometrical parameters of spiral coil antennas and the effect of them on inductive powering are reviewed. Considering the high price of conductive inks, development of FOM index, based on occupied area by the ink on substrate, can be an outlook of research. Printing the multilayer antennas for development of inductance [42] can be the next step of research. Application of other printing techniques e.g. flexography and gravure printing may cause to reach different FOM values for the same geometries. In addition, printing the spiral antennas on three-dimensional surfaces can improve the application of printed antennas for new products. Development of advanced software for functional printing, especially for printed antennas, is considerable. Also, finding a simple method for measurement of printed antennas can be useful.

References

- [1] J. J. Adams, E. B. Duoss, T. F. Malkowski, M. J. Motala, B. Y. Ahn, R. G. Nuzzo, *et al.*, "Conformal Printing of Electrically Small Antennas on Three-Dimensional Surfaces," *Advanced Materials*, vol. 23, pp. 1335-1340, 2011.
- [2] Adobe Systems Inc. 2010. "Illustrator CS5 release notes." [Online] Accessed 2015, Apr. 08. <https://helpx.adobe.com/illustrator/release-note/illustrator-cs5-release-notes.html>.
- [3] Adobe Systems Inc. 2011, Aug. 11. "Using Adobe® Illustrator® CS5." [Online] Accessed 2015, Apr. 09. http://help.adobe.com/archive/en_US/illustrator/cs5/illustrator_cs5_help.pdf.
- [4] Adobe Systems Inc. 2015. "Acrobat 9 Pro resources." [Online] Accessed 2015, Apr. 08. <https://www.adobe.com/support/documentation/en/acrobatpro/>.
- [5] Adobe Systems Inc. 2015. "Adobe InDesign CC." [Online] Accessed 2015, Apr. 09. <http://www.adobe.com/products/indesign.html>.
- [6] Adobe Systems Inc. 2015. "Adobe Photoshop CC." [Online] Accessed 2015, Apr. 09. <http://www.adobe.com/products/photoshop.html>.
- [7] Agilent Technologies Inc. 2009, Sep. 15. "Agilent E5061B network analyzer 5 Hz to 3 GHz technical overview." Accessed 2014, Oct. 08. <http://www.dipaul.ru/upload/iblock/fc1/fc13ec3e7fc751800c54d12a14038c4c.pdf>.
- [8] Agilent Technologies Inc. 2013, Aug. 02. "Agilent E5061B Network Analyzer Help." [Online] Accessed 2014, Nov. 11. <http://ena.support.keysight.com/e5061b/manuals/webhelp/eng/>.
- [9] Agilent Technologies Inc. 2013, Sep. 10. "Agilent impedance measurement handbook." [Online] Accessed 2014, Nov. 06. <http://cp.literature.agilent.com/litweb/pdf/5950-3000.pdf>.
- [10] O. J. Arenas, E. L. de la Jarrige, and F. Boone, "Creating screen-printed passive components for microwave applications," *Microelectronics International*, vol. 27, pp. 84-92, 2010.
- [11] E. Ashoori, F. Asgarian, A. M. Sodagar, and E. Yoon, "Design of double layer printed spiral coils for wirelessly-powered biomedical implants," in *Engineering in Medicine and Biology Society, EMBC, 2011 Annual International Conference of the IEEE*, 2011, pp. 2882-2885.
- [12] Autodesk Inc. 2010. "AutoCAD 2011 customization guide." [Online] Accessed 2015, Apr. 08. http://docs.autodesk.com/ACD/2011/ENU/pdfs/acad_acg.pdf.
- [13] Autodesk Inc. 2015. "AutoCAD." [Online] Accessed 2015, Apr. 08. <http://www.autodesk.com/products/autocad/overview>.
- [14] C. A. Balanis, *Modern antenna handbook*: John Wiley & Sons, 2008.
- [15] R. Brown, *RF/microwave hybrids: basics, materials and processes*: Springer, 2003.

-
- [16] CadSoft. 2011. "About EAGLE PCB design software." [Online] Accessed 2015, May. 11. <http://www.cadsoftusa.com/eagle-pcb-design-software/about-eagle/>.
- [17] T. P. Cencich and D. S. Filipovic, "Spiral Antennas," *Encyclopedia of RF and Microwave Engineering*, 2005.
- [18] J. Chang, T. Ge, and E. Sanchez-Sinencio, "Challenges of printed electronics on flexible substrates," in *Circuits and Systems (MWSCAS), 2012 IEEE 55th International Midwest Symposium on*, 2012, pp. 582-585.
- [19] K. Chen and Z. Zhao, "Analysis of the double-layer printed spiral coil for wireless power transfer," 2013.
- [20] Z. N. Chen, *Antennas for portable devices*: John Wiley & Sons, 2007.
- [21] S.-H. Cho, S.-H. Son, H.-J. Chung, and J.-B. Lee, "A wireless powered fully integrated SU-8-based implantable LC transponder," *Microsystem Technologies*, vol. 16, pp. 1657-1663, 2010.
- [22] F. Ellinger, *Radio frequency integrated circuits and technologies*: Springer, 2008.
- [23] P. A. D. Fabbro and M. Kayal, "Linear CMOS RF power amplifiers for wireless applications," 2010.
- [24] Fatboy brand. "NOKIA wireless charging pillow." [Online] Accessed 2014, Oct. 04. <http://www.fatboy.com/it/nokia-wireless-charging-pillow-online-shop>.
- [25] G. K. Felic, D. Ng, and E. Skafidas, "Investigation of Frequency-Dependent Effects in Inductive Coils for Implantable Electronics," *Magnetics, IEEE Transactions on*, vol. 49, pp. 1353-1360, 2013.
- [26] C. Fernandez, O. Garcia, R. Prieto, J. Cobos, S. Gabriels, and G. Van Der Borgh, "Design issues of a core-less transformer for a contact-less application," in *Applied Power Electronics Conference and Exposition, 2002. APEC 2002. Seventeenth Annual IEEE*, 2002, pp. 339-345.
- [27] C. Fernandez, R. Prieto, O. Garcia, and J. Cobos, "Coreless magnetic transformer design procedure," in *Power Electronics Specialists Conference, 2005. PESC'05. IEEE 36th*, 2005, pp. 1548-1554.
- [28] K. Finkensteller and R. Waddington, *RFID handbook: radio-frequency identification fundamentals and applications*: Wiley New York, 1999.
- [29] Gallus Holding AG. "Gallus Screeny: the screen printing plate for maximum printing quality." [Online] Accessed 2014, Sep. 26. <http://www.gallus-group.com/gallus/screen-printing/screen-printing-plates.aspx>.
- [30] K. N. Goh, S. R. M. Shukri, and R. B. H. Manao, "Automatic Assessment for Engineering Drawing," in *Advances in Visual Informatics*, ed: Springer, 2013, pp. 497-507.
- [31] K.-H. Gonschorek and R. Vick, *Electromagnetic compatibility for device design and system integration*: Springer, 2009.
- [32] J. W. Gooch, *Encyclopedic dictionary of polymers* vol. 1: Springer, 2010.
- [33] H. M. Greenhouse, "Design of planar rectangular microelectronic inductors," *Parts, Hybrids, and Packaging, IEEE Transactions on*, vol. 10, pp. 101-109, 1974.
- [34] P. Groche, M. Ibis, C. Hatzfeld, A. Stöckigt, and C. Gerlitzky, "Economic production of load-bearing sheet metal parts with printed strain gages by

- combining forming and screen printing," *International Journal of Material Forming*, pp. 1-14, 2014.
- [35] T. K. Gupta, "Handbook of thick-and thin-film hybrid microelectronics," *Handbook of Thick-and Thin-Film Hybrid Microelectronics*, by Tapan K. Gupta, pp. 424. ISBN 0-471-27229-9. Wiley-VCH, May 2003., vol. 1, 2003.
- [36] F. Hadley. 2007, Jun. 07. "Goodbye wires!" [Online] Accessed 2014, Oct. 04. <http://newsoffice.mit.edu/2007/wireless-0607>.
- [37] Henkel AG & Co. KGaA, "Acheson Electrodag PF-050," ed, 2011, May.
- [38] R. Ho and R. Drost, *Coupled Data Communication Techniques for High-Performance and Low-Power Computing*: Springer, 2010.
- [39] A. Hobby, "Fundamentals of screens for electronics screen printing," *Circuit World*, vol. 16, pp. 16-28, 1990.
- [40] E. Horvath, G. Harsanyi, G. Henap, and A. Torok, "Mechanical modelling and life cycle optimisation of screen printing," *Journal of Theoretical and Applied Mechanics*, vol. 50, pp. 1025-1036, 2012.
- [41] R. Horwood, "Towards a Better Understanding of Screen Print Thickness Control," *Active and Passive Electronic Components*, vol. 1, pp. 129-136, 1974.
- [42] A. B. Islam, S. K. Islam, and F. S. Tulip, "Design and Optimization of Printed Circuit Board Inductors for Wireless Power Transfer System," *Circuits and Systems*, vol. 4, p. 237, 2013.
- [43] B.-J. Jang, S. Lee, and H. Yoon, "HF-band wireless power transfer system: Concept, issues, and design," *Progress in electromagnetics research*, vol. 124, pp. 211-231, 2012.
- [44] J. Jeong, S. W. Lee, K. S. Min, and S. J. Kim, "A novel multilayered planar coil based on biocompatible liquid crystal polymer for chronic implantation," *Sensors and Actuators A: Physical*, vol. 197, pp. 38-46, 2013.
- [45] S.-E. Jo, S. Joung, J.-K. F. Suh, and Y.-J. Kim, "Improvement of wireless power transmission efficiency of implantable subcutaneous devices by closed magnetic circuit mechanism," *Medical & biological engineering & computing*, vol. 50, pp. 973-980, 2012.
- [46] U.-M. Jow and M. Ghovanloo, "Design and optimization of printed spiral coils for efficient transcutaneous inductive power transmission," *Biomedical Circuits and Systems, IEEE Transactions on*, vol. 1, pp. 193-202, 2007.
- [47] S. Kasap and P. Capper, *Springer handbook of electronic and photonic materials*: Springer, 2007.
- [48] KBA-Kammann GmbH. "K15 Q-SL Laboratory Screen Printer with motor driven squeegee and adjustable speed." Accessed 2014, Nov. 21. http://www.kba-kammann.com/en/container_printing_1/k15_q-sl/k15_q-sl_1.html.
- [49] K.-R. Kim, D.-H. Kim, and H.-J. Kim, "Magnetic Resonance Wireless Power Transmission Using a LLC Resonant Circuit for a Locomotion Robot's Battery Charging," in *Intelligent Robotics and Applications*, ed: Springer, 2013, pp. 31-37.
- [50] S. Konno, T. Yamamoto, and K. Koshiji, "Improvement of coupling coefficient by designing a spiral pattern formed on a printed circuit board," in *Wireless Power Transfer (WPT), 2013 IEEE*, 2013, pp. 167-170.

-
- [51] Leica Microsystems. 2015. "Imaging software integrates Leica automated microscopes and digital cameras Leica application suite." [Online] Accessed 2015, Mar. 12. <http://www.leica-microsystems.com/products/microscope-software/software-for-materials-sciences/details/product/leica-application-suite/>.
- [52] Leica Microsystems. 2015. "Versatile upright microscope for materials analysis Leica DM4000 M." [Online] Accessed 2015, Mar. 12. <http://www.leica-microsystems.com/products/light-microscopes/industrial-materials/upright-microscopes/details/product/leica-dm4000-m/>.
- [53] B. Lenaerts and R. Puers, *Omnidirectional Inductive Powering for Biomedical Implants*: Springer, 2009.
- [54] Y. Li, D. Lu, and C. Wong, *Electrical conductive adhesives with nanotechnologies*: Springer, 2010.
- [55] H.-C. Lin, P. Lin, C.-A. Lu, and S.-F. Wang, "High-frequency electrical properties of silver thick films measured by dielectric resonator method," *Japanese Journal of Applied Physics*, vol. 47, p. 7289, 2008.
- [56] L. Liu, H. Wang, Z. Zhang, Y. Li, and Z. Feng, "Wideband substrate integrated waveguide cavity-backed spiral-shaped patch antenna," *Microwave and Optical Technology Letters*, vol. 57, pp. 332-337, 2015.
- [57] S. Logothetidis, "Flexible organic electronic devices: Materials, process and applications," *Materials Science and Engineering: B*, vol. 152, pp. 96-104, 2008.
- [58] J. Masuch and M. Delgado-Restituto, "Design constraints for the inductive power and data link of an implanted body sensor," in *Circuit Theory and Design, 2009. ECCTD 2009. European Conference on*, 2009, pp. 425-428.
- [59] T. A. Milligan, *Modern antenna design*: John Wiley & Sons, 2005.
- [60] N. Misron, L. Q. Ying, R. N. Firdaus, N. Abdullah, N. F. Mailah, and H. Wakiwaka, "Effect of inductive coil shape on sensing performance of linear displacement sensor using thin inductive coil and pattern guide," *Sensors*, vol. 11, pp. 10522-10533, 2011.
- [61] Mitsubishi Polyester Film GmbH, "Hostaphan® GN," ed, 2013, Sep.
- [62] S. S. Mohan, M. del Mar Hershenson, S. P. Boyd, and T. H. Lee, "Simple accurate expressions for planar spiral inductances," *Solid-State Circuits, IEEE Journal of*, vol. 34, pp. 1419-1424, 1999.
- [63] National Instruments Corp. 2015. "NI DIAdem." [Online] Accessed 2015, Apr. 08. <http://www.ni.com/diadem/>.
- [64] Nicomatic (UK) Ltd, "NCS-500AG Silver conductive screen printable ink," ed, 2001, Jan. 05.
- [65] OE-A (Organic and Printed Electronics Association). 2013. "Organic and Printed Electronics Applications, Technologies and Suppliers 5th Edition." [Online] Accessed 2015, Mar. 05. http://www.oe-a.org/documents/10179/31903/OE-A_Brochure2013.pdf.
- [66] J. Olivo, S. Carrara, and G. De Micheli, "Modeling of printed spiral inductors for remote powering of implantable biosensors," in *Medical Information & Communication Technology (ISMICT), 2011 5th International Symposium on*, 2011, pp. 29-32.

-
- [67] J. Pan, G. L. Tonkay, and A. Quintero, "Screen printing process design of experiments for fine line printing of thick film ceramic substrates," *Journal of Electronics Manufacturing*, vol. 9, p. 203, 1999.
- [68] I. Papagiannopoulos, G. De Mey, and V. Chatziathanasiou, "Current distribution in circular planar coil," *Engineering Analysis with Boundary Elements*, vol. 37, pp. 747-756, 2013.
- [69] S. Partridge, "The Rôle of the Stencil in High Definition Screen Printing," *Circuit World*, vol. 13, pp. 4-13, 1987.
- [70] C. Peters and Y. Manoli, "Inductance calculation of planar multi-layer and multi-wire coils: An analytical approach," *Sensors and Actuators A: Physical*, vol. 145, pp. 394-404, 2008.
- [71] Plastic Logic Germany. "Smart watches: the start of the wearable electronics revolution?" [Online] Accessed 2014, Nov. 05. <http://media.plasticlogic.com/lib/docs/153532-pl-wp-wearables-final.pdf>.
- [72] Plastic Logic Germany. 2014. "Applications - Displays." [Online] Accessed 2014, Nov. 05. <http://www.plasticlogic.com/applications/displays/>.
- [73] C. Reig and E. Avila-Navarro, "Printed Antennas for Sensor Applications: A Review," *Sensors Journal, IEEE*, vol. 14, pp. 2406-2418, 2014.
- [74] D. E. Riemer, "The theoretical fundamentals of the screen printing process," *Microelectronics International*, vol. 6, pp. 8-17, 1989.
- [75] Robert McNeel & Associates. 2014. "Rhinceros design, model, present, analyze, realize..." [Online] Accessed 2015, Apr. 08. <https://www.rhino3d.com/>.
- [76] I. Rosu. 2010. "Small antennas for high frequencies." [Online]. YO3DAC / VA3IUL Accessed 2015, Mar. 17. <http://www.qsl.net/va3iul/>.
- [77] J. F. Salmerón, F. Molina-Lopez, D. Briand, J. J. Ruan, A. Rivadeneyra, M. A. Carvajal, *et al.*, "Properties and Printability of Inkjet and Screen-Printed Silver Patterns for RFID Antennas," *Journal of Electronic Materials*, vol. 43, pp. 604-617, 2014.
- [78] A. P. Sample, D. A. Meyer, and J. R. Smith, "Analysis, experimental results, and range adaptation of magnetically coupled resonators for wireless power transfer," *Industrial Electronics, IEEE Transactions on*, vol. 58, pp. 544-554, 2011.
- [79] H. G. Scheer, *Siebdruck-Handbuch*: Verlag Der Siebdruck Lübeck, 2007.
- [80] D. Schneider. 2010, Apr. 30. "A Critical Look at Wireless Power." [Online] Accessed 2014, Oct. 03. <http://spectrum.ieee.org/transportation/mass-transit/a-critical-look-at-wireless-power>.
- [81] S. Schramm. 2009, Mar. "Der Mann, der Strom durch die Luft schickt." [Online] Accessed 2014, Oct. 04. <http://www.zeit.de/zeit-wissen/2009/03/Soljadic>.
- [82] Sefar AG, "Screen printing mesh – Article list SEFAR® PET 1500," ed, 2014, Aug. 08.
- [83] Sensofar Corp. "PLu neox 3D optical profiler." [Online] Accessed 2015, Mar. 12. <http://www.sensofar.com/sensofar/products/neox/>.
- [84] D.-Y. Shin, Y. Lee, and C. H. Kim, "Performance characterization of screen printed radio frequency identification antennas with silver nanopaste," *Thin Solid Films*, vol. 517, pp. 6112-6118, 2009.

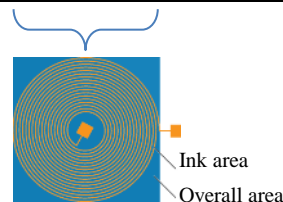
- [85] A. P. Shitvov, D. E. Zelenchuk, T. Olsson, A. G. Schuchinsky, and V. F. Fusco, "Transmission/reflection measurement and near-field mapping techniques for passive intermodulation characterisation of printed lines," in *Proc. Sixth Int. Workshop on Multipactor, Corona and Passive Intermodulation in Space RF Hardware, Valencia, Spain*, 2008, pp. 1-6.
- [86] H. Shoki, "Issues and Initiatives for Practical Deployment of Wireless Power Transfer Technologies in Japan," *Proceedings of the IEEE*, vol. 101, pp. 1312-1320, 2013.
- [87] J. Sidén, M. Fein, A. Koptuyg, and H.-E. Nilsson, "Printed antennas with variable conductive ink layer thickness," *IET Microwaves, Antennas & Propagation*, vol. 1, pp. 401-407, 2007.
- [88] L. R. Smith, H. Czichos, T. Saito, and L. Smith, *Springer handbook of materials measurement methods*: Springer, 2006.
- [89] H. Sugiyama, "Optimal designs for wireless resonant energy link with symmetrical coil pair," in *Microwave Workshop Series on Innovative Wireless Power Transmission: Technologies, Systems, and Applications (IMWS), 2011 IEEE MTT-S International*, 2011, pp. 247-250.
- [90] Sun Chemical Group Coöperatief U.A., "SunTronic™ PTF Silver CXT-0644," ed, 2013, Aug.
- [91] X. Sun, Y. Zheng, X. Peng, X. Li, and H. Zhang, "Parylene-based 3D high performance folded multilayer inductors for wireless power transmission in implanted applications," *Sensors and Actuators A: Physical*, vol. 208, pp. 141-151, 2014.
- [92] D. Sung, A. de la Fuente Vornbrock, and V. Subramanian, "Scaling and optimization of gravure-printed silver nanoparticle lines for printed electronics," *Components and Packaging Technologies, IEEE Transactions on*, vol. 33, pp. 105-114, 2010.
- [93] A. Syed, K. Demarest, and D. D. Deavours, "Effects of antenna material on the performance of UHF RFID tags," in *RFID, 2007. IEEE International Conference on*, 2007, pp. 57-62.
- [94] C.-M. Tai and C.-N. Liao, "Multilevel suspended thin-film inductors on silicon wafers," *Electron Devices, IEEE Transactions on*, vol. 54, pp. 1510-1514, 2007.
- [95] S. Tang, S. R. Hui, and H. Chung, "Characterization of coreless printed circuit board (PCB) transformers," in *Power Electronics Specialists Conference, 1999. PESC 99. 30th Annual IEEE*, 1999, pp. 746-752.
- [96] M. Taroni, C. Breward, P. Howell, J. Oliver, and R. Young, "The screen printing of a power-law fluid," *Journal of Engineering Mathematics*, vol. 73, pp. 93-119, 2012.
- [97] Trelleborg AB (publ). 2014, Mar. 13. "Screen Printing Squeegee Blades." [Online] Accessed 2014, Oct. 25. <http://www.trelleborg.com/Documents/Trelleborg%20Applied%20Technology/New/UNITEX-Screen-Printing-Squeegee-GV1.jpg>.
- [98] C. Tucker, K. Warwick, and W. Holderbaum, "A contribution to the wireless transmission of power," *International Journal of Electrical Power & Energy Systems*, vol. 47, pp. 235-242, 2013.

-
- [99] K. van Schuylenbergh and R. Puers, *Inductive Powering: Basic Theory and Application to Biomedical Systems*: Springer, 2009.
- [100] H. J. Visser, *Array and phased array antenna basics*: John Wiley & Sons, 2006.
- [101] J. Volakis, *Antenna Engineering Handbook, Fourth Edition*: McGraw-Hill Education, 2007.
- [102] J. F. Wager, D. A. Keszler, and R. E. Presley, *Transparent electronics*: Springer, 2008.
- [103] J. Wang, J. Li, S. Ho, W. Fu, Y. Li, H. Yu, *et al.*, "Lateral and angular misalignments analysis of a new PCB circular spiral resonant wireless charger," *Magnetics, IEEE Transactions on*, vol. 48, pp. 4522-4525, 2012.
- [104] G. White, C. Breward, P. Howell, and R. Young, "A model for the screen-printing of Newtonian fluids," *Journal of Engineering Mathematics*, vol. 54, pp. 49-70, 2006.
- [105] W. S. Wong and A. Salleo, *Flexible electronics: materials and applications* vol. 24: Springer, 2009.
- [106] W. Wu and Q. Fang, "Design and simulation of printed spiral coil used in wireless power transmission systems for implant medical devices," in *Engineering in Medicine and Biology Society, EMBC, 2011 Annual International Conference of the IEEE*, 2011, pp. 4018-4021.
- [107] Z. Wu, M. Jobs, A. Rydberg, and K. Hjort, "Hemispherical coil electrically small antenna made by stretchable conductors printing and plastic thermoforming," *Journal of Micromechanics and Microengineering*, vol. 25, p. 027004, 2015.
- [108] K. Zhu, H. Nii, O. N. N. Fernando, and A. D. Cheok, "Selective inductive powering in hardware-based paper computing," in *Ambient Intelligence*, ed: Springer, 2011, pp. 340-344.

Appendix

A1. Measured values for all of the samples

Ink	Printed sample	Geometric characteristics										Electric characteristics			
		Nominal size								Measured size		DC resistivity [Ω]	Parasitic capacitance [pF]	Inductance [μH]	Resonance frequency [Hz]
		Inner dia. [mm]	Outer dia. [mm]	Track width [mm]	Track gap [mm]	Number of turns	Track length [mm]	Ink area [mm ²]	Overall area [mm ²]	Track width [μm]	Track gap [μm]				
CXT-0644	Comparative C	8	35	1	0.5	8.31	562.52	562.52	1147.55	1043.83	439.32	31.3	12.73	1.53	36,081,155.64
		8	35	1	0.5	8.31	562.52	562.52	1147.55	Not measured	Not measured	39.9	12.71	1.52	36,228,119.12
		8	35	1	0.5	8.31	562.52	562.52	1147.55	Not measured	Not measured	34.6	12.76	1.58	35,463,898.52
	Comparative D	8	35	2	0.5	4.57	309.93	619.85	1097.36	2059.80	425.33	11.2	12.01	0.59	59,718,377.42
		8	35	2	0.5	4.57	309.93	619.85	1097.36	Not measured	Not measured	9.7	11.99	0.61	58,831,532.25
		8	35	2	0.5	4.57	309.93	619.85	1097.36	Not measured	Not measured	13.2	12.08	0.62	58,326,283.86
PF-050	Comparative A	8	35	0.25	0.5	17.66	1193.49	298.31	1185.95	340.09	399.81	60.1	13.22	6.21	17,574,332.09
		8	35	0.25	0.5	17.66	1193.49	298.31	1185.95	Not measured	Not measured	57.9	13.36	6.15	17,567,079.61
		8	35	0.25	0.5	17.66	1193.49	298.31	1185.95	Not measured	Not measured	58.1	12.93	6.31	17,628,948.71
		8	35	0.25	0.5	17.66	1193.49	298.31	1185.95	Not measured	Not measured	61.6	12.79	6.28	17,767,456.55
	Comparative B	8	35	0.5	0.5	12.99	877.95	438.96	1173.08	550.89	424.94	21.1	12.74	3.57	23,611,388.89
		8	35	0.5	0.5	12.99	877.95	438.96	1173.08	Not measured	Not measured	20.6	12.8	3.5	23,790,378.37
		8	35	0.5	0.5	12.99	877.95	438.96	1173.08	Not measured	Not measured	22.4	12.77	3.55	23,649,977.46
		8	35	0.5	0.5	12.99	877.95	438.96	1173.08	Not measured	Not measured	20.7	12.72	3.5	23,865,073.62
	Comparative C	8	35	1	0.5	8.31	562.52	562.52	1147.55	1041.30	445.02	7.1	12.68	1.59	35,463,546.72
		8	35	1	0.5	8.31	562.52	562.52	1147.55	Not measured	Not measured	7.6	12.66	1.57	35,716,893.37
		8	35	1	0.5	8.31	562.52	562.52	1147.55	Not measured	Not measured	7.5	12.6	1.56	35,916,398.75
		8	35	1	0.5	8.31	562.52	562.52	1147.55	Not measured	Not measured	7.8	12.65	1.58	35,617,755.64
	Comparative D	8	35	2	0.5	4.57	309.93	619.85	1097.36	2014.64	447.02	2.6	12.05	0.61	58,829,484.54
		8	35	2	0.5	4.57	309.93	619.85	1097.36	Not measured	Not measured	2.5	12.07	0.61	58,829,123.21
		8	35	2	0.5	4.57	309.93	619.85	1097.36	Not measured	Not measured	2.5	12.09	0.59	59,420,182.77
		8	35	2	0.5	4.57	309.93	619.85	1097.36	Not measured	Not measured	2.6	12.07	0.6	59,419,396.75
Final	51.55	80	1	0.15	12	2477.63	2477.66	6352.58	1035.27	72.75	35.1	14	14.44	11,199,348.05	
	51.55	80	1	0.15	12	2477.63	2477.66	6352.58	Not measured	Not measured	34.2	14.06	14.38	11,198,716.56	
	51.55	80	1	0.15	12	2477.63	2477.66	6352.58	Not measured	Not measured	36.8	13.95	14.5	11,196,164.00	
	51.55	80	1	0.15	12	2477.63	2477.66	6352.58	Not measured	Not measured	38.2	13.96	14.49	11,196,014.55	



A2. Silver ink NCS-500AG Nicomatic

NCS-500AG SILVER CONDUCTIVE SCREEN PRINTABLE INK

NCS-500AG has been formulated as a Silver Conductive Screen Printable ink ideal for use in flexible circuit, membrane switch, touch switches and other flexible applications. NCS-500AG is a general purpose polymer thick film silver-containing conductor for use only on print treated polyester or polycarbonate.

By using a unique combination of silver flake and the latest in resin technology, the NCS-500AG possesses excellent conductivity, abrasion resistance and printability.

It can be used with semi-automatic and manual printers and offers excellent residence time on the screen.

Typical Properties:

Appearance	Thick Silver Coloured Paste
Volume Resistivity ($\Omega/\text{sq cm}$)	$\leq 0.5 \times 10^{-4}$
Adhesion/Tape Pull	100/100 (no material removal)
Abrasion Resistance, Pencil Hardness (ASTM D3363-74)	2H
Solids Content	65%
Viscosity (poise) (RION VT-04, #2 spindle 25°C)	120 / 150
Cure Conditions	120°C for 2-3 mins 115°C for 3-5 mins
Circuit Line Thickness (printed with 270 mesh polyester)	5 ± 1 microns
Coverage (dependent on screen size and material)	20 x / 10 x / kg
Shelf Life	6 mths in unopened container

Processing:

Printing	Suitable for Manual, Semi-Automatic or High Process's
Screen Type	Polyester or Stainless Steel
Substrates	Polyester or Polycarbonate
Cleanup Solvent	MEK, MIBK, Acetone or similiar solvents
Storage	Store at ambient temp, some settling of solids may occur, stir vigorously before use

Safety & Handling:

The following precautions should be exercised when handling:

- Avoid prolonged contact with skin. If contact with skin occurs, wash immediately with soap and water
- Use with adequate ventilation, avoid prolonged breathing of vapour.
- Dangerous if swallowed - DO NOT CONSUME

The performance characteristics are influenced and affected by printing technique, nature of substrate, curing time, curing temperature and type of drying equipment.

Before adopting our products for commercial use, the user assumes responsibility for determining fitness of use in their particular application and process. Nicomatic makes no warranties and assumes no liability in connection with any use of this information.

Specification subject to change without prior notice

NICOMATIC (UK) LTD

Unit 8, Campus Five, Third Avenue, Letchworth, Hertfordshire SG6 2JF England

Tel: +44(0)1462 677886 Fax: +44(0)1462 677499

email: sales@nicomatic.co.uk http: //www.nicomatic.co.uk

Jan 05/01

A3. Silver ink SunTronic™ PTF CXT-0644 Sun Chemical



SunTronic™

Technical Data Sheet

SunTronic™ PTF Silver CXT-0644

Product Description

SunTronic™ PTF Silver CXT-0644 is a screen printable conductive ink specifically designed for fine resolution printing (<100 microns).

The ink exhibits very low line spreading, high conductivity and excellent adhesion to various substrates, including glass, PET, ITO and other transparent conductive films.

CXT-0644 is specifically suitable for printing of conductive traces in touch panel manufacture.

Typical Properties

Pigment	Silver
Binder	Thermoplastic
Viscosity (25 °C, 20 sec ⁻¹), Pa.s	75 - 85
Solids (120 °C), %	82 - 85
Sheet Resistivity, Ω/sq/mil	
120 °C/30 min	<0.014
150 °C/30 min	<0.010
Volume Resistivity, Ω/cm	
120 °C/30 min	<3.5x10 ⁻⁵
150 °C/30 min	<2.5x10 ⁻⁵

Processing and Handling Guidelines

PRINTING

CXT-0644 is supplied as ready-to-use ink. It should be stirred prior to printing as some sedimentation may occur over time. If thinning is necessary, use a maximum of 3% of ER-SOLV04 thinner by weight.

CXT-0644 is suitable for use on hand, semi-automatic or fully automatic screen printing machines. Polyester or Stainless screens with mesh count 255-420 threads/inch (100-165 threads/cm) can be used depending on desired ink film thickness and resolution. For very fine lines, stainless screen mesh is preferred. Cleaning with ER-SOLV04 thinner followed by cleaning with Acetone is recommended. Relevant Material Safety Data Sheet (MSDS) should be read carefully prior to using this product.

DRYING

Typical drying temperature may range from 120-200 °C (248-392 °F) depending on temperature tolerance of the substrate. Drying time may range from 2-30 minutes. Higher drying temperature and/or longer drying times will result in better electrical performance, adhesion and mechanical properties.

Optimum drying conditions should be established for particular equipment used by the customer.

STORAGE AND SHELF LIFE

Store in sealed containers in a cool, dry place (10-25 °C/50-77 °F). Shelf life of the product in unopened container is 6 months from the date of shipment.

Although the information presented here is believed to be reliable, Sun Chemical Corporation makes no representation or guarantee to its accuracy, completeness or reliability of the information. All recommendations and suggestions are made without guarantee, since the conditions of use are beyond our control. There is no implied warranty of merchantability or fitness for purpose of the product or products described herein. In no event shall Sun Chemical Corporation be liable for damages of any nature arising out of the use or reliance upon the information. Sun Chemical Corporation expressly disclaims that the use of any material referenced herein, either alone or in combination with other materials, shall be free of rightful claim of any third party including a claim of infringement. The observance of all legal regulations and patents is the responsibility of the user. Aug 2013

Sun Chemical Electronic Materials, 2445 Production Drive, St. Charles, IL 60174, USA; Tel +1 (630) 513-5348, Fax +1 (630) 587-5226
www.sunchemical.com

A4. Silver ink Acheson Electrodag PF-050 Henkel

Technical Data Sheet



Electrodag PF-050

May 2011

PRODUCT DESCRIPTION

Electrodag PF-050 provides the following product characteristics:

Technology	Thermoplastic
Appearance	Silver
Filler Type	Silver
Solvent	Dibasic ester
Product Benefits	<ul style="list-style-type: none"> • Conductive • Screen printable • Excellent flexibility • Low electrical resistance • Long screen residence time • Long shelf life • Good adhesion • No thinning required • Process ease • Superior fine line printability
Cure	Heat cure
Application	Conductive Ink

TYPICAL CURING PERFORMANCE

Recommended Curing Conditions

15 minutes @ 121°C or
3 minutes @ 140°C

Percent Volatiles

VOC, g/l	751
----------	-----

The above cure profile is a guideline recommendation. Cure conditions (time and temperature) may vary based on customers' experience and their application requirements, as well as customer curing equipment, oven loading and actual oven temperatures.

TYPICAL PROPERTIES OF CURED MATERIAL

Electrical Properties

Volume Resistivity, ohm/sq/mil	<0.01
--------------------------------	-------

Electrodag PF-050 is designed for production of flexible circuitry. This material can be used on a variety of substrates.

TYPICAL PROPERTIES OF UNCURED MATERIAL

Solids Content by Weight, %	68.5
Viscosity, Brookfield - RVT, mPa·s (cP): Spindle 6, speed 20 rpm, @ 30°C	17,500
Density, kg/l	2.39
Theoretical coverage, m ² /kg: @ 10 μm coating thickness	11
@ 25 μm coating thickness	4.4
Shelf Life, from date of qualification in original seal, year	1
Flash Point °C	74

TYPICAL SCREEN PRINTING PROCESS

Recommended Thickness	
Dried, μm	7.5 to 12.5
Emulsion Thickness	
Solvent resistant emulsion, μm	15 to 25
Recommended Squeegee	
Urethane for all screens, durometer	80
Recommended Screen Type	
Polyester screen, mesh	195 to 305
Stainless steel screen, mesh	200 to 270

GENERAL INFORMATION

For safe handling information on this product, consult the Material Safety Data Sheet, (MSDS).

DIRECTIONS FOR USE

1. Electrodag PF-050 should be thoroughly stirred prior to use. Avoid rapid stirring as this causes air entrapment.
2. Bring product to room temperature prior to use..
3. Electrodag PF-050 is supplied ready for use. Should thinning become necessary, dilute 1 to 4% by weight with Electrodag™ DBE (dibasic ester)..
4. Keep product container tightly closed when not in use.

Clean-up

To clean screen and equipment, use Methyleneketone (MEK) or similar solvents

Storage

Store product in the unopened container in a cool dry well ventilated area. Storage information may be indicated on the product container labeling.

Optimal Storage: 5 to 20°C. Storage below 5°C or greater than 20°C can adversely affect product properties.

Material removed from containers may be contaminated during use. Do not return product to the original container. Henkel Corporation cannot assume responsibility for product which has been contaminated or stored under conditions other than those previously indicated. If additional information is required, please contact your local Technical Service Center or Customer Service Representative.



Not for product specifications

The technical data contained herein are intended as reference only. Please contact your local quality department for assistance and recommendations on specifications for this product.

Conversions

$(^{\circ}\text{C} \times 1.8) + 32 = ^{\circ}\text{F}$
 $\text{kV/mm} \times 25.4 = \text{V/mil}$
 $\text{mm} / 25.4 = \text{inches}$
 $\text{N} \times 0.225 = \text{lb}$
 $\text{N/mm} \times 5.71 = \text{lb/in}$
 $\text{N/mm}^2 \times 145 = \text{psi}$
 $\text{MPa} \times 145 = \text{psi}$
 $\text{N}\cdot\text{m} \times 8.851 = \text{lb}\cdot\text{in}$
 $\text{N}\cdot\text{m} \times 0.738 = \text{lb}\cdot\text{ft}$
 $\text{N}\cdot\text{mm} \times 0.142 = \text{oz}\cdot\text{in}$
 $\text{mPa}\cdot\text{s} = \text{cP}$

Note

The data contained herein are furnished for information only and are believed to be reliable. We cannot assume responsibility for the results obtained by others over whose methods we have no control. It is the user's responsibility to determine suitability for the user's purpose of any production methods mentioned herein and to adopt such precautions as may be advisable for the protection of property and of persons against any hazards that may be involved in the handling and use thereof. In light of the foregoing, **Henkel Corporation and its affiliates ("Henkel") specifically disclaims all warranties expressed or implied, including warranties of merchantability or fitness for a particular purpose, arising from sale or use of Henkel products. Henkel specifically disclaims any liability for consequential or incidental damages of any kind, including lost profits.** The discussion herein of various processes or compositions is not to be interpreted as representation that they are free from domination of patents owned by others or as a license under any Henkel patents that may cover such processes or compositions. We recommend that each prospective user test his proposed application before repetitive use, using this data as a guide. This product may be covered by one or more United States or foreign patents or patent applications.

Trademark usage

All trademarks in this document are trademarks and/or registered trademarks of Henkel in the US and elsewhere.

Reference 0.2

Americas
+1.888.943.6535

Europe
+44.1442.278.000

Asia
+86.21.3898.4800

For the most direct access to local sales and technical support visit: www.henkel.com/electronics

A5. PET film Hostaphan® GN



Hostaphan® GN

Glass clear film

Hostaphan® GN is a glass clear biaxially oriented film, made of polyethylene terephthalate (PET) and is characterized by its high transparency and surface gloss and its low haze accompanied by its excellent mechanical strength and dimensional stability.

Hostaphan® GN is one or two side chemically treated for improved slip and processability as well as for improvement of the adhesion of coatings and printing inks. Details see next page!

Typical properties

Property	Thickness µm	Units	Value		Test Method	Test Conditions
			MD	TD		
MECHANICAL						
Tensile strength	50-125 175-250	N/mm ²	180 175	230 220	ISO 527-1 and ISO 527-3 Sample type 2	Test speed 100 %/min.; 23 °C, 50 % r.h.
Elongation at break	50-125 175-250	%	190 175	130 120	ISO 527-1 and ISO 527-3 Sample type 2	Test speed 100 %/min.; 23 °C, 50 % r.h.
Young's Modulus	50-125 175-250	N/mm ²	4100 3900	4900 4600	ISO 527-1 and ISO 527-3 Sample type 2	Test speed 1 %/min.; 23 °C, 50 % r.h.
F5-value (stress to obtain 5% elongation)	50-125 175-250	N/mm ²	105 110	105 110	ISO 527-1 and ISO 527-3 Sample type 2	Test speed 100 %/min.; 23 °C, 50 % r.h.
THERMAL						
Shrinkage	50-175 250	%	1.0 1.0	0.1 0.9	DIN 40634	150°C, 15 min.
OPTICAL						
Transparency	50-250	%	91		ASTM-D 1003-61 method A	-
Haze (for 1-side treated film)	50, 75 96, 100 125 175 250	%	0.5 0.6 0.6 1.1 1.5		ASTM-D 1003-61 method A	Enlarged measurement angle
Yellowness Index	50, 75 96, 100 125 175 250	-	1.5 2.0 2.5 2.8 3.0		ASTM E313-96/ D65	
SURFACE						
Roughness Ra value	50-250	nm	10		DIN 4768	Cut off 0.25 mm



Kasteler Str. 45 • 65203 Wiesbaden/Deutschland • Tel.: +49 611 96203 • Fax.: +49 611 9629357



Property	Thickness μm	Units	Value		Test Method	Test Conditions
			MD	TD		
PHYSICAL/CHEMICAL						
Density	50-250	g/cm ³	1.4		ASTM-D 1505-68 method C	23°C

MD = Machine direction, TD = Transverse direction

Product description:

Hostaphan® GN 4600A/460I/4660A:

The chemical treatment of these grades provides excellent adhesion primarily to water based coatings and printing inks.

Hostaphan® GN 4600A: One side treated, treated side wound out.

Hostaphan® GN 460I: One side treated, treated side wound in.

Hostaphan® GN 4660A: Two side treated.

Hostaphan® GN CT010/CT01I/CT01B:

The chemical treatment of these grades provides excellent adhesion primarily to solvent based coatings and printing inks.

Hostaphan® GN CT010: One side treated, treated side wound out

Hostaphan® GN CT01I: One side treated, treated side wound in

Hostaphan® GN CT01B: Two side treated

Applications:

- Membrane touch switches
- Imaging/Business graphics
- Printing
- Labels

Product advantages:

- Suitable for all standard printing processes (offset, flexographic, rotogravure and book printing).
- Glass clear films with smooth surfaces for excellent optics.
- Outstanding heat resistance.



Kasteler Str. 45 • 65203 Wiesbaden/Deutschland • Tel.: +49 611 96203 • Fax.: +49 611 9629357



Delivery program Hostaphan® GN

Thickness	Yield		Roll length	Roll diameter	Roll length	Roll diameter
	μm	g/m^2				
50	70	14.3	3 200	485	6 400	670
67	94	10.7	3 200	560	6 400	770
75	105	9.5	2 000	475	4 000	650
96	134	7.4	1 600	480	3 200	655
100	140	7.1	1 600	485	3 200	670
125	175	5.7	1 280	485	2 560	670
175	245	4.1	800	475	1 600	630
250	350	2.9	600	475	1 200	650

Other roll lengths on request. Core diameter: 152.4 mm (6")

Rolls are preferably supplied with knurls.

For detailed information of available grades please contact your local sales representative or directly us.

The properties shown in this technical data sheet only apply to the film itself. We cannot guarantee the properties of an intermediate or final product made from or using the film. Instead, the intermediate or final product must be subjected to standard industrial testing.

This data sheet reflects our state of knowledge at the time this was prepared. The purpose is to provide an overview of the characteristics of our products and their potential uses. It neither guarantees specific properties nor the suitability of products in specific applications. The user must observe industrial property rights, such as patents or trademarks. The quality of our products is covered by the terms of the General Conditions of Sale of MITSUBISHI POLYESTER FILM GmbH.

Edition 09/13



Kasteler Str. 45 • 65203 Wiesbaden/Deutschland • Tel.: +49 611 96203 • Fax.: +49 611 9629357

Curriculum Vitae

Personal status

Name: Ardeshir

Surname: Hakimi Tehrani

Date of birth: 1978

Nationality: Iranian

Education

1. Printing Technology (Doctor of Philosophy, Technische Universität Darmstadt, 2012-2015).
2. Industrial Design (Master of Art, University of Tehran, Cumulative GPA: 19.30/20, 2006-2008).
3. Printing Technology (Bachelor of Art, Art University of Tehran, Cumulative GPA: 18.37/20, 2003-2008).
4. Industrial Design (Bachelor of Art, Art University of Tehran, Cumulative GPA: 18.56/20, 2001-2006).

Honors

Graduated in the first rank of the Industrial Design, M.A. (2008).

Graduated in the first rank of the Printing Technology, B.A. (2008).

Graduated in the first rank of the Industrial Design, B.A. (2006).

The winner of “Iran’s National Science Olympiad” in industrial design (the ministry of science, research and technology of Iran, 2006).

Publications (books)

“The generalities of industrial design”, (2010) Tehran, Mirdashti Publications.

“Printing techniques and materials in packaging design”, (2009) Tehran, Mirdashti Publications.